Critical Velocity Modelling of High-Speed Rail Lines

Sara Mezher

Doctor of Philosophy

Heriot-Watt University

School of Energy, Geoscience, Infrastructure and Society

December, 2017

Abstract

Increased train speeds result in elevated railway track vibrations. This is undesirable because high track deflections can cause rapid track degradation and safety concerns. To understand the relationship between train speed and track vibrations and to investigate remedial measures, this thesis presents three computational approaches.

The first method is intended for use during the early design stage of a new line, and is capable of predicting the speed at which track deflections will be greatest (aka the 'critical speed'). The method analyses the dispersion relationships of the track and the soil and uses their intersection to compute the critical speed. It is advantageous because the procedure is fast and fully automated, thus removing the need for two dimensional image processing, which is often required for dispersion analysis. The model is validated using larger 2.5D finite element simulations. Using the method, a variety of track-soil variables is investigated to determine their influence on the critical speed, including: track type, track depth, track mass, railpad stiffness and soil layer configuration.

The second approach is intended for use on sections of new high speed line, where the train speed is found to be greater than 50% of the critical speed (e.g. calculated using the first approach). It is designed to calculate the relationship between train speed and track deflection, known as the dynamic amplification function. It, therefore, allows designers to determine track displacements for a range of speeds and the effect of changing different track-soil properties. The proposed method is semi-analytical, and couples a thin layer finite element formulation for the soil with an analytical approach for the track. The model is validated using field data from the Ledsgård site, Sweden, and then used to investigate axle spacing, train passage direction, slab tracks and soil stiffness.

The third approach is intended for detailed analyses of complex critical velocity sites and for cases where mitigation measures require appraisal. The model is a three dimensional finite

element model developed using the commercial software ABAQUS. It is a fully coupled train-track-soil system which considers train-track interaction. It is validated using field data from two European sites (Ledsgård, Sweden and Carregado, Portugal) and strong agreement is found. The method is then extended to simulate potential remediation measures such as stone columns and slab track.

The three approaches are used to conclude that, in general, increasing rail bending stiffness and railpad stiffness results in an increased critical velocity for ballasted track. However, for concrete slab tracks, these variables have minimal effect because slab track already has a significant bending stiffness. It is also found that soil saturation results in a reduced critical velocity and that if the soil has a deep uppermost layer, the critical speed is equal to the shear velocity of that layer. In terms of vibration levels, it is concluded that increasing the stiffness of the supporting soil results in a significant reduction in track vibration. This is particularly true for the case study of Ledsgård, Sweden, which has a low stiffness layer sandwiched between two stiffer layers. For vibration mitigation methods, it is found that the use of stone columns is an effective method to reduce track deflections, and that they should be deployed to a depth covering the softest soil layers.

Acknowledgements

The work of this research could not have been achieved without the help of the following individuals:

Dr. David Connolly (1st supervisor, Heriot-Watt University) – His consistent support, constant feedback and knowledge of modelling techniques made the project easier and more exciting.

Prof. Omar Laghrouche (2nd supervisor, Heriot-Watt University) and **Prof. Peter Woodward** (3rd supervisor, University of Leeds) – Their intensive knowledge of earthquake engineering /ground dynamics effects of high-speed trains added to my understanding throughout the research.

Dr. Pedro Alves Costa (University of Porto) – His knowledge and support in providing numerical knowledge was pivotal for the semi-analytical models developed in this research.

Mr Kaitai Dong (Heriot-Watt University) – His support in developing and assisting with the modelling techniques were of great importance throughout the project.

ACADEMIC REGISTRY

Research Thesis Submission

Name*:*	Sara Mezher		
School:	Energy, Geoscience, Infrastructure and Society (EGIS)		
Version: *(i.e. First, Resubmission, Final)*	Final version	Degree Sought:	PhD

Declaration

In accordance with the appropriate regulations I hereby submit my thesis and I declare that:

1) the thesis embodies the results of my own work and has been composed by myself

2) where appropriate, I have made acknowledgement of the work of others and have made reference to work carried out in collaboration with other persons

3) the thesis is the correct version of the thesis for submission and is the same version as any electronic versions submitted*.

4) my thesis for the award referred to, deposited in the Heriot-Watt University Library, should be made available for loan or photocopying and be available via the Institutional Repository, subject to such conditions as the Librarian may require

5) I understand that as a student of the University I am required to abide by the Regulations of the University and to conform to its discipline.

6) I confirm that the thesis has been verified against plagiarism via an approved plagiarism detection application e.g. Turnitin.

* *Please note that it is the responsibility of the candidate to ensure that the correct version of the thesis is submitted.*

Signature of Candidate*:*		Date:	

Submission

Submitted By *(name in capitals):*	
Signature of Individual Submitting:	
Date Submitted:	

For Completion in the Student Service Centre (SSC)

Received in the SSC by *(name in capitals):*			
1.1 Method of Submission *(Handed in to SSC; posted through internal/external mail):*			
1.2 E-thesis Submitted (mandatory for final theses)			
Signature:		Date:	

Table of Contents

List of Tables

List of Figures

Nomenclature

b	Half-track width
c	Damping coefficient
c_d	Dilatational wavespeed (P-wave)
c_P	Railpad damping
C	Damping matrix
d	Material deformation
E	Elasticity modulus
E_r	Nonlinear modulus of elasticity
EI	Bending stiffness
F	Force
f	Frequency
G	Shear modulus
g	Gravitational acceleration
H	Soil depth
H_i	Hermite shape functions
h	Average of normal strains
I	Vector of the internal force
K	Stiffness matrix
K_{Hz}	Hertzian coefficient

k	Stiffness
k_1	Fourier image of coordinate x
k_2	Fourier image of coordinate y
L	Element dimension
M	Mass matrix
m	Mass
N	Imposed load by wheel-rail interaction
n	Natural frequency number
n	Degree of freedom number
P	Vertical load
p	Mean stress
q	Mean shear stress
r_{irr}	Rail surface irregularity
s	Track support stiffness
t	Time
Δt	Time increment
u	Displacement
$\dot{u}$	Velocity
$\ddot{u}$	Acceleration
V_p	Compression wave velocity
V_R	Rayleigh wave velocity
V_s	Shear wave velocity

V_T	Train speed
x	Depth of the receiver
α_c, β_c	Constants proportional to mass and stiffness matrices
ν	Poisson's ratio
ρ	Density
ξ	Damping
ω	Angular frequency
ε	Normal strain
γ	Shear strain
σ	Normal stress
τ	Shear stress
ε	Normal strain
λ	Wavelength
λ_l	First Lamé parameter
λ^*	Dynamic Lamé parameter
μ_l	Shear modulus/second Lamé parameter
μ^*	Dynamic Lamé parameter
Ω	Driving frequency of the moving load

Chapter 1 Introduction

1.1 Overview and General Considerations

The development of railway tracks has been growing rapidly in recent years, allowing trains to go at higher speeds. Trains that travel at a speed greater than $200\ km/h$ are known as high speed trains (UIC). When the operational speed exceeds $400\ km/h$, they are categorised as ultra-speed trains (HS2 line in the UK) (DFT, 2010; Woodward et al., 2012b). Travelling at such speeds shortens travel duration and increases capacity. The critical velocity occurs when the speed of the train coincides with the ground surface wave velocity and observed phenomena are related to critical velocities: formation of surface waves (ground Mach cone development) and track uplift caused by waves interaction. These phenomena cause track damage due to increased deflections, and, thus, increase concerns about safety and maintenance work (e.g. tamping and Measured Shovel Packing (MSP) methods) (Claisse & Calla, 1992). The development and transmission of vibrations also affect the far field areas.

Due to excessive track vibrations, significant safety, social and economic concerns arise, which emphasise the importance of this research:

- Safety effects:

The development of vibrations is one of the causes of rail derailment with recent examples around the world, such as the TGV derailment in France, in 2015, which was not a critical velocity problem; however, it was reported as being caused by excessive speed, resulting in the death of 10 people (Jethro, 2015). The consequences of damage and accidents raise the awareness of the importance of critical velocity investigation.

- Social effects:

Excessive track vibrations affect the comfort of train passengers. In addition, transmitted ground vibrations lead to structural vibration and internal noise in nearby structures. This affects the safety and comfort of the occupants of nearby structures and public facilities (e.g. schools, hospitals etc).

- Economic effects:

Frequent exposure to vibrations causes track degradation, thus, leading to increased maintenance and renewal. The average cost of maintenance and renewal per kilometre of track length across Europe was 62 million Euros in 2006, with a cost of approximately 170 million Euros in the United Kingdom (Smith et al., 2008). A constant increase in the number of renewed track parts was reported in the United Kingdom, for example: concrete sleepers were renewed along $335\,km$ in the $2010-2011$ financial year, while sleepers were renewed along $439\,km$ in $2011-2012$ (ORR-Data). In addition to maintenance and renewal, mitigation methods can be applied (e.g. railpads, trenches for the farfield), which increase the overall cost and time of service delays.

Analysing critical velocity effects throws up a number of challenges for railway engineers. Different studies have been conducted to predict the behaviour of the ground under certain effects using three-dimensional software modelling; however, due to the high complexity and nonlinearity of soil and track components, a large body of research is still ongoing. Being able to predict the response of the ground will be beneficial to future construction projects on new railway tracks. Also, modelling the dynamic problems will help in the design of mitigation strategies to reduce these effects.

1.2 Objectives

The main aim of this work is to propose a framework for combining approaches to tackle the challenges raised by critical velocity effects and improve knowledge in the railway field. The objectives of this research are summarised by the following points:

1- Prediction of critical velocity value:

Quick indication of critical velocity value is beneficial in the early design stage to provide the speed for which additional investigation is required.

2- Assessment of factors influencing critical velocity:

Different factors including the properties of train, track and soil affect the value of critical velocity for a specific track. It is important to monitor the effects of these factors on dynamic amplification at critical conditions in order to assist in reducing the effects.

3- Track optimisation and investigation of different track stabilisation techniques:

After determining the critical velocity value and its effects, different stabilisation methods are analysed and compared in order to come up with the most efficient solution, which reduces the dynamic effects and overall construction cost.

1.3 Original Developed Approaches

The main focus of this research is to analyse and predict critical velocity effects on track behaviour and ground response as mentioned in the research objectives. Modelling approaches are developed that provide accurate prediction and allow the effects of different train and track properties on the ground behaviour to be tested.

1- Developing an analytical approach for critical velocity value prediction:

One of the aims is to improve different analytical methods in terms of efficiency in determining critical velocity. Dispersion analysis is used for soil and track systems. The applicability of dispersion characteristics is direct for surfaces on homogeneous soil in order to compare the natural soil wave speed with the load speed. However, this is more complex for multi-layered ground. This analytical method has been modified previously for railway track systems by many researchers. The research aims to improve the dispersion analysis further in order to achieve minimal run time with less computational capability. The key contribution in this approach is in producing dispersion relations between the wave apparent velocity and frequency for track and soil systems, which avoids post-processing in determining critical velocity. It is important to test the changes in track and soil properties and their relation to critical velocity values; thus, this approach will be used to investigate different properties (track type, track depth, saturation etc.).

2- Developing a semi-analytical approach for producing DAF curves:

Since the dispersion analytical approach is used merely for critical velocity calculations, a semi-analytical approach is developed in order to calculate the 3D ground displacements and produce Dynamic Amplification Factor (DAF) curves. DAF curves are beneficial in investigating the change rate in ground response with the increase in train speed. The key contribution is the combination of modelling the track analytically, while modelling the soil numerically using the Thin Layer Method (TLM), a technique which makes use of finite element methods. The benefits of a semi-analytical approach lie in reduced total simulation time in comparison to fully numerical models; thus, the model results in fast production of DAF curves in order to test different track and train properties (axle loading, axle spacing etc.) effects on the ground behaviour at critical velocities.

3- Developing a 3D numerical approach for a fully coupled train-track-soil system:

Another objective is to develop a numerical model using finite element software in order to assess the behaviour and solutions. The chosen software is ABAQUS, which is a 3D finite element software widely used across companies for different types of model. In comparison to the semi-analytical approach, the accuracy is higher in numerical models since the track is expected to be modelled using finite element methods, which allows for a reduction in element size to increase accuracy. In addition, the soil can be meshed in three dimensions, unlike for TLM where the soil layers are meshed vertically. This is applicable when producing model displacements and 3D response along the track, far field and various depths of soil models, including strains and stresses. The key contribution is defining subroutines for a lumped mass vehicle system, which calculate the interaction forces between the train and the track. This allows one simulation to be run for a full train-track-soil system, instead of the use of sub-modelling. Figure 1.1 shows a comparison between simulation time for the three approaches. The numerical approach was run on Scientific Linux with Core i7 processor, while the other two approaches were run on Microsoft with Core i5 processor.

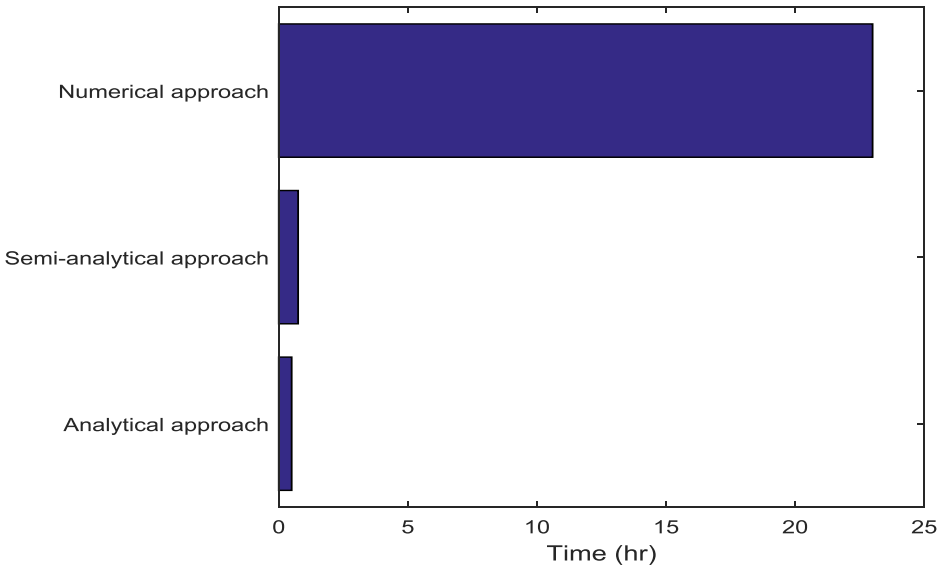

Figure 1.1 Simulation time comparison between the developed analytical, semi-analytical and numerical approaches

Additionally, the aim is to use this approach in testing mitigation strategies. In future investigations, critical velocities and the dynamic amplifications caused by them are taken into consideration in order to come up with the best stabilisation technique if required. Being able to model the solutions helps to reduce maintenance and failure costs, provides comfort for passengers and ensures the safety of residents in nearby areas. It is also important that these solutions are cost effective and environmentally friendly. The numerical approach is chosen to model mitigation strategies rather than the semi-analytical approach, as it allows for modelling inhomogeneous ground in three dimensions, which is required for modelling some of the chosen stabilisation techniques in this research (e.g. stone columns). Stone columns, concrete slabs and asphalt tracks are some of the mitigation strategies considered in this research.

1.4 Thesis Outline

The following presents the description of the chapters included in the thesis:

Chapter 2 includes a brief description of track components and various sources of vibrations associated with increasing train speeds: wave propagation and transmission phenomena, vehicle dynamics and their effects on the ground. The chapter also explains the general behaviour of the soil under cyclic loading and the effects of the track and soil nonlinearities. Train track interaction is also introduced as it is a major problem for train-track systems modelling. Critical velocities are defined in this chapter, in addition to their effects including the ground Mach cone and resonance phenomena.

Chapter 3 is devoted to the literature review. Modelling aspects are discussed and explanations are made between different analytical and numerical modelling approaches. The chapter also covers previous research on the ground behaviour and modelling mitigation strategies for the adopted case (Ledsgård site, in Sweden). Modelling approaches for dispersion analysis of track and ground systems are included in this chapter.

Chapter 4 focuses on the dispersion analysis. The developed simplified approach that produces dispersion relations in velocity against frequency is explained. The method is applied to the track system and soil system. Both ballasted and slab tracks are modelled. Validation of the track model is included for ballasted tracks, in addition to the validation of critical velocity calculations. After validation, different parameters are studied using sensitivity tests including ballast depth, slab depths, comparison between both track types, slab mass, rail bending stiffness, railpad stiffness, soil saturation, and depths of soil layers.

Chapter 5 includes a simple semi-analytical analysis carried out using MATLAB software for quick determination of the ground response and Dynamic Amplification Factors. The formulation of the track is done with analytical equations and Green's functions are used for the ground system. The model is validated for the X2000 train track in Sweden. Additional slab track models are also presented in this chapter for the same train track. The results are also compared to previous research outcomes. Soil properties are changed to stiffer soil to study the effects on the behaviour. Different changes to the vehicle system are applied including different axle spacing and running the vehicle in opposite directions.

Chapter 6 explains the numerical approach aspects that are adopted in the study using ABAQUS software. Different modelling techniques for the soil or track models are compared. Finite element implementation includes explicit time integration, material properties, a definition of boundary conditions, modelling of train-track interaction and shape functions considered for the rail elements. The results of initial testing under a stationary train are included. The chapter explains the loading application and the user-defined subroutines used with ABAQUS to define the train system and interaction with the track. Two cases of train tracks are modelled and validated: the X2000 train track in Sweden and the Alfa-Pendular train in Portugal. The chapter also includes the modelling of slab tracks.

Chapter 7 includes the analysis and critical velocity effects of the simulations that are carried out in ABAQUS software. For the Swedish track, the stresses and octahedral shear strain plots underneath the rail are presented and discussed, in addition to contour plots of the ground vibrations and ground Mach cone formations. The chapter also presents an analysis of mitigation strategies: stone columns, which are validated using actual field results from the Swedish site before and after stabilisation. Different properties of the stone columns are

tested. In addition, the chapter includes slab and asphalt track models. A summary and list of findings arising from this work and recommendations for future research are included in the final chapter.

Chapter 2 Background

2.1 Introduction

The chapter includes background information and basic aspects of track components. It is important to develop an understanding of the sources of ground vibrations; thus, the wave propagation phenomena, vehicle dynamics and train-track interactions, which contribute to railway-generated ground vibrations, are explained in this chapter. Nonlinearity behaviour of the soil and ballast material under static/quasi static/dynamic loading is included, which helps to clarify the effects of critical velocities on the track and ground. The definition of these critical speeds and their effects are explained in this section. Vibration and wave transmission in railway tracks are some of the critical velocity effects. Finally, modelling aspects are briefly introduced in this chapter.

2.2 Track Components

The main components of a conventional ballasted track are shown in Figure 2.1. The rail distributes the load of the vehicle vertically and horizontally to the sleepers. The fasteners hold the rail in place and prevent it from moving on top of the sleepers. The main role of railpads, especially soft railpads, is to prevent high vibrations being transmitted to the sleepers. The sleepers fix the super-structure in the ballast to stop the system from moving vertically, horizontally or along the passage direction (Banimahd, 2008; Selig & Waters, 1994).

Moving to the sub-structure, the ballast resists the forces that are transmitted from the sleepers to hold the super-structure in place. It also provides drainage and contributes to distribution of forces to the lower layers. Since the ballast consists of coarse granular

material, the sub-ballast layer helps to protect the subgrade from the penetration of ballast components. This layer also reduces the stresses applied to the subgrade and soil layers beneath the track (Banimahd, 2008).

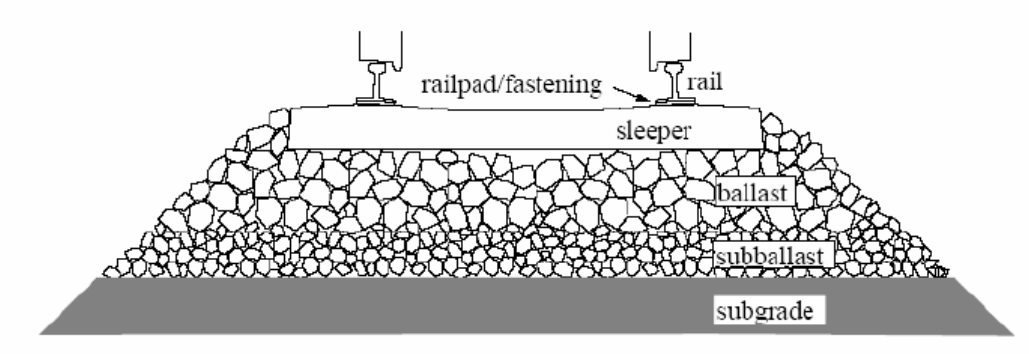

Figure 2.1 Railway ballast track components (Dahlberg, 2006)

Slab tracks, on the other hand, consist mainly of the rail, slab layer, Hydraulically Bonded Layer (HBL), Frost Protection Layer (FPL) and the subgrade. Figure 2.2 shows the components of the Rheda 2000 slab track, in Germany (RailOne, 2011) as an example. The HBL is a mixture of soil, water and cement, which increases the strength and stability of the track. The FPL layer is usually made of compacted permeable soil (RailOne, 2011). The slab track material is concrete; however, asphalt slabs are used on some occasions (Serdelová & Vičan, 2015). Slab tracks provide higher lateral track resistance, reduction of structure height and lower maintenance requirements than ballasted tracks. Another advantage is that they avoid the churning of ballast particles at high speeds (Esveld & Markine, 1998). Precast slabs and on-site poured slabs can be applied. The design of the slab tracks depends on soil conditions. For soils that are expected to have large settlements, reinforcement can be applied in the slab at the neutral line (e.g. Rheda 2000) or at the top and at the bottom of the slab. The latter provides larger bending strength. In addition to the reinforcement, other techniques can be used to improve the strength (e.g. bridge-like structures as the substructure) (Esveld & Markine, 1998).

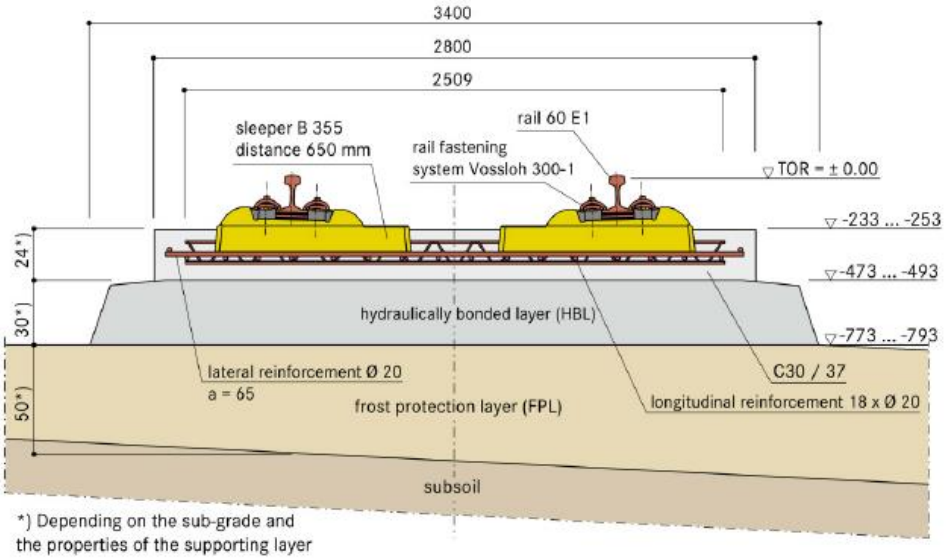

Figure 2.2 Railway slab track components (RailOne, 2011)

2.3 Sources of Ground Vibrations

2.3.1 Wave propagation phenomena

The induced stress pattern spreads away from the source, as a result, the stresses cause vibration in the surrounding soil, and the waves are different in the ground layers due to variations in surface geometry and stiffness of soil. Shear waves, compression waves and Rayleigh waves are the main types of stress wave, which vary depending on soil properties. The spreading of waves can be described by the transmission of energy density contained in wave-fronts, which is expressed in relation to two components: kinetic energy (depending on soil density and wave velocity) and potential energy (depending on stress and strain) (Shearer, 2009). Due to the variation in mechanical and geometrical characteristics of the soil, the stress waves that infiltrate the layer of soil are further complicated by the wave and surface interactions that affect the propagation and wave amplitude. The interactions between waves and soil layers include:

1) Refraction: the energy transmitted between boundaries of soil layers has an altered wave path due to different velocities/properties between layers;
2) Reflection: the energy reflected at boundaries depends on the angle the wave has with the boundaries and is also caused as a result of changes in soil properties;
3) Dispersion: soil characteristic that describes speed and frequency of wave propagation in soil layers;
4) Diffraction: the waves are diffracted due to the presence of cracks; and
5) Attenuation: energy loss is due to anelastic processes or internal friction (intrinsic attenuation).

Ground-borne energy has variations caused by the magnitude of excitation, and also varies due to the different types of waves that pass through it. The amount of energy exerted by a circular disc that oscillates vertically to an isotropic homogeneous half-space is approximately 67% Rayleigh waves, 26% shear waves and 7% compression waves (Banimahd, 2008; Miller & Pursey, 1955).

Body waves consist of compression (P-waves) and shear waves (S-waves), while surface waves mainly consist of Rayleigh waves. The stiffness of the layer through which the waves are passing can determine the speed of the surface and body waves, where compression waves are considered to be the initial waves at any point in the ground, followed by shear waves, then Rayleigh waves. The vibrations caused by P-waves cause volume change by compression and expansion in the direction of the propagated wave. The S-waves do not change the volume of the material and they propagate in a perpendicular direction to the direction of the travelling wave. The Rayleigh waves are dispersive in nature, and they reduce with depth. The particles in a Rayleigh wave have an elliptical path that moves counter clockwise. The seismic wave-fields consist of P-wave component (P), vertical S-wave component (SV), and horizontal S-wave component (SH). The seismic modes are shown in Figure 2.3. The equations governing the measurement of the waves' velocities in an elastic medium are:

Compression wave velocity: $V_p = \sqrt{\frac{E(1-\nu)}{\rho(1+\nu)(1-2\nu)}}$ (2.1)

Shear wave velocity: $V_s = \sqrt{\frac{E}{2\rho(1+\nu)}}$ (2.2)

Rayleigh wave velocity: $V_R \approx \frac{0.87+1.12\nu}{1+\nu} V_s$ (2.3)

where E is the elasticity modulus, ν is Poisson's ratio, and ρ is density of the elastic medium. The ground vibration is assumed to be at low frequency (under $20\ Hz$ normally, according to Hall (2000)) and higher frequencies are filtered by the super-structure attenuation, which is formed by the uneven riding of the wheel of the train. In addition, the vibrations formed can also be filtered by the ballast layer.

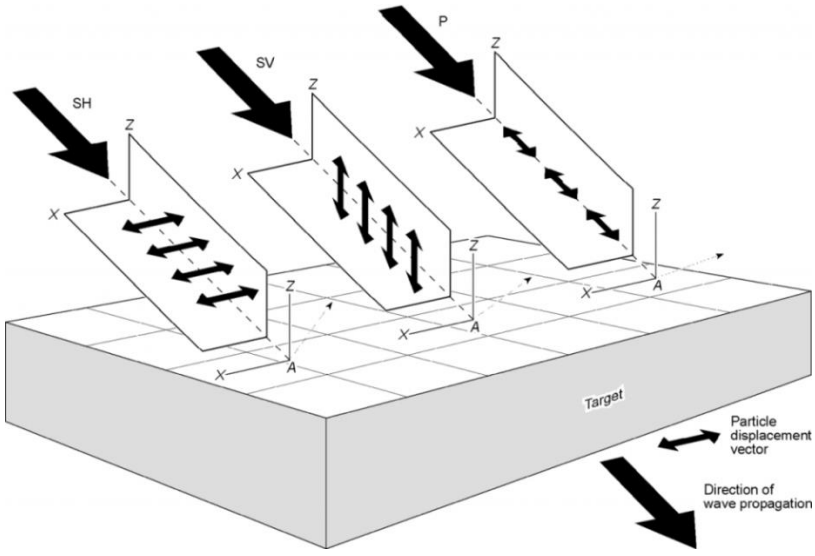

Figure 2.3 Seismic modes in the wave-field (Edward, 2007)

2.3.2 Vehicle dynamics

In order to maintain the rigid body modes of the vehicle's body and bogie, vehicle suspensions are used and designed for that purpose to have a sufficient buffer zone that isolates passengers from the vibration. Also, the vehicle suspensions are used to reduce the unsprung mass effects on the vehicle, which can decrease the dynamic loads placed on the wheel-rail interface. At low frequencies (below $20\,Hz$), the track behaves as a stiff spring. On the other hand, when the frequencies exceed $20\,Hz$, the inertia of the track is of greater importance, as demonstrated by the complete isolation of suspension, other than the unsprung mass from the rest of the vehicle. A better definition of "high" frequencies, for present usage and purposes, refers to those above $20\,Hz$, where the track dynamics become highly significant and vehicle dynamics play a lesser role in the interaction between all parameters. This clearly demonstrates passenger comfort, stability and curving as phenomena occurring under low frequencies (Knothe & Grassie, 1993). Many problems which are related to different parts of the train and rail components: bogie, unsprung mass, wheel/rail interactions, are discussed further by Knothe and Grassie (1993).

When stationary, the weight of the train results in a stress pattern around the immobile vehicle, which moves with the train's movement. The present system is a significant source of train-induced ground vibration that results in uplift stress waves found even with the absence of the periodic irregularities in the vehicle. The primary constraints, such as the wheel axle spacing, train speed and axle weight, can play a major role in the structural response of the track, which can also be excited by secondary constraints. An example of secondary constraints is the unsymmetrical riding of the train caused by the wheel defects that creates fluctuating forces on the track, and results in non-uniform support outcomes (Banimahd, 2008; Hall, 2000). Hall (2000) studied different sources of vibration, such as induced stress waves by the track structural responses, discontinuity on the track, vibration source at interface between wheel and rail and various supports for the vehicle.

Several types of mechanisms can be used to identify railway-generated ground vibration data, which can affect the total ground vibration level at various frequency bands (Krylov et al., 2000). These mechanisms are divided into several types, such as:

- Wheel axle pressure on the track;
- Effects of un-welded rail joints;
- Equality and evenness of rails or wheels;
- Dynamically generated forces of carriage and wheel axle vibrations that are induced due to unevenness of rails and wheels;
- The commonly used mechanism based on the quasi-static pressure of wheel axles on the rail track.

2.3.3 Train-Track Interaction

When modelling railway tracks for critical velocity analysis, it is essential to take wheel-rail interaction into consideration. As this interaction is the source of excitation, geometrical irregularities are the cause of large forces, which, in the long run, cause damage to vehicle components, rail corrugations or other track components leading to the need for increased maintenance. Train speed is a major factor affecting the interaction between the wheel and the rail, especially at turnouts due to rail discontinuity, and thus, it increases the vibrations (Zhai et al., 2001). Apart from the irregularities that are related to the rail and wheel, any structural irregularities and stiffness variations of the track can cause oscillations of the interaction force. The variations of track stiffness can be caused by the change of ballast depth due to decrease of void sizes or generation of excess pore water pressure along with other factors, which result in stiffness reduction (Banimahd, 2008).

Figure 2.4 illustrates the components of the vehicle showing the wheel and the bogie with the suspension systems. In terms of modelling, the interaction can be represented by rigid bodies and springs and dampers. For simplicity and since the primary and secondary suspension systems are modelled as springs, a Hertzian spring is often used to model the interaction as discussed in detail in Chapter 6 (Kouroussis et al., 2014; Woodward et al., 2012a).

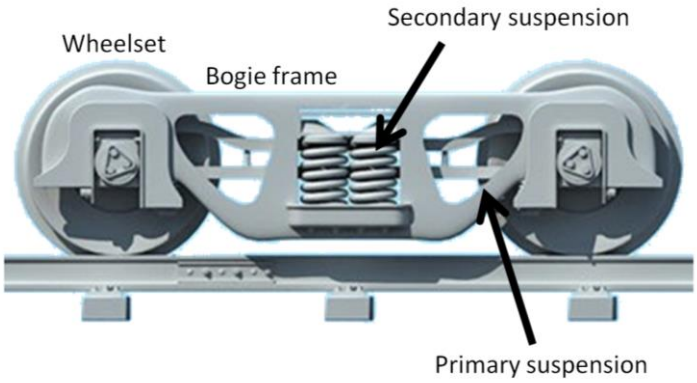

Figure 2.4 Components of train/track interaction (Gandoza3DModels)

2.4 Soil properties and Behaviour under Cyclic Loading

2.4.1 Static, quasi-static and dynamic loading

Static load denotes the weight of the rail freight wagons that does not change over long periods of time. When the ideal conditions of perfect rail surface and wheel tread are considered, this creates an identical force between the wheel-rail contact loading and the static wheel force itself. Quasi-static loading changes marginally over long periods of time, as the summation of the effect of train speed and static load, along with the track support and geometrical properties (curvature, roughness and super elevation). On the other hand, dynamic loading is a time-dependent parameter, which changes its magnitude significantly over short time periods. Such changes are dependent on the duration of abnormalities (Remennikov & Kaewunruen, 2008). The loads induced by the train have three components based on direction. The horizontal forces are significantly small, which can be ignored in the modelling procedures, and only dynamic vertical loads are taken into consideration. The dynamic load is calculated by totalling the static load of the train with the dynamic forces induced from the wheel-rail irregularities. To simplify the calculation of the dynamic loads, F_{dyn}, a factor which is known as the Dynamic Amplification Factor (DAF) can be multiplied by the static force, F_{static} (Equation (2.4)).

$$F_{dyn} = DAF.F_{stat} \tag{2.4}$$

Different theories cover the calculation of DAF. A few of these theories are presented in Table 2.1.

Reference	Equation	
(Esveld, 2001)	$\begin{cases} DAF = 1 + t_m\varphi & V < 60 \\ DAF = 1 + t_m\varphi\left(1 + \dfrac{V-60}{140}\right) & 60 \le V \le 200 \end{cases}$	(2.5)
(AREA, 1996)	$DAF = 1 + \dfrac{5.2V}{D_w}$	(2.6)
(Srinivasan, 1969)	$DAF = 1 + \dfrac{0.017V}{\sqrt{k}}$	(2.7)
(C. Clark, 1957)	$DAF = 1 + \dfrac{19.65V}{D_w\sqrt{k}}$	(2.8)

Table 2.1 Summary of different adaptations for DAF calculations

φ is an empirical factor, and Table 2.2 presents the values taken based on track quality (Esveld, 2001). t_m is the multiplication factor of standard deviation, which depends on the confidence interval. V is the train speed, D_w is the diameter of the wheel, and k is the track modulus and the values are $7\ MN/m/m$ for poor tracks, $14\ MN/m/m$ for average tracks and $21\ MN/m/m$ for good quality tracks (Stewart & O'Rourke, 1988).

Track condition	φ
Very good	0.1
Good	0.2
Bad	0.3

Table 2.2 Classification of empirical factor φ

2.4.2 Nonlinearity in ballast/sub-ballast

One reason behind the complexity of modelling tracks and soil is due to the nonlinearity of the materials. The passage of the train causes cyclic loading on the track layers. Traffic load is carried mainly by the granular soils (ballast/sub-ballast) in a well-compacted form. It is important to identify permanent deformation, which affects performance in the long run, and resilient behaviour, which is instantaneous recoverable deformation of granular soil due to cyclic loading. The resilient behaviour can be calculated using triaxial tests to calculate the resilient modulus by dividing repeated deviator stress over the axial strain after unloading (Figure 2.6) (Seed et al., 1962). The deviatoric stress is the stress that causes distortion in the body, and it is calculated by subtracting the mean stress from the normal principal stresses ($\sigma_1 - p, \sigma_2 - p$ and $\sigma_3 - p$). Figure 2.5 shows the notations used for normal and shear stresses, (a), and principal stresses, (b), throughout the thesis. The mean stress, p, is the average of the normal principal stresses (Equation (2.9)). The deviatoric strain is related to the deformation at a constant volume, and it is calculated by subtracting the average of the normal strains, h (Equation (2.10)), from the normal strains ($\varepsilon_1 - h, \varepsilon_2 - h$ and $\varepsilon_3 - h$).

The resilient behaviour of the soil is nonlinear and it is affected by the density, moisture content and stress-strain relation (Banimahd, 2008). Different studies by Knutson and Thompson (1977) and Monismith et al. (1967) discuss the effect of confining pressure and mean stress on the resilient modulus, as it increases with bulk stress. Moreover, Haynes and Yoder (1963) report a decrease in the resilient modulus as the moisture content is increased, while Hicks (1970) discusses an increase in the modulus as the optimum density is increased. Seed and Idriss (1970) discuss the effect of the shear strain (deviatoric) on the resilient modulus, which decreases as the deviatoric strain is increased (Seed & Idriss, 1970). This is

not always true as the interaction between both mechanisms has to be considered as, in some cases when the shear failure is not reached, the increase of deviatoric stress or strain causes a slight increase in the resilient modulus (Hicks & Monismith, 1971; Sweere, 1990). Uzan (1985) states that the increase in shear strain in dense granular soil causes a particle rearrangement, which increases the material volume, and thus, increases the resilient modulus.

$$p = \frac{\sigma_1+\sigma_2+\sigma_3}{3} \tag{2.9}$$

$$h = \frac{\varepsilon_1+\varepsilon_2+\varepsilon_3}{3} \tag{2.10}$$

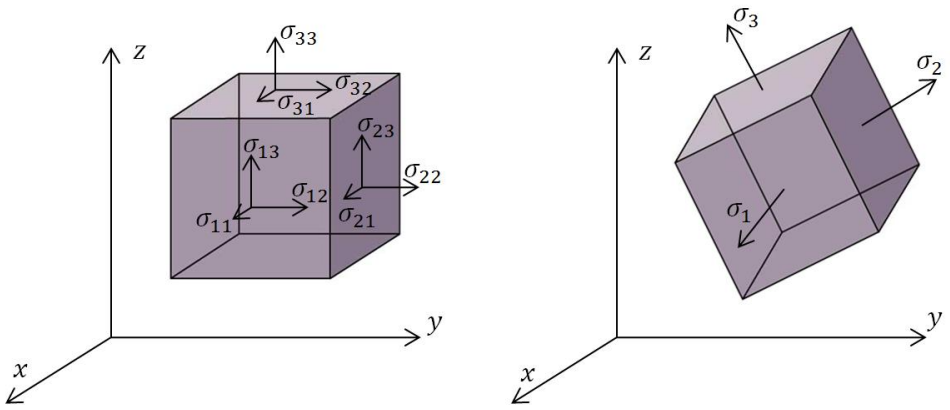

a) Normal and shear stresses b) Principal stresses

Figure 2.5 Stresses in a given coordinate system and principal stresses

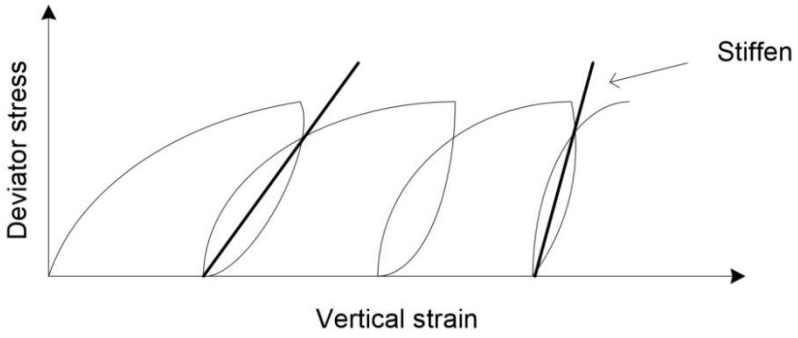

Figure 2.6 Behaviour of soil under cyclic loading (Selig & Waters, 1994)

2.4.3 Nonlinearity in clayey subgrade

For the subgrade material and the soil layers underneath the track, other factors included in this section, which affect the resilient modulus, should be taken into consideration. As the subgrade soil resilient behaviour changes under various loadings, it is essential to understand the three different categories of influence, namely:

- Stress/pressure condition;
- The structure and type of soil;
- The water content and soil density.

Subgrade that consists of clay layers is the main soil type discussed in this section, since clay has low permeability and large water-holding capacity due to its small particles. Studies show that increasing moisture content results in a lower value of resilient modulus (Elfino & Davidson, 1989). Other studies by Thompson and Robnett (1979) prove that the modulus increases with an increase in the unconfined compression strength in clay, and decreases with an increase in the degree of saturation. In addition, the resilient modulus is larger for increasing density based on the findings of Thompson and Robnett (1979).

In terms of modelling nonlinearity, the soil stiffness and damping values of the track and soil layers vary. They are calculated using the proposed Equation (2.11) for Young's modulus, (Uzan, 1992) and Equation (2.12) for damping ratio (Rollins et al., 1998), which are applied

to the finite element analysis rather than constant Young's modulus and damping values. However, if the model assumes a linear behaviour, a reduction in the stiffness should be considered as the train speed increases.

$$E_r = k_1 P_{atm} \left(\frac{3p}{P_{atm}}\right)^{k_2} \left(1 + \frac{q}{P_{atm}}\right)^{k_3} \quad (2.11)$$

$$\xi = d_1 + (d_2(1 + 0.15(100\gamma^{dev})^{-0.9})^{0.75}) \quad (2.12)$$

where P_{atm} is the atmospheric pressure, p is the mean stress (Equation (2.9)), and q is the shear stress (Equation (2.13)) relating triaxial values. k_1, k_2 and k_3 are material parameters donated by negative values for softening and positive values for hardening of the behaviour. γ^{dev} is the deviatoric strain (Equation (2.14)), and d_1 and d_2 are material properties.

$$q = \frac{1}{\sqrt{2}}[(\sigma_1 - \sigma_2)^2 + (\sigma_1 - \sigma_3)^2 + (\sigma_2 - \sigma_3)^2]^{0.5} \quad (2.13)$$

$$\gamma^{dev} = \frac{1}{\sqrt{2}}[(\varepsilon_1 - \varepsilon_2)^2 + (\varepsilon_1 - \varepsilon_3)^2 + (\varepsilon_2 - \varepsilon_3)^2]^{0.5} \quad (2.14)$$

2.5 Critical Velocity Effects

As the high speed on weak soil amplifies the ground response, it is important to understand what these effects are in order to reduce the problem. Research to define the critical velocities, how to determine their values and monitor their effects, is ongoing (Madshus & Kaynia, 2000; Woodward et al., 2012b). The two major effects that are caused in the ground are surface wave transmission (ground Mach cone) and track resonance. These two effects are defined briefly in this section.

2.5.1 Ground Mach cone effects

The ground Mach cone is a phenomenon created when the speed of the vehicle approaches Rayleigh wave velocity, which results in higher track displacements and higher values of vibration at ground surface level. The track is assumed to be in a critical condition (critical velocity) as the train speed approaches the Rayleigh wave velocity of the ground surface, and creates an asymmetric profile of the vibration (Woodward et al., 2012a). The ground Mach cone ratio is used to verify the track conditions, as stated in Table 2.3.

Ground Mach Cone Ratio (GM)	**Track Condition**
$1 > GM > 0$	Sub-critical conditions
$GM = 1$	Critical conditions
$GM > 1$	Super-critical conditions

Table 2.3 Ground Mach cone ratios and corresponding track conditions

The main aspect of a Mach cone effect being formed, when ground wave velocity is exceeded, is the transmission of surface Rayleigh waves, which are highly dependent on the fundamental natural ground frequencies. The transmission of these waves is also dependent on Poisson's ratio, stiffness of the ground layer and density of the soil. Ground Mach cone ratio is defined as follows (Krylov, 1995):

$$\mathrm{GM} = \frac{\mathrm{V_T}}{\mathrm{V_R}} \tag{2.15}$$

where $\mathrm{V_T}$ is the speed of the train and $\mathrm{V_R}$ is the Rayleigh wave velocity of the ground surface. At GM ratio between 0.5 and 1 (sub-critical conditions), the wave propagation results in a gradual increase the dynamic deflection above the static deflection with low lateral track vibrations. When GM is equal to 1 (critical conditions), the surface waves are transmitted

with high lateral vibrations away from the track, leading to higher transient deflections described as a ratio to the static displacements. Taking into consideration the displacements in multi-layered soil is essential when the behaviour of the ground is difficult to identify due to the differences of Rayleigh wave velocities in each layer (Woodward et al., 2012b).

When the ratio of the ground Mach cone exceeds 1 (i.e. the train speed exceeds the velocity of Rayleigh waves in super-critical conditions), the dynamic response of the track begins to decrease. Such a formation of Mach cone can be identified by the angle between the formed waves and the track level, and is described as "Mach Angle Theory" (Equation (2.16)).

$$\alpha = \sin^{-1}\frac{1}{GM} \tag{2.16}$$

where the total angle is 2α (Figure 2.7).

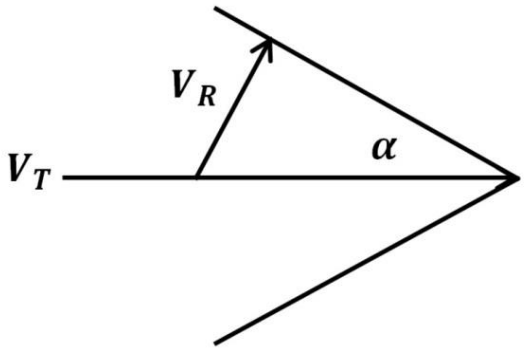

Figure 2.7 Mach cone angle (Woodward et al., 2012a)

2.5.2 Track resonance

Track resonance is observed as a result of the increase in train speed, which can be shown once the primary loading frequency is equal to the natural frequency. The loading wavelength, λ_p, is explained as the centre-to-centre distance of the double bogie, which can be used to measure the "Resonant Train-Track Velocity", V_{RTT}, as defined by Woodward et al. (2013) (Equation (2.18)). Both the track components and train components are parameters that affect the loading frequency. On the other hand, the cut-off frequency (ground natural frequency) is a significant factor in the wave propagation. To determine the frequency, the following equations are used:

$$f_n = \frac{V_p(2n-1)}{4H} \tag{2.17}$$

$$V_{RTT} = \lambda_p f_n \tag{2.18}$$

The soil is assumed to be homogenous in fully isotropic conditions. The critical depth of the soil can be calculated for a known loading frequency using the following equation, where f_L is the loading frequency (Woodward et al., 2012a):

$$H_{crit} = \frac{V_p(2n-1)}{4f_L} \tag{2.19}$$

The frequencies where resonance occurs depend on the soil's material properties and geometry (Kramer, 1996). Resonance causes the uplift effect of the track, which, in turn, causes significant damage to the track, especially if poor suspensions in the train are found (Woodward et al., 2012a).

2.6 Modelling Aspects

In order to develop a better understanding of the ground behaviour, different modelling methods are considered. The most commonly adopted method for modelling railway tracks is the Finite Element Method (FEM), which is a numerical method for solving unknowns at discrete number of points by dividing a system into smaller parts (finite elements), and then assembling into a large system of equations to solve the entire model. The flexibility of FEM has led to it being widely used for railway vibration modelling techniques where the seismic wave equation is introduced into the procedure. It is also capable of analysing complicated geometric models. Modelling of structures/buildings can be suitably analysed using FEM; however, computational efficiency is still an issue. As the domain size increases, the run time increases, which can create an obstacle to modelling large offsets. The modelling software offers two types of analyses: implicit and explicit finite element analyses. Implicit analysis requires a series of iterations to obtain equilibrium, while for explicit analysis, the nodal accelerations are solved directly. Explicit analysis also provides a stability time limit and it does not require matrix inversion over time steps, unlike implicit analysis. Therefore, explicit analysis is more common for cases that include material nonlinearities and contact treatments. Many researchers have adopted FEM in combination with other methods (e.g. Boundary Element Method) to study the behaviour of the ground under high-speed trains. These methods are reviewed in Chapter 3.

The Boundary Element Method (BEM) is a numerical method that solves partial differential equations by formulating integral equations. The method uses boundary conditions to fit boundary values into integral equations and it constructs a mesh over a modelled surface, which makes it more efficient in terms of computational requirements than FEM for problems with small surface to volume ratio. However, BEM can result in large unsymmetrical matrices depending on the size of the problem.

Frequency and time domains are the two main methods used to analyse data, and are widely practiced in several fields such as acoustics, electronics, telecommunications, etc. The outcomes of both methods can be converted from the time domain functions to frequency domain functions and vice versa. Fast Fourier Transformation (FFT) is the most commonly

used transformation. There are two main uncertainties about the frequency domain method (Knothe & Grassie, 1993):

1- The assumption that steady state solution always exists; however, it has not been determined if it is always true or if stability limit exists close to the critical speeds;
2- The fact that the usage of frequency domain models takes into account the linear behaviour of the model, but there are some nonlinearities in the suggested system;

Other uncertainties about frequency and time domain methods are related to factors that contribute to the irregularities found in practice, such as: defective railpads and fastenings, poorly supported sleepers and the unequal spacing of sleepers.

2.7 Summary

This chapter includes a description of the source of vibration and how vibrations are transmitted in soil layers, in addition to soil behaviour under dynamic moving loads generated by high-speed trains. The ground waves, from surface to body waves, are also explained within the chapter. The transmission of these waves is affected by different interactions between the waves and soil layers. Railway-generated vibrations are caused by the forces induced from the moving train, which is affected by various factors (e.g. discontinuities, surface irregularities of wheels and rail, unwelded rail joints, etc.). Static loading is applied on the track, which is equal to the weight of a stationary train. For a moving train, quasi-static loading results as a combination of static loads and the effects of train speed. The dynamic loading is described as the dynamic forces induced from wheel-rail irregularities, in addition to the static load of the train.

The critical velocity effects include surface wave transmission in addition to amplified vibrations beneath the track, which cause track damages and affect the nearby structures and comfort of passengers. Based on observations from previous research, it is proposed that

there are, in fact, three main factors affecting the ground response: exceeding Rayleigh wave velocity, loading frequency coinciding with natural frequency of the ground and the axial configuration of the train. Modelling aspects, which have been used in previous research for modelling approaches explained in Chapter 3, were briefly introduced in this chapter.

Chapter 3 Literature Review

3.1 Introduction

In order to be able to develop a fully-coupled model and study critical velocity effects, it is essential to review the methods developed by previous researchers for railway tracks. This section firstly looks at different approaches and hybrids used for high-speed tracks including model configurations and adopted assumptions. The modelling approaches include analytical, semi-analytical and numerical methods. Secondly, models developed previously for the Ledsgård site, in Sweden, are reviewed since it represents the main case adopted in this research. Lastly, previous research on dispersion analysis is included as this method is adopted and modified throughout this research.

3.2 Modelling Approaches

3.2.1 Analytical modelling approaches

Different studies have been carried out to predict the behaviour of high-speed trains and compare the outcomes with the actual field results. In order to develop a method to model the track, it is suggested that the behaviour of a moving load as a point load placed on an elastic half-space is identified (Frýba, 1972; Kenney, 1954; Lamb, 1904). Knothe and Grassie (1993) used beam elements to describe the rail, and elastic foundation to describe the track. These assumptions help in investigations of low-frequency track characteristics. The Euler-Bernoulli beam on continuous support was used by Timoshenko (1954); however, since continuous support neglects the effect of sleepers, discontinuous support was introduced by Mead (1970) to model the sleepers, which is useful for higher frequencies. Other researchers (Chen et al., 2001; Suiker et al., 1998) used Timoshenko beams rather than

Euler-Bernoulli beams in order to account for the shear deflections. In terms of foundation modelling, Winkler foundations were used by Auersch (1996), and viscoelastic foundations by Metrikine and Popp (2000). However, elastic half-space foundations produce higher accuracy (Knothe & Wu, 1998), as wave propagation damping and coupling between sleepers cannot be modelled correctly by viscoelastic foundations.

Krylov (1995) and Degrande and Lombaert (2001) used an analytical approach to investigate the train wheel approximated movement to be considered as a dynamic point load. An analytical approach was used to define the track, and Green's function was integrated into the process to calculate the soil response under the track for far field vibrations. These methods took individual sleepers and two soil layers into consideration. Other methods were proposed by Dieterman and Metrikine (1996) and Barros and Luco (1995).

Takemiya and Bian (2005) modelled the rail as a Euler-Bernoulli beam on discrete sleepers, with a spring connection representing railpads. The ground was modelled by a multi-layered half-space. The dynamic interaction between the track and ground was simulated by sub-structuring, where the displacement compatibility and force equilibrium between the structures were met through the mass/spring system. The coupled equations between the beam and soil compliance through the inertia of sleepers and stiffness of railpads were solved in the frequency-wave-number domain by applying the Fourier transform method.

Sheng et al. (2003) and Thompson (2008) modelled the track analytically in the frequency domain, but the soil response was solved as an integral transformation approach. This modelling method is considered to be a semi-analytical approach. A coupled train-track-soil system was developed by Sheng et al. (2004) using receptance methods for the vehicle and track systems, and layered half-space for the soil. These alternative approaches formed more accurate results in comparison with the measured displacements at Ledsgård, Sweden. Xia et al. (2010) followed a similar multibody vehicle and track systems as Sheng et al. (2004), however, Green's functions were used to calculate the response of the ground. Cao et al. (2011) developed a vehicle system by modelling the wheel-rail interaction using Hertzian contact springs. The authors investigated a poroelastic half-space under a moving train in the frequency-wavenumber domain using inverse Fourier transformation. Other semi-analytical approaches were developed by Hussein and Hunt (2007) and Jones (2010). In addition, a

semi-analytical approach was combined with finite element modelling techniques by Triepaischajonsak and Thompson (2015).

3.2.2 Numerical modelling approaches

Moving to numerical modelling of free field vibrations, finite element method is commonly used for numerical modelling for critical velocity investigations. Furthermore, combined methods are used, which are referred to as hybrid models. The Finite Element Method (FEM) is combined with the Boundary Element Method (BEM) to model the wave propagation at large offsets, where BEM uses green functions to calculate the propagation of vibration at large offsets as accurately as possible. Near field vibration and complex track arrangements are handled by the FEM approach, whereas BEM simulates the far field vibration. Structural vibration in the region of the adjacent soil can be challenging to calculate using BEM close to the boundary element regions due to the evaluation of singular integrals on the boundaries. Furthermore, introducing large unsymmetrical matrix formulation between BEM and FEM can demand computational power that is excessive.

Another method used is the scaled boundary finite element method (SBFEM) (Ekevid & Wiberg, 2002), or the finite element thin layer method (FETLM) (Kausel, 1981), which uses a series of horizontal thin layers to overcome the issue of boundary reflection in the frequency domain. This process can decrease the computational run time that can produce efficient boundary absorption during the analysis; therefore, it facilitates modelling approaches. Examples of 2D, 2.5D and 3D numerical methods are described below:

1- 2D numerical methods:

2D models reduce computational requirements compared with 3D models. Balendra et al. (1989) used a plane strain finite element method for vibration transmission investigations. Their study included investigating vibrations traveling from a subway into buildings above. Yang et al. (2009) studied the stress change in ballasted track beds using finite element 2D models in ABAQUS software. It was concluded that stresses caused by dynamic effects

increase significantly when train speed exceeds the Rayleigh wave speed. Other finite element 2D models for critical velocities have been developed by Chahour et al. (2014), Ferrara et al. (2013), and Nsabimana and Jung (2015).

2- 2.5D numerical methods:

In order to decrease the computational requirements, reduction in the track-soil modelling formulation to 2.5D was proposed, whereby the track is considered to be invariant in the direction of the moving train. The track-soil model is two-dimensional, while the excitation is considered to be three-dimensional. Hanazato et al. (1991) used a combination of finite element and extended thin layered element models to study vibrations, while Francois (2012) used a combined finite element and boundary element methods in order to prevent wave reflection at the boundaries. Yang et al. (2003) used a finite element 2.5D model where infinite element solutions were used to terminate the unbounded soil domain. The simulations were run for different train speeds passing on layered soil.

Combined FEM and BEM were developed for 2.5D models by Costa et al. (2012b). The 2D cross section only is required and the track-soil model is considered to be invariant along the track. The coordinates along the track are subjected to Fourier transform to perform a domain transformation. Figure 3.1 shows the coupling of the 2.5D finite element and boundary elements models: the latter is used for the ground. The interaction between the track and soil for pure finite element models is governed by the dynamic equilibrium equation. For this example, the coupling between the FEM track and BEM ground domains is performed by finite element formulation, where the dynamic behaviour of the BEM domain is governed by comprising the transformation of the flexibility matrix into a dynamic stiffness matrix (Costa et al., 2012a). Equivalent linear formulation was proposed by Alves Costa et al. (2010), and it was successfully validated between the measured and predicted outcomes of Ledsgård, Sweden.

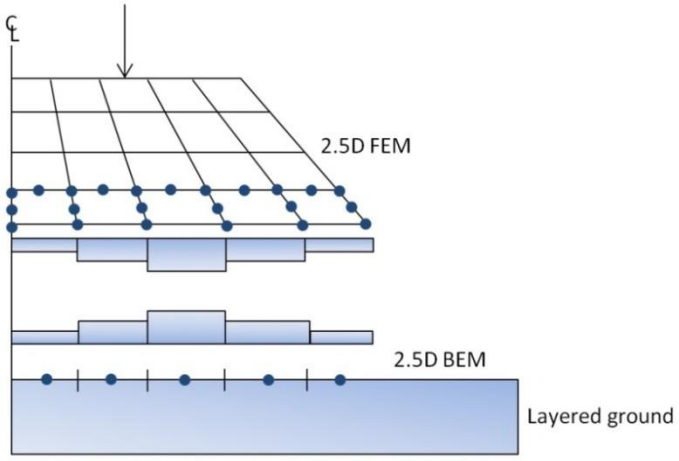

Figure 3.1 2.5D FEM-BEM coupling (Costa et al., 2012b)

3- 3D numerical methods:

Due to the assumption of invariant model properties in one axis for 2.5D models, modelling non-continuous components (e.g. sleepers), buildings or mitigation strategies is not possible. Therefore, 3D models are developed in time and frequency domains for finite element modelling. Using time domain analysis allows the model to implement nonlinear analysis (Paixão et al., 2015), but analysis run times are increased. In order to solve this obstacle, modal sub-structuring was introduced to the element model analysis to contribute to decrease in the number of degrees of freedom and increase efficiency (Arlaud et al., 2014; Ferreira & Lopez-Pita, 2015).

Pure finite element models have the challenge of defining boundary conditions in order to prevent wave reflections within the soil space. Kouroussis et al. (2009) used two techniques: infinite element implementation in ABAQUS software in order to enhance the absorption of waves and, in addition, modelling the soil in spherical domain. Hall (2003) also used ABAQUS to develop a moving load on a 3D track-soil model; however, defining the contact between the wheel and the rail is a challenge in the software, which makes it difficult to simulate dynamic effects. Thus, Kouroussis et al. (2011) suggested sub-modelling in order to account for dynamic excitation: multibody vehicle modelling and soil modelling, separately. First order interaction effects are considered since the two systems are solved independently.

Other 3D approaches used the combination of finite element and boundary element methods (Galvín et al., 2010); however, the soil is defined as 1D since Green's functions were used for the differential equations solutions. Other 3D models were developed by Varandas et al. (2011), Connolly et al. (2013), El Kacimi et al. (2013), and Shih et al. (2014).

Several other examples of variations of models include: the Thin Layer Method (Bian et al., 2016), the discrete element method to analyse ballast settlement at critical speed (Huang & Chrismer, 2013), and combined Finite Element (FE) and Boundary Element (BE) methods (Andersen et al., 2007; Colaço et al., 2016; Galvín et al., 2010), which were developed to remove the necessity of absorbing boundary conditions.

Research was also carried out by Yang et al. (2003), whose study has been implemented to model the finite/infinite element of layered soils under high-speed trains and which took into consideration factors such as damping ratio, shear wave speed and depth of stratum. In the study by Yang et al. (2003), two train speeds were chosen, $c = 100\,m/s$ and $70\,m/s$, to investigate the super-critical and sub-critical ranges. The conclusions verified from the parametric studies:

1- The higher the shear wave speeds of soil, the lower the response of both super-critical and sub-critical conditions, but increasing the damping ratio decreases only the super-critical speeds for dynamic loads with no oscillations.
2- The damping of soil has a significant effect on the degree of attenuation, which occurs at higher frequency values. The response is affected by damping at higher frequencies that attenuates faster than damping at lower frequencies; however, at lower values of damping ratio, a longer distance is required for the full effect of the damping to be observed.
3- Stratum depth plays a major role in vibration propagation, and occurs due to the cut-off frequency. At that point, no waves can infiltrate outwards, and the variation can be observed for different speeds, c, and frequencies, f_o. With higher values of speeds, the cut-off frequency gets closer to approaching that of the plane strain study. For cut-off frequency = 0, the vibration caused by lower values of frequency can be suppressed by the bedrock layer.

4- For soil layers with $f_o = 0$, the critical speed of the train at locus near the source can be verified from the speed of the Rayleigh wave of the top layer of the soil, but the locations in a long distance from the source have maximum response at higher speeds.
5- The transfer function becomes more complicated when both cut-off frequency and frequencies of multi-layers are considered, which results in variation from case to case. It is hard to predict the outcomes of each case; however, field experiment or accurate numerical analysis can be a useful asset in finding a reasonable model, taking into account variation in soil properties.

3.2.3 Vehicle modelling and vehicle/track interaction

The track is subjected to a wide diversity of loads applied by the vehicle system. As mentioned previously, dynamic load points representing the axle loads have been used in different models (e.g. Krylov (1995)). For more accurate representation of the vehicle, a system of masses (car, bogie and wheel) and springs/dampers (primary and secondary suspensions) was used in previous work (e.g. El Kacimi et al. (2013)). However, the mentioned approaches do not take into account lateral forces exerted on the rail. In order to analyse the dynamic behaviour accurately between the vehicle components in interaction with the rail, complex 3D multibody formulations were used (e.g. Pombo and Ambrósio (2004)).

Different factors affect the vehicle/track interaction, including the nonlinearities of the interaction, location of actual contact points, dynamic loading etc. Previous work used theoretical transfer functions to relate the parameters of the vehicle and the track. A method was developed by Mauer (1995) using inverse transfer function of track recording vehicles in order to determine track irregularities. Using a mass/spring damper, transfer functions between the wheels and car body acceleration were used by Esveld (2001).

The most commonly applied method for the normal contact problem is the Hertz theory (Hills et al., 1993); however, other methods, for example the Boussinesq theory (Remington & Webb, 1996), allow characterisation of stress distribution on the contact surface. Different

studies addressed nonlinear creep forces between the wheel and rail (e.g. Scheffel et al. (1994)) and the nonlinear response of a wheelset to lateral rail irregularities (e.g. Law (1974)). Kalker's programs (CONTACT or FASTSIM) were used for tangential contact problems (Knothe & Grassie, 1993). A study by Pombo and Ambrósio (2008) implemented parameterisation methodology for track geometry, including irregularities, and parameterisation for wheel and rail surfaces, in addition to the calculation of normal and tangential contact forces. Other methods, which consider rail irregularities, were presented by Wu and Thompson (2001) and Clark et al. (1982).

3.3 Previous Research related to Ledsgård, Sweden

The Ledsgård site has experienced high vibrations since the opening of the X2000 train service (Holm et al., 2002). The train line connects Gothenburg and Malmo, and has a maximum operational speed of approximately $200\ km/h$. It has $50\ m$ deep weak clay soil with low shear wave velocity and critical velocity effects have clearly been observed. Seismic tests were performed on this site to obtain ground response, which makes it suitable for research purposes. A study was carried out by Madshus and Kaynia (2000) who used the VibTrain computer program to model the Ledsgård track. Green's functions were used to define the ground system and the rail system was defined by beam with infinite elements.

The authors predicted the ground response for a speed of $70\ m/s$, which is greater than the actual speed of the X2000. Madshus and Kaynia (2000) observed the large dynamic amplifications that arose due to the rail/embankment/ground system responses, which occur as a result of a train passing at speed close to the critical value. The study clarified that the dispersion curve of the first Rayleigh mode is the controlling factor in the critical speed; nevertheless, the embankment profile at the site and the load distances of the train can also play a big role in such a case. The degrees of coincidence between the wavelengths for the site and load distances are major factors in the degree of dynamic amplification. The dynamic amplitudes can change with the changing speed of the train, unlike the quasi-static

amplitudes, and it is shown that dynamic amplitudes can increase significantly with the approach of critical values of speed (Madshus & Kaynia, 2000).

The results are presented in Figure 3.2 in comparison with a calibration study carried out at Heriot-Watt University using DART3D software and developed by Woodward et al. (2013). There is good agreement about the overall shape between both studies and field results for various speeds; however, it is noted that there is a significant difference between peak values that remains to be investigated. It is suggested that the amplitude is highly affected by the loading frequency. In the calibration study of DART3D for speed $45\ m/s$, good agreement of the nonlinear analysis values met the field results. The Mach cone starts to form at this speed. For $51\ m/s$ speed, a linear analysis with constant stiffness was simulated. The response resulted in a lower value at the end and damped the oscillation at the tail, which was assumed to be due to the length of the mesh and the effects of viscous boundaries. Another nonlinear analysis run for the same speed of $51\ m/s$ produced a good approximation response to the field results. It is better to adapt a nonlinear analysis, since plasticity and pore water pressure are generated when the train moves at a high speed (Madshus & Kaynia, 2000; Madshus et al., 2004; Woodward et al., 2013).

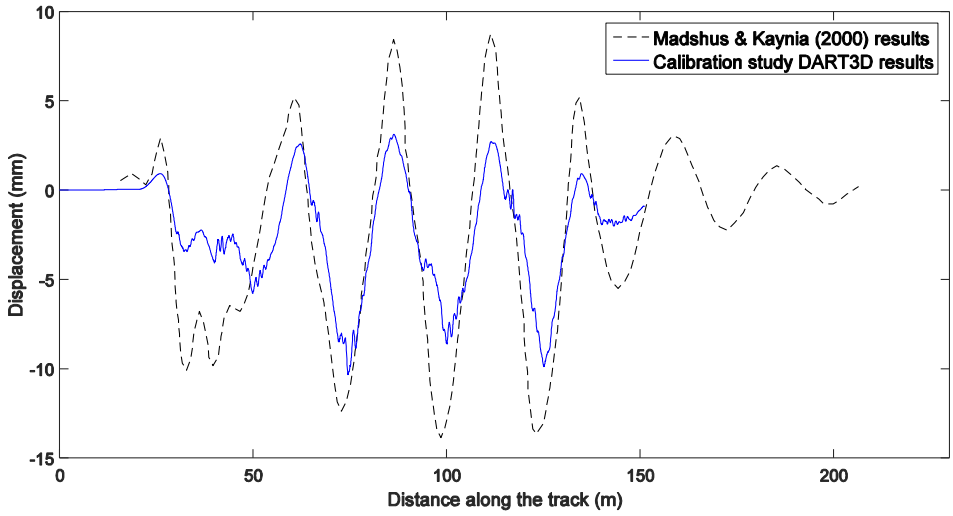

Figure 3.2 Vertical displacement response (speed $70\ m/s$) (Madshus & Kaynia, 2000)

In addition to nonlinearity, other factors also affect the response, such as axial loading. For the X-2000 train, Kaynia et al. (2000) carried out a study running an analysis for the southbound train and the northbound train. There was a notable difference in response between both runs. Kaynia et al. (2000) suggest that the axial loading sequence changes the magnitudes and pattern of the response. Due to different axial configurations between the front and rear cars in the train, the initiated Mach cone is different and; thus, influences the effects in the ground. In addition to axial loading, railpads have an effect on the response. Railpads absorb a segment of rail vibrations; therefore, they reduce the stiffness of the upper part of the track and allow the rail elements to rotate more flexibly without damaging the sleepers (Kouroussis et al., 2014).

Moreover, for the X-2000 train, Madshus and Kaynia (2000) present their findings in a frequency-wavenumber domain, $R(\omega, k)$, rather than the time domain, using the following equation:

$$R(\omega, k) = H(\omega, k) \cdot P(\omega, k) \tag{3. 1}$$

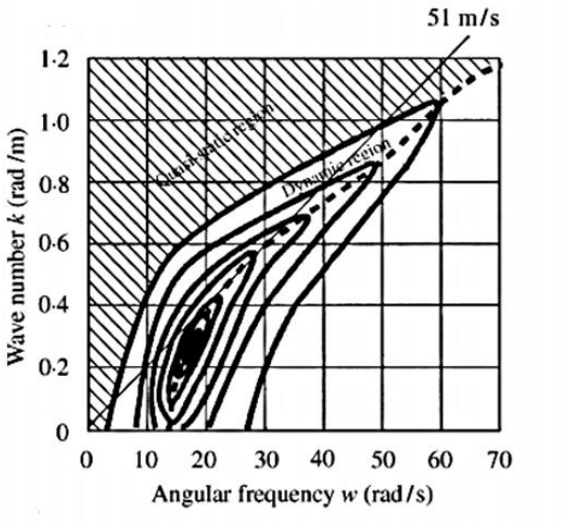

a) Dynamic transfer function

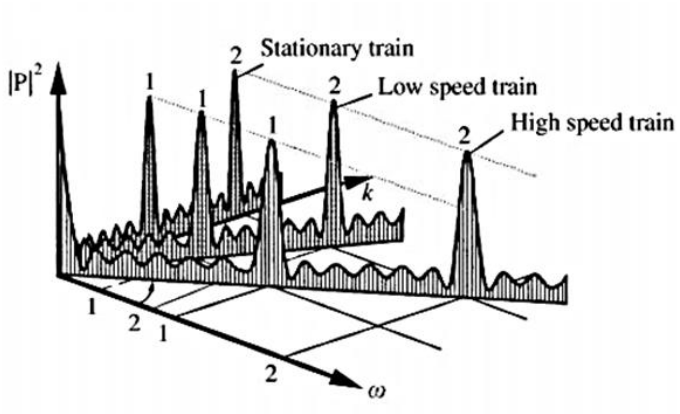

b) Excitation function of the train load

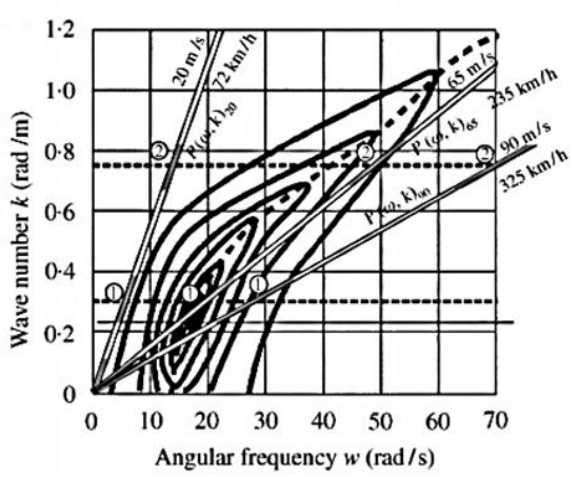

c) Response in frequency-wavenumber domain

Figure 3.3 Response calculations in the frequency-wavenumber domain (Madshus & Kaynia, 2000)

where $H(\omega, k)$ is a dynamic transfer function and $P(\omega, k)$ is the excitation function of the train load. Figure 3.3 (a) represents $H(\omega, k)$, which shows the highest dynamic amplification at the dotted line (peak in (ω, k)). The steepest tangent line of the curve represents the slowest Rayleigh wave, which has a velocity of $51\ m/s$. The hatched region characterises the quasi-static region where no waves are forming. Moving to Figure 3.3 (b), which shows $P(\omega, k)$ in a three-dimensional plot of different speeds ($20, 65$ and $90\ m/s$). The peaks in the function relate to wavelengths equal to the distances between the main loads. These values are projected onto the (ω, k) plane in Figure 3.3 (c), which shows the response

$R(\omega, k)$. The peaks of speed $65\ m/s$ are located in the dynamic region of the plane, where the highest amplification occurs. Based on these outcomes, Madshus and Kaynia (2000) state that the lowest Rayleigh velocity, $51\ m/s$, is not the critical speed, since there is no coincidence between the peaks of $H(\omega, k)$ and $P(\omega, k)$, while coincidence occurs for the speed $65\ m/s$ (Madshus & Kaynia, 2000). Krylov et al. (2000) confirm that there are two main critical velocities: the Rayleigh surface wave velocity and the minimum phase velocity when bending waves start to propagate in the track. He described the second velocity as the critical velocity.

3.4 Dispersion Analysis

One of the objectives of this research is to facilitate the dispersion analysis in calculating critical velocity of high-speed rail lines, which is carried out in Chapter 4; thus, this section includes previous research on dispersion analysis application for track-soil systems. Soil layers have different dispersion characteristics, which are related to speed and frequency of wave propagation in a system. Free vibration properties help to determine the vibrations in the ground. Dispersion diagrams are a suitable tool for analysing ground wave propagation modes as a frequency function. The normalisation of each response for each frequency was implemented to the highest value at a certain frequency, as suggested by Triepaischajonsak et al. (2011), which created a clear verification of the recognised wavenumbers. For layered soil configuration, the outcomes demonstrate that the high frequency content follows the features of the upper layer of the soil. However, the lower frequencies are connected to the substratum, which gives an indication of the oscillation frequency of the soil surface (Kouroussis et al., 2014). Tests can be performed on existing sites to determine the dispersion curve, for example: multichannel analysis of surface wave (MASW) test. In addition, this can be calculated numerically by using the existing geotechnical data (SPT) and converting them into elastodynamic material properties (Connolly et al., 2014).

The dispersion curves of the soil can be modelled using the Thompson-Haskell approach. Sheng et al. (2003) looked at dispersion curves for the soil and compared them against

moving load curves in order to determine the critical velocity of the system. The authors also looked at dispersion relations for multi-layered ground. The modes of the ground describe the free propagating waves in the horizontal direction of the train passage direction, and there are two types: P-SV and SH modes. For the SH modes, the particles only vibrate in a direction parallel to the ground surface, which is perpendicular to the direction of horizontal propagation. For the P-SV modes, particles move vertically and horizontally in the propagation direction (Sheng et al., 2003). The formulation of dispersion curves for multi-layered soil over half-space is described by Jones (1987) and Sheng (2001)

Costa et al. (2015) came up with a simplified approach that investigated the relationship between the dispersion of the soil and the track. They also developed a simple model for track-embankment-ground systems. The track dispersion was calculated analytically and soil dispersion was modelled using the Thompson-Haskell approach. The validation was carried out using the 2.5D numerical model developed by Costa et al. (2012b). Post-processing is required to obtain the critical velocity following the wavenumber-frequency domain transformation. This simplified method has been proven to give accurate results.

The phase velocity of Rayleigh waves, which is the speed of propagation of waves, is frequency-dependent in vertically heterogeneous media. An example presented by Foti et al. (2014) for two layers over half-space, shows vertical particle motion with frequency (Figure 3.4 (a)) in order to explain that the dispersion curve is affected by the variation of parameters of medium with depth. For high frequency, the particle motion occurs in the first layer, which indicates that Rayleigh wave velocity is controlled by the properties of the upper layer. The particle motion extends for three layers for low frequency, indicating that the Rayleigh wave velocity is affected by a combination of the properties of all three layers. Assuming the stiffness increases with depth for the three layers (the shear wave velocity is the lowest for the upper layer), for high frequency (short wavelength), the propagation velocity of the Rayleigh wave is slightly lower than the shear velocity of the upper layer, while for low frequency (long wavelength), it has a higher velocity since it is affected by the underlying stiffer layers. Figure 3.4 (b) shows the phase velocity plotted against wavelength. Due to the relationship between wavenumber and frequency, the dispersion curve is then displayed in Figure 3.4 (c) between the phase velocity and the frequency. For vertically inhomogeneous

dispersive media, the propagation speed of the Rayleigh waves generated by harmonic sources is known as the "apparent" or "effective" phase velocity (Foti, 2000). The superposition of different Rayleigh propagation modes creates a waveform, and the apparent phase velocity is the propagation speed of this waveform. This understanding was the inspiration for modelling the track-soil systems for velocity-frequency dispersion curves that allow the critical velocity to be determined immediately from the figure. The method for calculating apparent velocities by Foti et al. (2014) is discussed in Chapter 4.

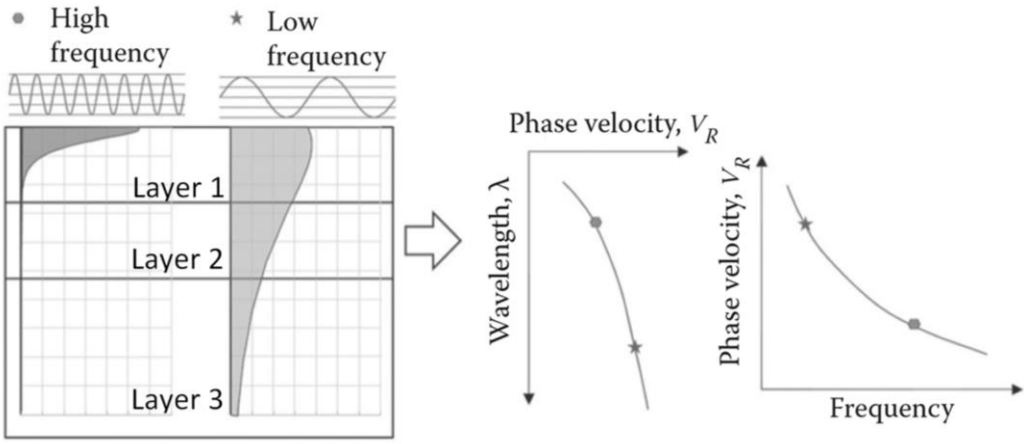

(a) (b) (c)

Figure 3.4 Geometric dispersion of Rayleigh waves: (a) vertical particle motion with depth for high and low frequencies, (b) phase velocity plot against the wavelength, and (c) dispersion curve (Foti et al., 2014)

Auersch (2005) discussed detailed and simplified methods to plot the dispersion in terms of velocities against the frequencies of the soil. Another approximated method for homogeneous half space known as the "Dispersal Soil Method" is explained in this section, which calculates the vibrations of the ground (Auersch, 2005). Dispersion curves of single and multi-layered soil tracks were studied for different shear wave speeds. The exact approach for obtaining dispersion curves is calculated according to the wavenumber and the frequency using the Thompson-Haskell approach (Sheng, 2001).

The following figures (Figure 3.5 and Figure 3.6) show the dispersion curves for multi-layered soil using the Thompson-Haskell approach presented in 2D image. The apparent velocities are presented in dashed curves as shown in the figures, for two layers and three layers, respectively, to create a simpler way of presenting the plots in linear format. For two-layered soil, the change in speed happens at frequency (20 Hz), while for three-layered soil, it happens at two frequencies (20 Hz and 50 Hz) (Auersch, 2005). For the first figure (Figure 3.5), a soft layer (100 m/s) is on top of a stiff layer (200 m/s); similarly in the second figure (Figure 3.6), the stiffness increases with depth. The figures show that the wave speed reduces at higher frequencies.

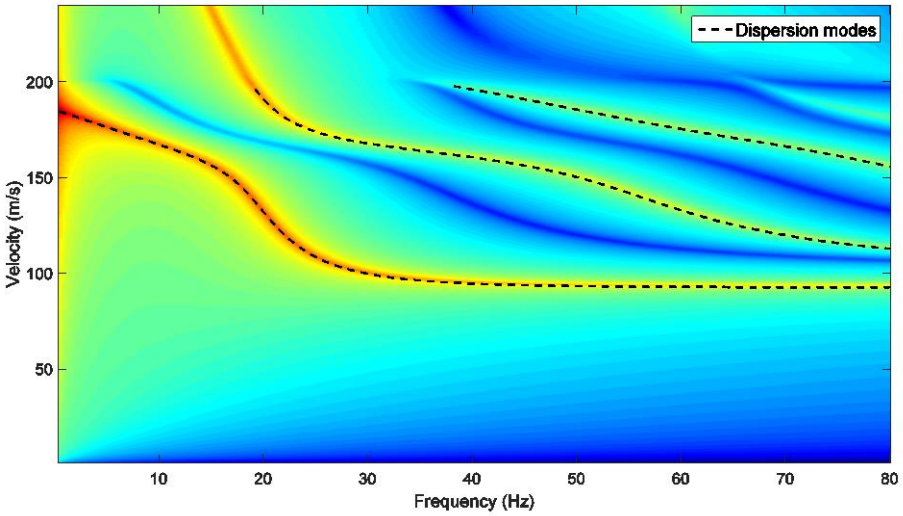

Figure 3.5 Dispersion curves (2 layers) $(100, 200\ m/s)$

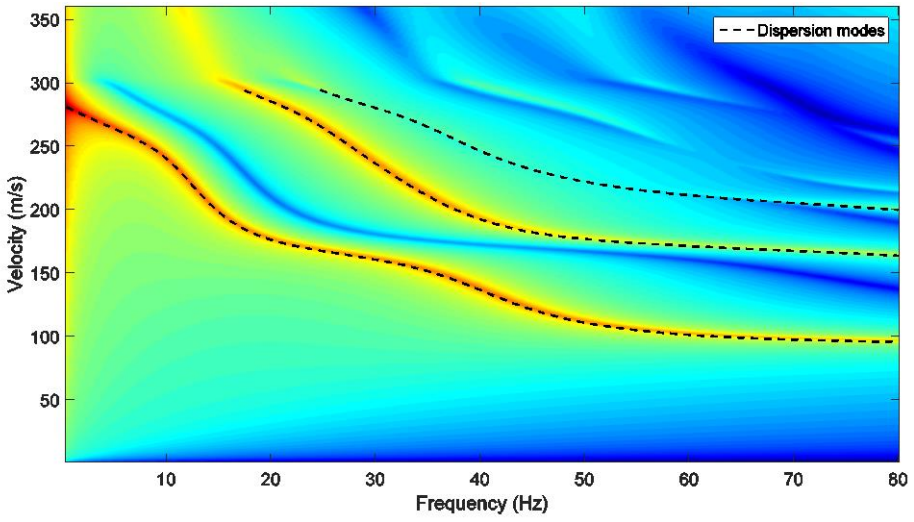

Figure 3.6 Dispersion curves (3 layers) $(100, 200, 300\ m/s)$

1- Approximated method of calculating velocity-frequency dispersion curves

Approximated formulae are derived to calculate the speeds by Auersch (2005) as shown below for two layers (Equation 3.2) and multi-layers (Equation 3.3), respectively:

$$V(f) = V_1 + (V_2 - V_1)0.5(1 + cos\frac{\pi}{2}\frac{f}{f_1}) \tag{3.2}$$

$$V(f) = V_1 + \sum_{i=1}^{n-1}(V_{i+1} - V_i)0.5(1 + cos\frac{\pi}{2}\frac{f}{f_i}), \quad \text{with } f_i = \frac{V_i}{3h_i} \tag{3.3}$$

i corresponds to the layer. The approximated method is then compared to the dispersion plot using apparent velocity, which is explained in Section 4.2.2 of Chapter 4 (Figure 3.7).

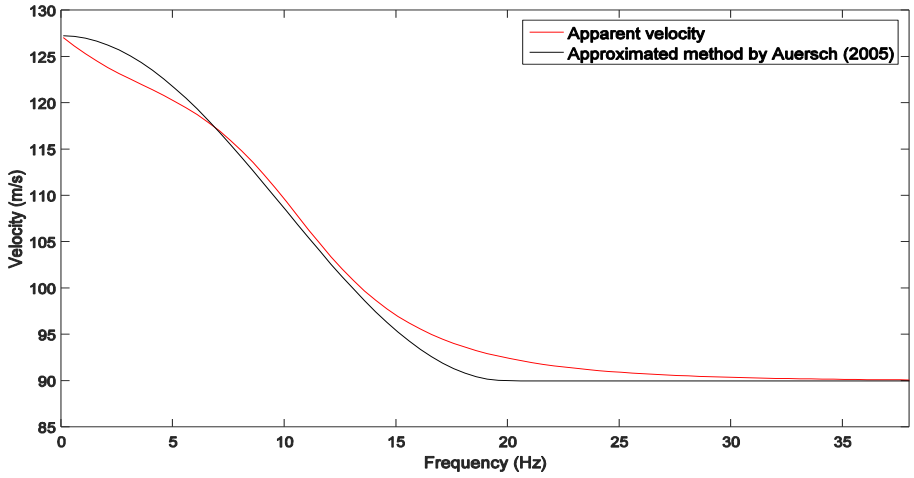

Figure 3.7 Apparent velocity and approximated method of soil with two layers (Auersch, 2005)

2- Approximated Dispersal Soil Method

Another approach is approximated for the homogeneous half-space where G is the shear modulus, r is the distance from the vibration source, v is the Poisson's ratio, and $r_0^*$is the beginning of the far field. To obtain the dispersion in frequency-speed plot, the velocities are calculated as follows:

$$V(r,f) = \frac{P\omega}{2\pi G r}\begin{cases} 1-v & r^* \le r_0^* \\ \sqrt{\frac{r^*}{r_0^*}} & r^* > r_0^* \end{cases} \tag{3.4}$$

$$r^* = \frac{\omega r}{V_s} \tag{3.5}$$

The far field, which is dominated by the Rayleigh waves attenuates with $r^{-0.5}$ and the near field attenuates with r^{-1}. However, the effects of resonance and other modifications need to be added to this method in order to consider inhomogeneous soil (Auersch, 2005).

3.5 Summary

Modelling aspects carried out by previous researchers are described in this chapter from analytical to numerical approaches, mainly those relevant to the adopted case of the Swedish track for the X2000 train. The following approaches are summarised, and they assisted in choosing the methods for developing the models carried out in this research.

Different analytical and semi-analytical methods assumptions are discussed for rail, track and soil models, in addition to train models. Rail elements can be modelled as beam elements (Timoshenko or Euler-Bernoulli beams), while sleepers can be modelled as continuous or discrete elements. Different types of foundations were tested in previous research (e.g. elastic and viscoelastic foundations). When soil vibrations are of interest, modelling approaches have been developed to account for multi-layered soil over half-space, applying different methods to avoid wave reflections within the soil model. Green's functions were included in the methods applied to calculate the ground response, which could also be calculated numerically, as in semi-analytical methods (e.g. with FETLM). Lumped mass vehicle systems were developed, instead of applying vertical point loads for more accurate representation of the train-track-soil system. The forces generated from wheel-rail interaction have an effect on the induced vibrations; thus, the interaction forces have been considered in previous research.

For a numerical tool, FEM is the most commonly adopted method for modelling railway tracks. The method can be coupled with other modelling approaches (e.g. BEM). Previous research has been developed in ABAQUS software, and validated by previous researchers (e.g. Hall (2000)). Numerical 2D models were developed, as they reduce computational requirements compared to 3D models. Alternatively, 2.5D models were developed assuming the track is invariant in the direction of train passage. However, in order to model non-continuous components (e.g. sleepers), buildings or mitigation strategies, 3D models were used in previous research.

The case of the X2000 train, in Sweden, is adopted, due to the availability of test results before and after the ground stabilisation was applied to the site. Previous research was devoted to calculate the response in time domain of the Swedish site using different tools

(e.g. VibTrain, DART3D, etc.), and the results were compared to actual field results. Further analysis was carried out for the response in frequency-wavenumber domain including the dynamic transfer function and excitation function in order to investigate critical velocity effects at Ledsgård.

In addition, the dispersion analysis is covered in this chapter as it was used in previous research to determine critical velocity values, which can be used for quick investigations on a particular site with known ground parameters. Previous work was devoted to creating dispersion curves for full train-track-soil systems (e.g. Costa et al. (2015)). Further research is needed to improve the dispersion analysis to eliminate post-processing procedures. From previous discussion points, the thesis aims to produce several new methods that are capable of predicting critical velocities and their effects, in order to test different properties and mitigation strategies and develop better understanding of ground behaviour.

Chapter 4 Dispersion Analysis

4.1 Introduction

This chapter presents an analytical approach for predicting critical velocities. Dispersion properties of a structure are related to the speed and frequency of waves propagating within it. The higher wave lengths of the Rayleigh waves travel to the lower layers of the soil with different properties and at variable speeds causing dispersion (Kramer, 1996; Kumar et al., 2006). In this chapter, the dispersion curves have been produced from the function of frequency and wave velocity rather than the function of wavenumber and frequency as discussed earlier in Chapter 3. This resulted in a direct reading of the speed without the need for post-processing.

This chapter clarifies the simplified method that was used in this research by developing a fully analytical approach using a code on MATLAB that presents the dispersion curves of the track and the soil layers showing the wave speed against the frequency. The method includes the track and soil as an uncoupled system even if, in reality, they are coupled, due to the different dispersion relations between both systems (Kouroussis et al., 2015). The validation section includes the soil model validation, using the Thompson-Haskell approach, and critical velocity validation, using a numerical approach carried out by Costa et al. (2015). Finally, soil profiles were created using sensitivity analysis to study the effects of different track/soil parameters on critical velocities.

4.2 Simplified Approach of Track-Ground Systems

This method follows the dispersion analysis of uncoupled systems: the track, which could be a ballasted or slab track, and the layered ground underneath. It allows for the prediction of

critical velocities of higher modes of soil with different depths. The model is entirely analytical, and this means it was not necessary to model a train system. It can be applied to either new or existing sites by using a drop-weight test, multi-channel analysis, or collecting geotechnical data from SPT, etc. (Connolly et al., 2014). However, for this chapter, the material properties of the soil have been based on assumptions.

The wave speed was calculated automatically, a method which does not require any post-processing, to obtain the dispersion curves. The following Figure 4.1 shows the dispersion curves calculated in the wavenumber and velocity domains, respectively. For the wavenumber domain, Figure 4.1 (a), the velocity was obtained by calculating the gradient of a straight line connecting the origin and the intersection point between the track and soil dispersion curves, while, for the velocity domain, Figure 4.1 (b), the wave speed can be read directly from the y-axis point of the intersection without the need to calculate the gradient.

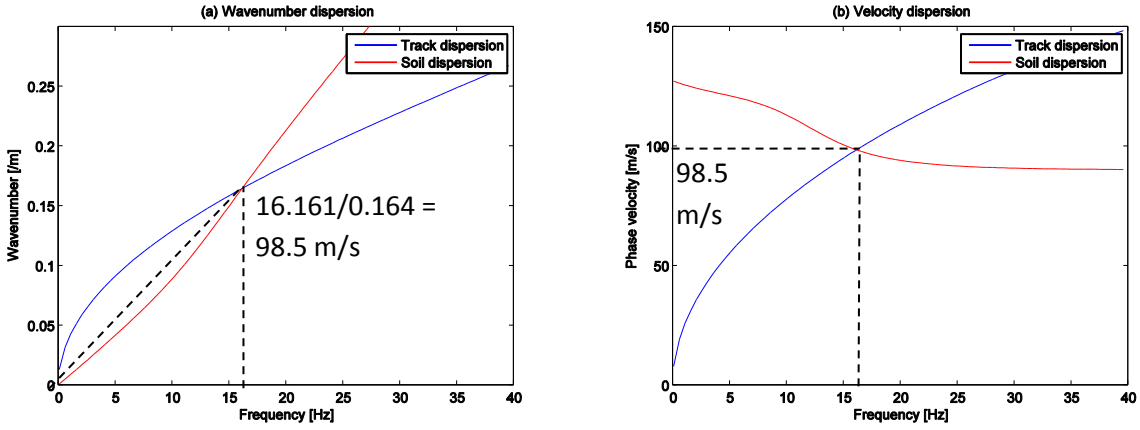

Figure 4.1 a) Wavenumber and b) velocity dispersion relations

4.2.1 Track model development

The track was assumed to be infinite and two-dimensional to allow for calculation of the dispersion in the wavenumber domain. It was also assumed that the track does not change in the direction of train passage (Zou et al., 2015). Figure 4.2 shows the components of a

typical ballasted track, thus the equation is as shown below (Equation 4.1) (Costa et al., 2015), where k_1 is the wavenumber, m_r and m_s are the mass of rail per metre and the equivalent distributed mass of the sleepers, respectively, k_p^* is the stiffness of the railpad including damping, V_b is the ballast compression wave speed, E_b is the ballast Young's modulus, h_b is the ballast height, $2b$ is the track width and u_r, u_s and u_b refer to rail displacement, sleeper displacement, and ballast displacement in the lower boundary respectively:

$$\begin{bmatrix} EI_r k_1^4 + k_P^* - \omega^2 m_r & -k_P^* & 0 \\ -k_P^* & k_P^* + \frac{2\omega E_b^* b\alpha}{\tan\left(\frac{\omega h_b}{V_b}\right)V_b} - \omega^2 m_s & \frac{-2\omega E_b^* b\alpha}{\sin\left(\frac{\omega h_b}{V_b}\right)V_b} \\ 0 & \frac{-2\omega E_b^* b\alpha}{\sin\left(\frac{\omega h_b}{V_b}\right)V_b} & \frac{-2\omega E_b^* b\alpha}{\tan\left(\frac{\omega h_b}{V_b}\right)V_b} + k_{eq} \end{bmatrix} \times \begin{Bmatrix} \tilde{u}_r(k_1,\omega) \\ \tilde{u}_s(k_1,\omega) \\ \tilde{u}_{bb}(k_1,\omega) \end{Bmatrix} = \begin{Bmatrix} \tilde{P}(k_1,\omega) \\ 0 \\ 0 \end{Bmatrix} \quad (4.1)$$

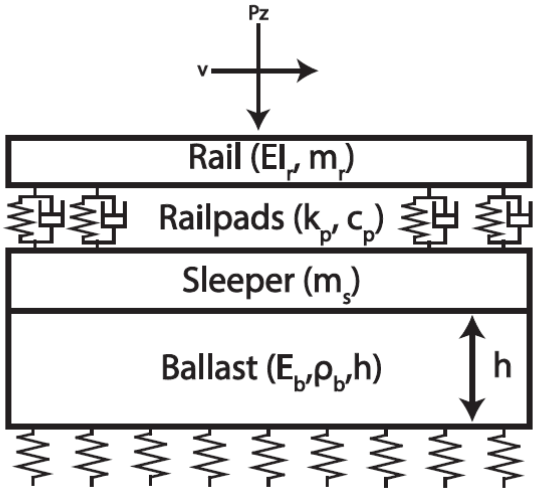

Figure 4.2 Ballast track model

And the system equation for the slab is shown below, where EI_s is the slab bending stiffness:

$$\begin{bmatrix} EI_r k_1^4 + k_P^* - \omega^2 m_r & -k_P^* \\ -k_P^* & EI_s k_1^4 + k_P^* - \omega^2 m_s \end{bmatrix} \times \begin{Bmatrix} \tilde{u}_r(k_1,\omega) \\ \tilde{u}_l(k_1,\omega) \end{Bmatrix} = \begin{Bmatrix} \tilde{P}(k_1,\omega) \\ 0 \end{Bmatrix} \tag{4.2}$$

$$k_{eq}(k_1,\omega) = \frac{2\pi}{\int_{-\infty}^{+\infty} \tilde{u}_{zz}^G(k_1,k_2,0,\omega)\left(\frac{sin(k_2 b)^2}{(k_2 b)^2}\right)dk_2} \tag{4.3}$$

To represent the stiffness from the underlying layer, a spring foundation was considered (k_{eq}) as shown in Figure 4.2 and Figure 4.3 (Steenbergen & Metrikine, 2007), where k_2 is the Fourier image of coordinate y and $\tilde{u}_{zz}^G$ is the wavenumber-frequency Greens function of the vertical displacement of the ground. If the difference between the ballast and soil is high, the inclusion of the spring foundation stiffness increases accuracy, otherwise, it has minimal effect on critical velocities (Kouroussis et al., 2011; Verbraken et al., 2011). The equivalent stiffness of the foundation (Equation (4.3)) was not included in this model; however, it was added to the system in the semi-analytical model in Chapter 5. Then the dispersion response is calculated by computing the determinant of the stiffness matrix.

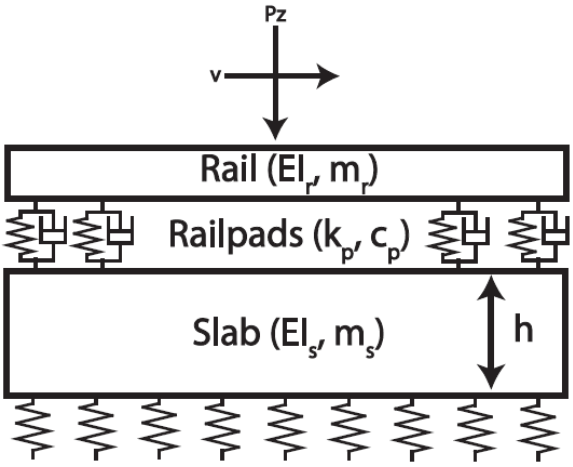

Figure 4.3 Slab track model

4.2.2 Soil model development

The soil dispersion curve was calculated in the wavenumber domain (Foti et al., 2014). As mentioned earlier, integration post-processing was used to produce the two-dimensional dispersion. The response was obtained for a point on a three-dimensional surface exactly at the excitation point ($0\,m$ distance). Note that all the soil layers were assumed to be horizontal. Equation (4.4) is used to calculate the apparent phase velocity V_{app} (individual modal velocity contribution) (Foti et al., 2014), where r is the distance of the receiver from the excitation source, x is the depth of the receiver, M is the number of modes, V_{RP} is the phase velocity, U_r is group velocity, r_1 and r_2 are the displacement eigenfunction, and I_R is the first Rayleigh energy integral:

$$V_{app}(r,x,\omega) = \frac{2\omega \sum_{i=1}^{M}\sum_{j=1}^{M}\left\{\frac{r_2(x,k_i,\omega)r_2(x,k_j,\omega)r_2(0,k_i,\omega)r_2(0,k_j,\omega)\cos[r(k_i-k_j)]}{[(V_{RP})_i(U_R)_i(I_R)_i][(V_{RP})_j(U_R)_j(I_R)_j]\sqrt{k_i k_j}}\right\}}{\sum_{n=1}^{M}\sum_{m=1}^{M}\left\{\frac{r_2(x,k_n,\omega)r_2(x,k_m,\omega)r_2(0,k_n,\omega)r_2(0,k_m,\omega)(k_n+k_m)\cos[r(k_n-k_m)]}{[(V_{RP})_n(U_R)_n(I_R)_n][(V_{RP})_m(U_R)_m(I_R)_m]\sqrt{k_n k_m}}\right\}} \tag{4.4}$$

$$(I_R)_j = \frac{1}{2}\int_0^{\infty}\rho(x)\left[(r_1^2)_j + (r_2^2)_j\right]dx, \qquad j = 1, M \tag{4.5}$$

$$\begin{cases} r_1(x) = \frac{V_R s B_4}{\omega(1-\frac{V_R^2}{2V_S^2})}\left[e^{-r_* x} - (1-\frac{V_R^2}{2V_S^2})e^{-sx}\right] \\ r_2(x) = \frac{V_R^2 r_* s B_4}{\omega^2(1-\frac{V_R^2}{2V_S^2})}\left[(1-\frac{V_R^2}{2V_S^2})^{-1}e^{-sx} - e^{-r_* x}\right] \end{cases} \tag{4.6}$$

where r and s are parameters depending on wavenumber, frequency and wave speeds: $r_*^2 = k^2 - \frac{\omega^2}{V_P^2}$ and $s^2 = k^2 - \frac{\omega^2}{V_S^2}$.

Since the primary mode is more dominant than the higher modes, the number of modes, M was chosen to be 1. The first Rayleigh energy integral and displacement eigenfunction were calculated from Equations (4.5) and (4.6) (Foti et al., 2014). The constant B_4 was determined from the boundary stress-free conditions at the surface of the half-space as x approaches infinity. The phase velocity is the speed of single wave propagation, and the group velocity is the velocity of the group of waves, as shown below:

$$V_{RP} = \frac{\omega}{k} \tag{4.7}$$

$$U_R = \frac{\partial \omega}{\partial k} \tag{4.8}$$

The apparent Rayleigh phase velocity required more calculations than the track; therefore, to increase efficiency, the phase velocity was reduced by optimising the frequency range so that the calculations were performed at a certain cut-off frequency. As shown in Figure 4.4 and Figure 4.5, the dispersion curve is constant after a certain point at the higher frequencies (at $35\ Hz$ and $25\ Hz$, respectively). The phase velocity remains constant because higher frequency energy is unable to propagate deep into the soil: it is confined near the surface. Hence, the velocity after this point was assumed to be similar to the phase velocity of the upper layer since the higher frequency response is governed by the top layer. This helped to reduce the run time; nevertheless, this optimisation needs further investigation. The following formula was used to calculate the cut-off frequency, where V_{s1} is the shear wave speed of the top layer, H_1 is the height of the layer, and μ is the cutoff factor taken as 1 (Auersch, 2014).

$$\omega_{cut-off} = \mu \left(\frac{V_{s_1}}{H_1}\right) \tag{4.9}$$

The results, shown in Figure 4.4, are an example of the cut-off frequency implementation. As a limitation, it was difficult to test the efficiency increase since the frequency range was chosen based on an arbitrary upper limit.

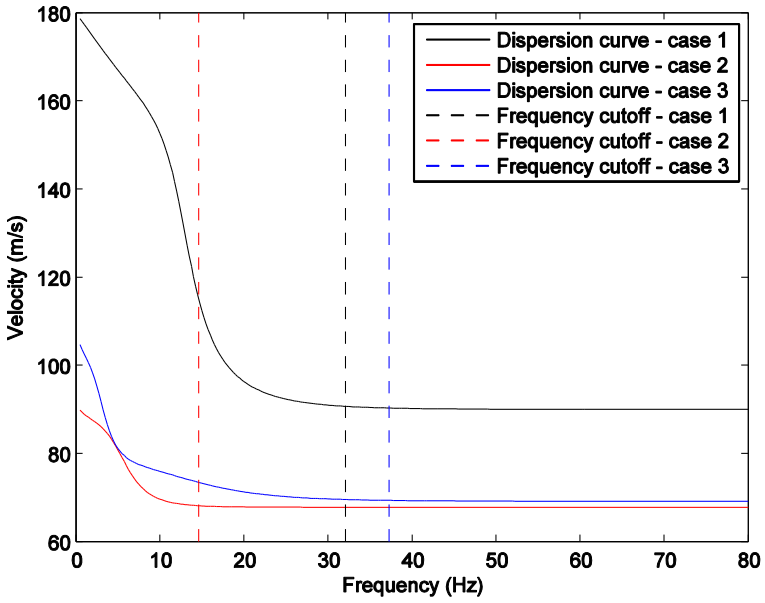

Figure 4.4 Optimisation of frequency cut-off

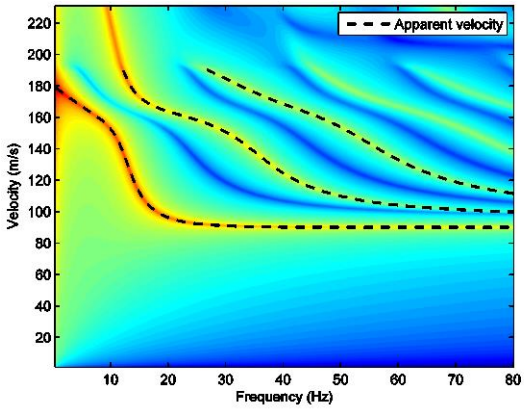

a) Profile 1

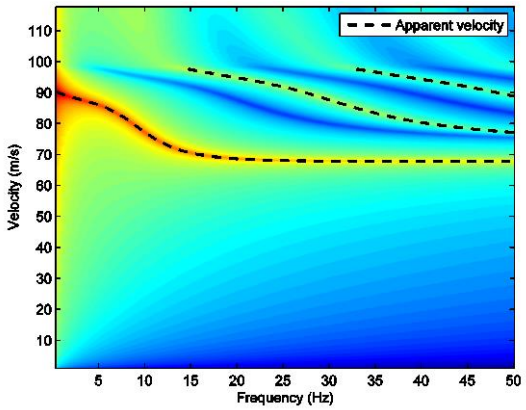

b) Profile 2

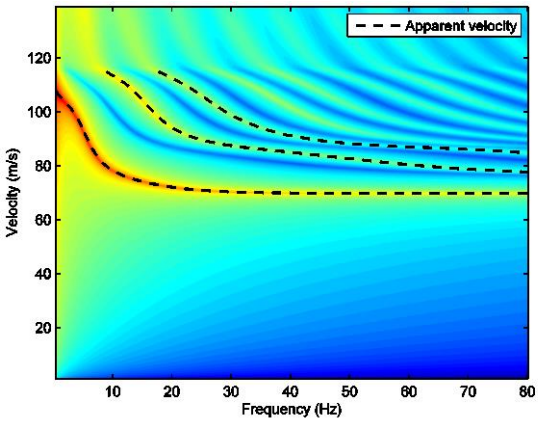

c) Profile 3

Figure 4.5 Apparent dispersion curve comparison

4.3 Validation of Simplified Approach

The dispersion of the soil was validated by comparing the apparent velocity calculations with 2D image produced by the Thompson-Haskell approach, while the critical velocities were compared to the values obtained from a numerical method carried out by Costa et al. (2015). The Dynamic Amplification Factory (DAF) curves were calculated from both methods and compared for track and slab systems.

4.3.1 Soil model validation

Three soil profiles were created to validate the analytical code as shown in Figure 4.6, where the first two consisted of a homogeneous half-space underlying an upper layer, and the third profile had two upper layers.

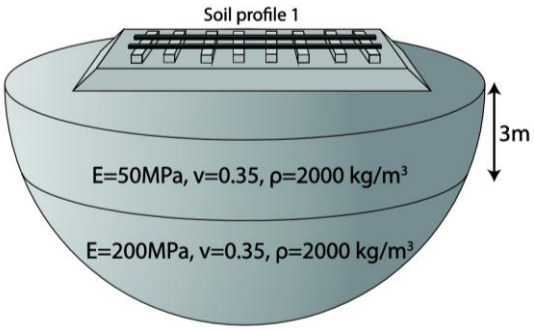

a) Profile 1

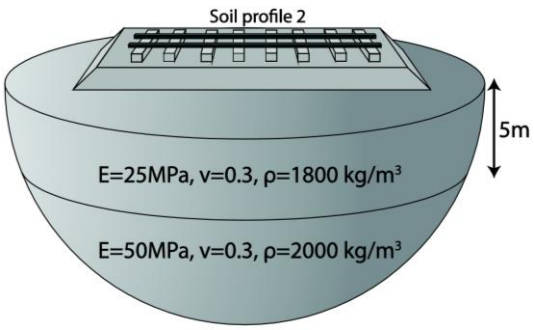

b) Profile 2

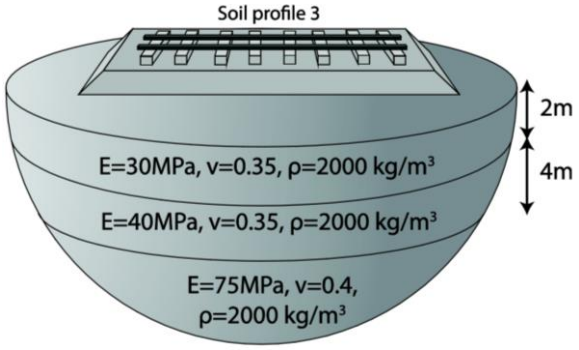

c) Profile 3

Figure 4.6 Soil profiles

The 2D image dispersion curve was calculated using the Thompson-Haskell approach for the first three modes as shown in Figure 4.5 for soil Profiles 1, 2 and 3 (Sheng et al., 1999). The figures also show the dispersion curve calculated using the analytical approach in comparison with Thompson-Haskell dispersion results. There is good agreement between the two approaches. In addition, the analytical code is able to take any layer height into consideration, while Thompson-Haskell is not suitable for modelling thick soil layers (Liu, 2010). Post-processing was not necessary for extracting the primary mode at each frequency when calculating the apparent velocity, since it was performed analytically. Nonetheless, the apparent velocity approach is only applicable for normally dispersive media, while numerical methods are also used for inversely dispersive media.

4.3.2 Validation of Critical velocity calculations

Using each of the soil profiles in Figure 4.6, the critical velocity was calculated for a ballasted track and two slab tracks with different heights (Slab 1, $h = 0.3\,m$ and Slab 2, $h = 0.45\,m$). Table 4.1 shows the properties of the tracks. Since experimental data is not available for critical velocities, a numerical solution, which was previously validated, was used (Costa et al., 2015).

Component	Property	Ballasted track	Slab track	Description
Rail	EI_r	12.9	12.9	Bending stiffness (MNm^2)
	m_r	120	120	Mass (kg/m)
Railpad	k_P	500	500	Stiffness (MN/m)
	c_P	0.25	0.25	Damping (MNs/m)
Sleeper	m_s	490	-	Mass (kg/m)
Ballast/Slab	h	0.35	0.35	Height of ballast/slab (m)
	E	130	30,000	Young's modulus (MPa)
	b	1.25	1.25	Half-track width (m)
	ρ	1700	2500	Density (kg/m^3)

Table 4.1 Ballast and slab track properties

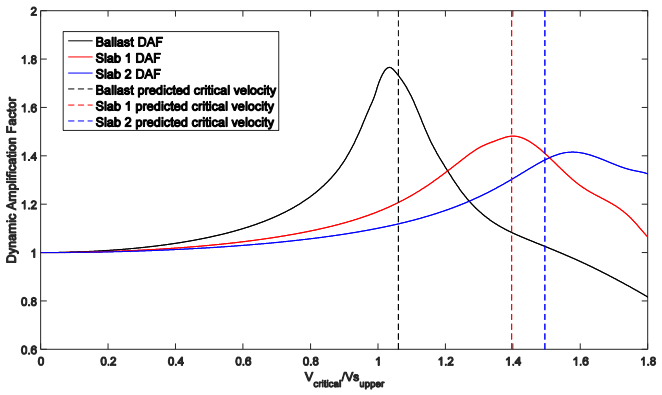

a) Profile 1

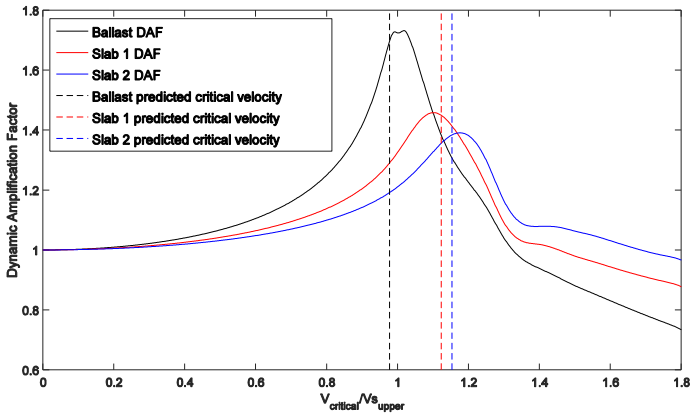

b) Profile 2

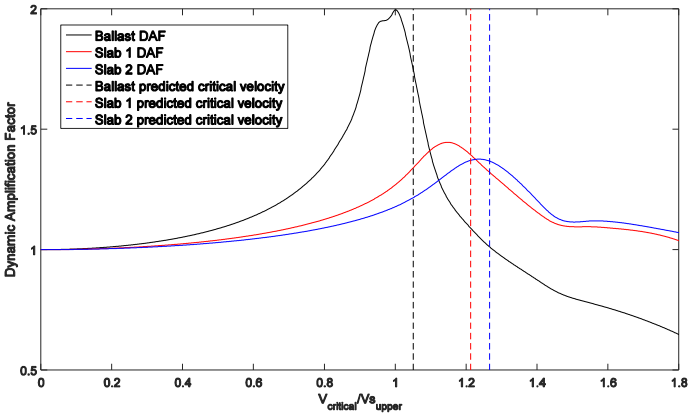

c) Profile 3

Figure 4.7 Dynamic amplification

Using the numerical solution, the dynamic amplification factor (DAF) was calculated as shown in Figure 4.7 for the soil profiles. The peak of the curves matched the critical velocity since these curves show the extent of the increase in track displacements at a certain speed. For the x-axis, the critical speed is divided by the shear wave speed of the top soil layer. The dotted lines represent the critical velocities using the analytical code to be compared to the peaks of the DAF curves. Figure 4.8 and Figure 4.9 show the ground displacements produced by the model. Table 4.2 summarises the accuracy between the analytical critical velocities and those obtained from the numerical solution, which were a good match. The

mean error is 3.39% for the ballast track and 2.53% and 2.98% for the slab tracks, for heights $0.3\,m$ and $0.45\,m$, respectively. As the overall mean error is 2.97%, the code is highly accurate (97% approximately), which is acceptable for critical velocity calculations, considering the soil testing methods errors when computing model input parameters.

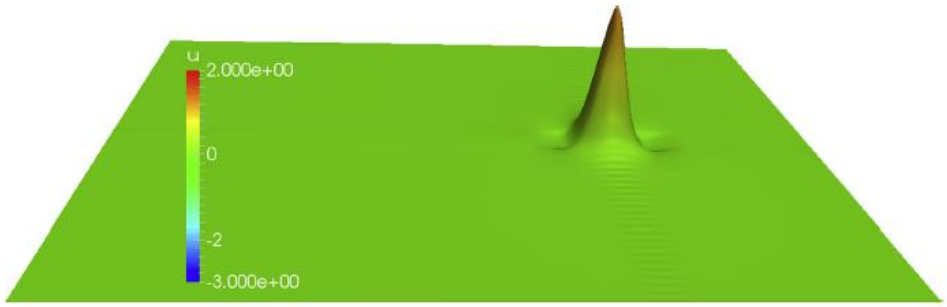

Figure 4.8 Normalised ground displacement at different load speeds ($\frac{V_{critical}}{V_{s_{upper}}} = 0.7$)

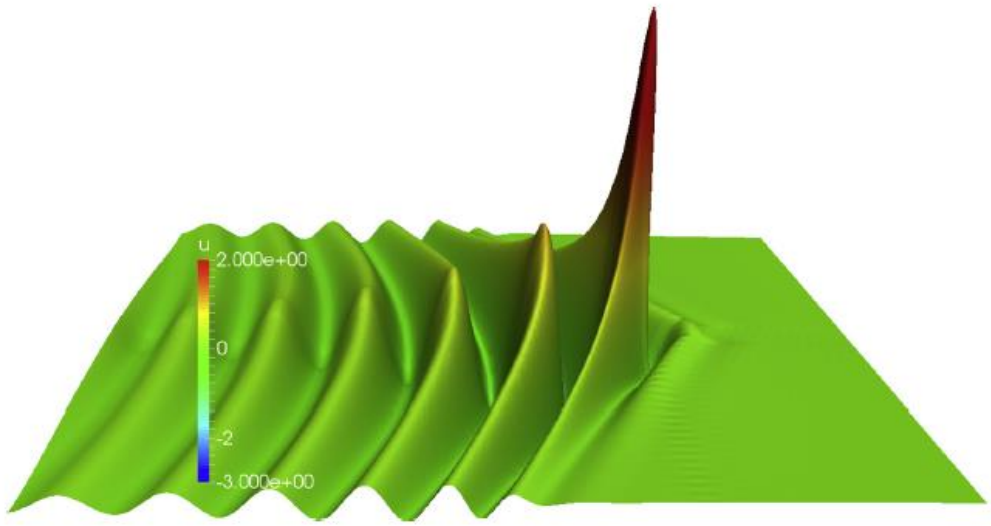

Figure 4.9 Normalised ground displacement at different load speeds ($\frac{V_{critical}}{V_{s_{upper}}} = 1.05$)

Track	Approach and Error	Soil Profile		
		1	**2**	**3**
Ballast	Numerical approach (m/s)	99.60	73.45	74.61
	Analytical approach (m/s)	102.08	71.45	78.31
	Error (%)	2.49	2.73	4.96
Slab 1	Numerical approach (m/s)	134.81	80.54	85.79
	Analytical approach (m/s)	134.39	82.08	90.39
	Error (%)	0.31	1.91	5.36
Slab 2	Numerical approach (m/s)	151.55	85.88	92.50
	Analytical approach (m/s)	143.88	84.32	94.40
	Error (%)	5.06	1.81	2.05
Mean error (%)		2.62	2.15	4.12
Overall mean error (%)		2.97		

Table 4.2 Validation results of critical velocity values obtained from a previously validated numerical model and the dispersion analytical model

4.4 Comparisons and Analysis of Parameters

The code may be beneficial for new high-speed line design, in order to allow the different effects on the critical speed of the site, due to its short run time, to be studied. It is difficult to produce conclusions for non-engineered soil regarding critical velocities, thus, general conclusions from empirical findings can make new track designs easier. Therefore, 1000 random soil profiles were generated by an algorithm using a sensitivity analysis test to study different effects. The statistical distribution of wave speeds over certain geographical regions was not available for the soil profiles, yet the profiles are still useful for comparisons. The study includes ballast and slab track comparisons, track height effects, rail bending stiffness, soil saturation, railpad stiffness, railpad damping and other factors related to deep soil layers.

Several assumptions were applied: shear wave velocity and density were normally distributed and Poisson's ratio and the number of layers were uniformly distributed. The maximum number of layers was seven. For shear wave velocity, density and Poisson's ratio, the mean material properties were $65\,MPa$, $2000\,kg/m^3$ and 0.35, respectively, while the standard deviation for the shear wave velocity and density were $16.25\,MPa$ and $200\,kg/m^3$. Material properties depend on each other, for example: the density and Young's modulus; thus, any profiles that resulted in unrealistic combinations were removed. The stiffness of soil layers increases with depth, to a maximum depth of $20\,m$. An infinite half-space underlies the soil layers. The critical velocity was then calculated for each layer using the analytical code. Monte-Carlo Sensitivity Analysis was used for factors affecting the critical velocity, while ensuring that the same 1000 profiles were used for each analysis for consistency. The cut-off frequency equation was not used for these profiles. The overall results may not represent in-situ soils due to their irregularities; therefore, they were only used for comparisons.

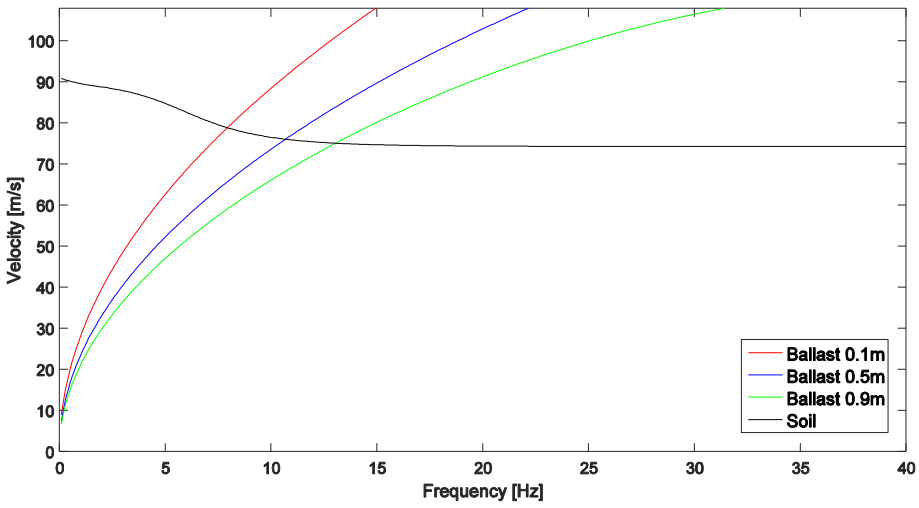

Figure 4.10 Ballast height calculations (Profile 3)

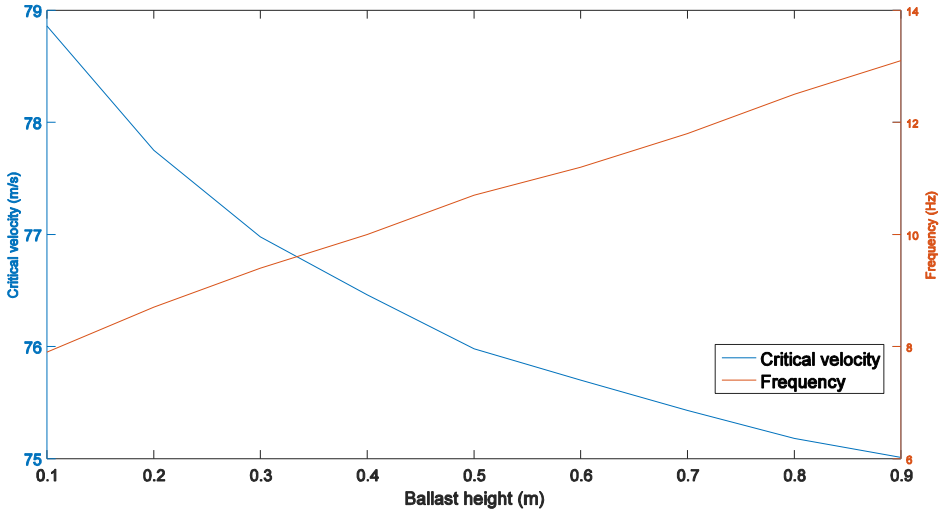

Figure 4.11 The effect of ballast height on critical velocity

4.4.1 Ballast height

Three ballast heights were considered, as shown in Figure 4.10 which indicates the dispersion curves. Critical velocity is reduced due to the reduction of wave propagation speed within a track when ballast height is increased. This is caused by an increase in track stiffness due to the increase in height and not because of changes to the bending stiffness of the track. The critical velocity is presented in Figure 4.11 ranging from $0.1\,m$ to $0.9\,m$ ballast height. The critical speed across the range is reduced by 5.1% ($4\,m/s$).

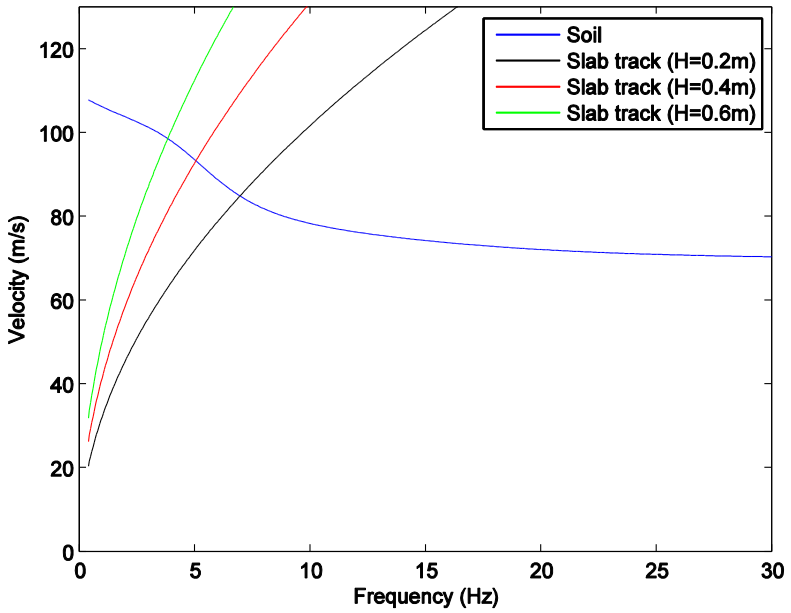

Figure 4.12 Slab height calculations (Profile 3)

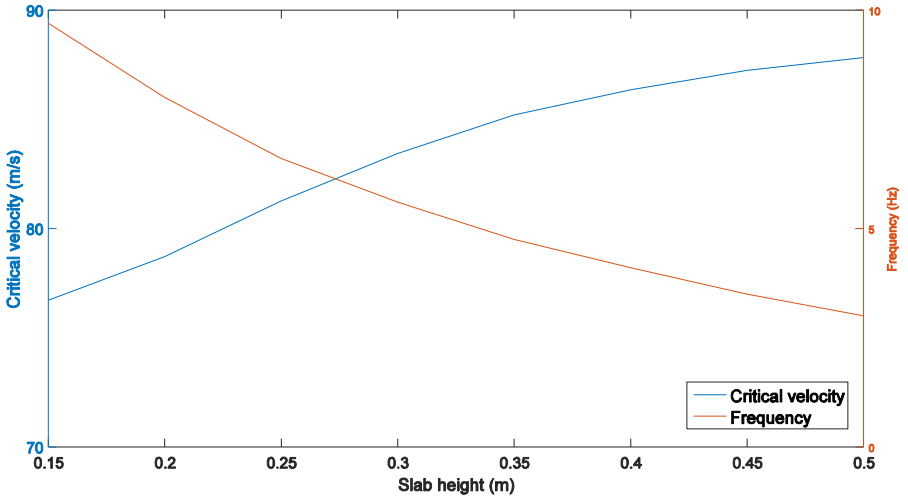

Figure 4.13 The effect of slab height on critical velocity

4.4.2 Slab height

Three slab tracks were considered: $0.2\,m, 0.4\,m,$ and $0.6\,m,$ and the results are shown in Figure 4.12. The critical speeds are higher when the slab height is increased, as the curve is plotted in the lower frequency range. The track stiffness increases as the slab thickness increases. Figure 4.13 shows the critical velocities and frequencies for slabs with a thickness ranging from $0.15\,m$ to $0.5\,m$. Across the range, the critical speed increases by 12.5% ($11\,m/s$) while the frequency decreases by 72.2% ($6.5\,Hz$).

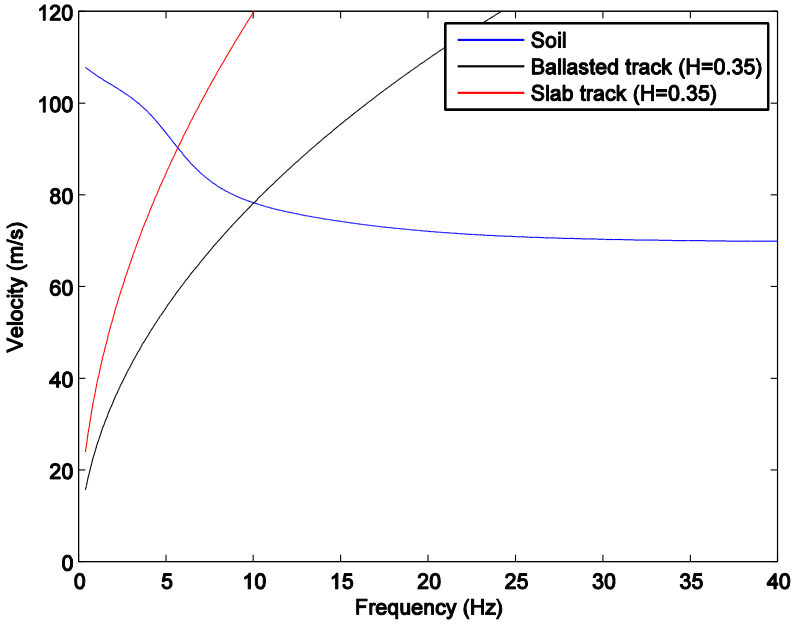

Figure 4.14 Ballast and slab calculations (Profile 3)

4.4.3 Slab versus ballast tracks

Both tracks have different dispersion properties. Slab tracks have higher critical velocities due to their high bending stiffness, which is more desirable as they are not affected by dynamic amplification. Considering the same track thickness for both ballasted and slab ($0.35\,m$), Figure 4.14 shows the results computed for soil Profile 3. The critical speed for

the ballasted and slab tracks are 78.3 m/s and 90.4 m/s, respectively. Analysing the 1000 soil profiles, the average critical speed is 129.4 m/s for ballasted tracks and 144.1 m/s for slab tracks. The average increase is approximately 11% (14 m/s).

The ballast track critical velocities occur at high frequencies while the slab track critical velocities occur at low frequencies: an average of 15.7 Hz, 51% lower than the ballasted track for 0.35 m track height. The speed of wave propagation in the slab is high, thus the low frequencies dominate the dispersion response. It is important to note that if the top soil layer is very thick, the increase in bending stiffness of the slab tracks will have minimal effect. The wave speed of the upper layer is low, which causes critical velocity reduction resulting in issues for both track types.

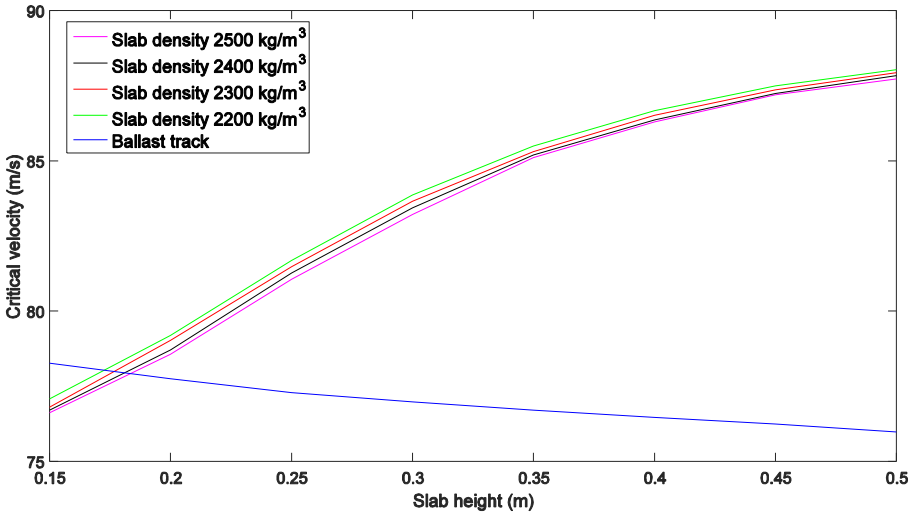

Figure 4.15 The effect of track height and slab mass on critical velocity

4.4.4 Slab mass

The mass of the slab can be changed by changing the density of concrete and slab height. Figure 4.15 shows the results of four different concrete densities ranging from 2200 kg/m^3 to 2500 kg/m^3. Differences in slab height were investigated in Section 4.4.2, they

demonstrated variations in critical velocities; however, for the densities, the variations in critical velocities were relatively small ($2.5\,m/s$). Testing two slab heights: $0.15\,m$ and $0.5\,m$, for a density of $2500\,kg/m^3$, the critical speed increased from $77.5\,m/s$ to $88.6\,m/s$. Increasing the density resulted in a small reduction in critical velocities as shown in Figure 4.15.

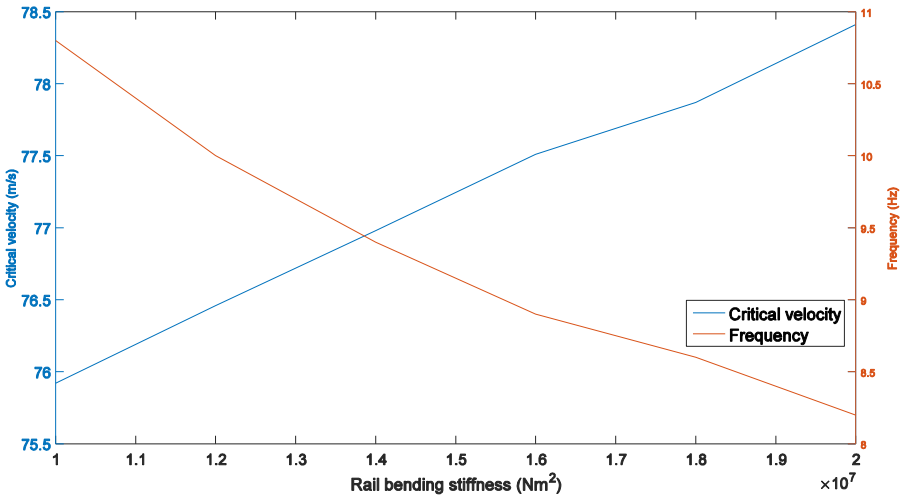

Figure 4.16 The effect of rail bending stiffness on ballast tracks

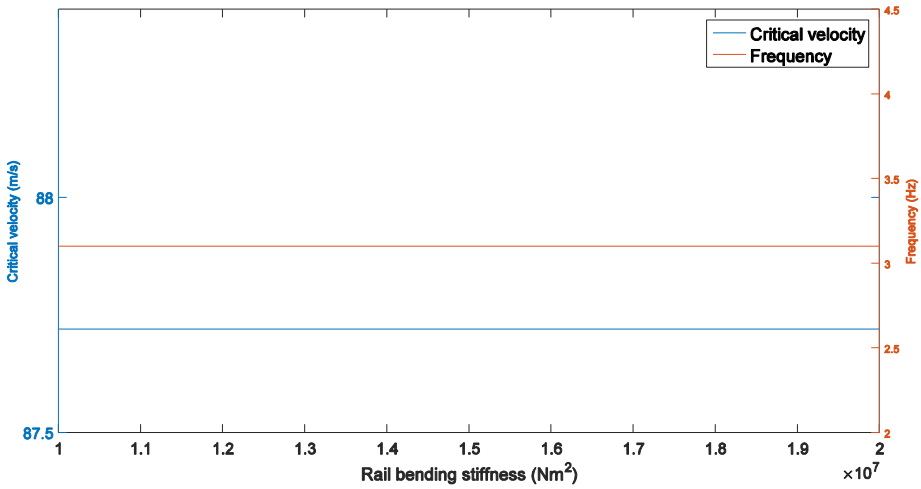

Figure 4.17 The effect of rail bending stiffness on slab tracks

4.4.5 Rail bending stiffness

The rail bending stiffness was altered for both ballasted and slab tracks, as shown in Figure 4.16. The change in critical velocities for the slab track was very small compared to the change for the ballasted track. The critical velocity increased as the rail bending stiffness increased. For a ballasted track, the change was $2.5\,m/s$ for rail bending stiffness ranging from $1 \times 10^7\ Nm^2$ to $2 \times 10^7\ Nm^2$, while it was almost zero for a slab track (Figure 4.17). The ballasted tracks had a lower bending stiffness than the slab, so an increase in the rail bending stiffness had a major effect on the increase in critical velocity. Similarly for the frequency, an increase in rail bending stiffness caused a decrease in the frequency for the ballasted track, while for the slab track, the effect was minimal.

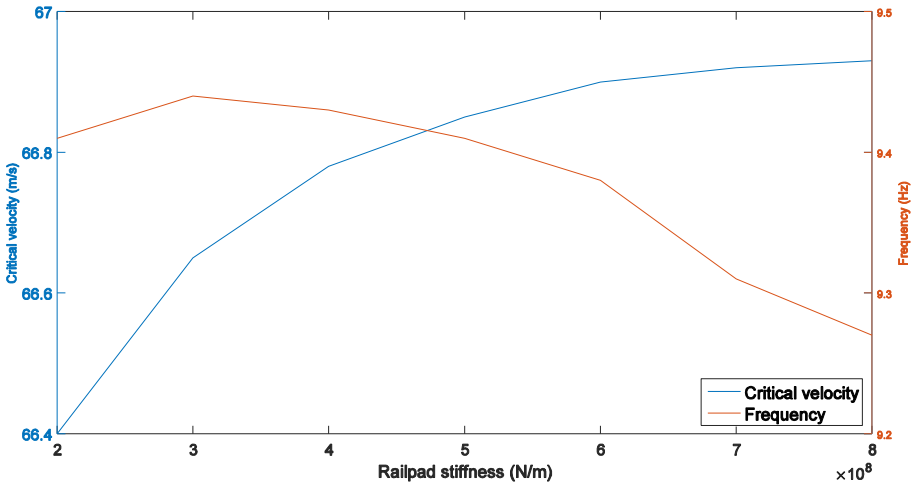

Figure 4.18 The effect of railpad stiffness on critical velocity for ballast tracks

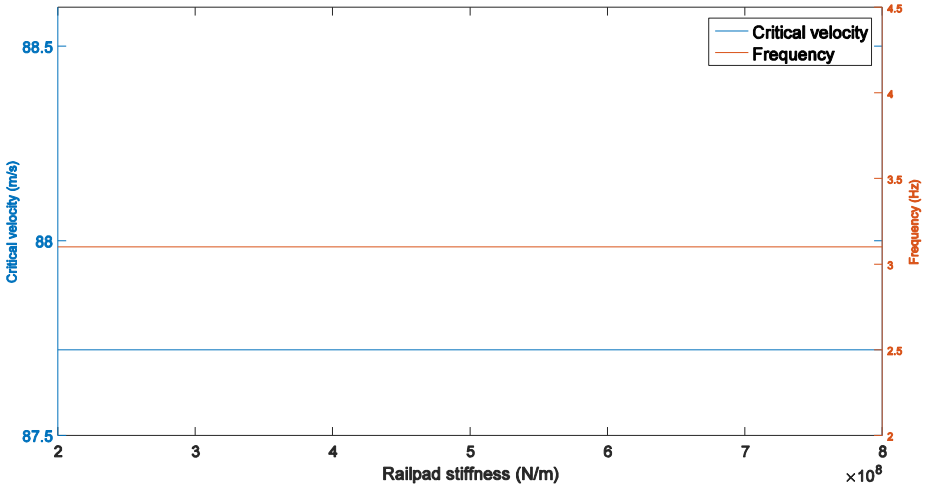

Figure 4.19 The effect of railpad stiffness on critical velocity for slab tracks

4.4.6 Railpad stiffness

Railpad stiffness was also tested for ballasted and slab tracks. The increase in railpad stiffness caused the critical velocity to increase (Figure 4.18). The stiffness ranged from $2 \times 10^8\ N/m$, which is considered to be a soft railpad, to $8 \times 10^8\ N/m$, which is considered to be a stiff railpad. However, the increase in critical velocity for a ballasted track was only 0.75%, and there was almost no influence on the slab tracks (Figure 4.19). In conclusion, the railpad does not affect the critical velocities. This result is similar to the conclusion drawn by Wei et al (2014) that for the critical velocity range (for low frequency vibration), the railpad stiffness is negligible.

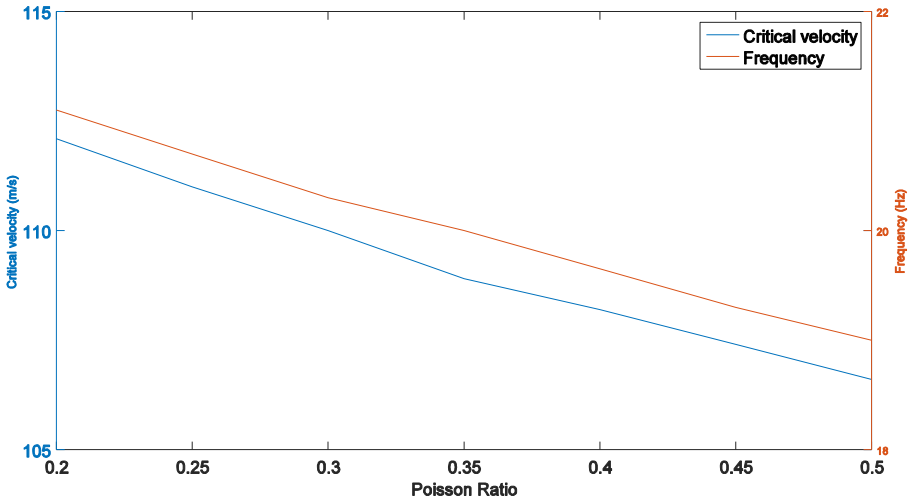

Figure 4.20 The effect of soil saturation on ballast tracks

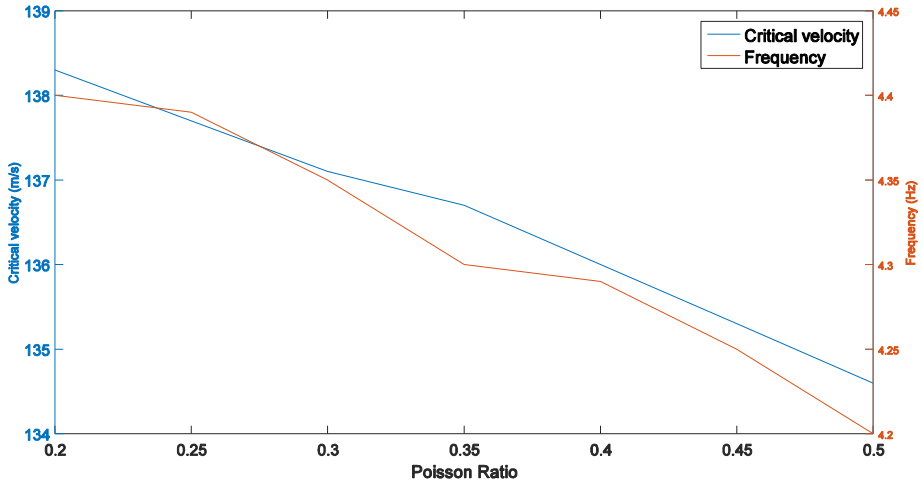

Figure 4.21 The effect of soil saturation on slab tracks

4.4.7 Soil saturation

It is important to consider saturation of the soil in lines constructed near water sources as the groundwater level changes. The Poisson's ratio values were changed ranging from 0.2 and 0.5 for the 1000 soil profiles, in order to study the saturation effect. In Figure 4.22, a fully

saturated soil ($v = 0.5$), shows an increase in the compression wave speed to a speed comparable with water, while it has no effect on shear wave speed because of the lack of shear strength of water. Poisson's ratio value was changed for both ballasted and slab tracks as shown in Figure 4.20 and Figure 4.21. As the ratio was increased, the critical velocities for both tracks decreased. The effect was larger on ballasted tracks, as the critical velocity decreased by 5.4% ($6.2\ m/s$). The slab track critical velocity decreased by 2.5% ($3.4\ m/s$).

Figure 4.23 shows the effect of soil saturation on soil dispersion relations. The elastodynamic relationships shown in Figure 4.22 show that the change in Poisson's ratio has minimal effect on Rayleigh wave speeds, which means it does not affect the critical velocity greatly. Figure 4.23, for a ballasted track, shows that this is true at very low frequencies (below $5\ Hz$). However, there was a difference in critical velocities, noticed in the middle frequency range. The top layers are governed by the Rayleigh wave velocity at high frequencies, and the lower layers are dominated by the shear wave velocity at lower frequencies. Thus, the Poisson's ratio is influential on the dispersion between these values, which is an essential finding as the critical velocities occur in this middle frequency range (intersection point between track and ground dispersion curves). For a slab track, Figure 4.21, the intersection occurs at a lower frequency, where the effect is minimal. In reality, the change in saturation also has an effect on density, which might influence the data obtained in this section, as only the Poisson's ratio was changed. The soil saturation can be altered using Biot's theory alternatively. Furthermore, changing the depth and Young's modulus of the soil layers changed the relations of different Poisson's ratios: where the maximum or minimum effects occur at certain frequencies.

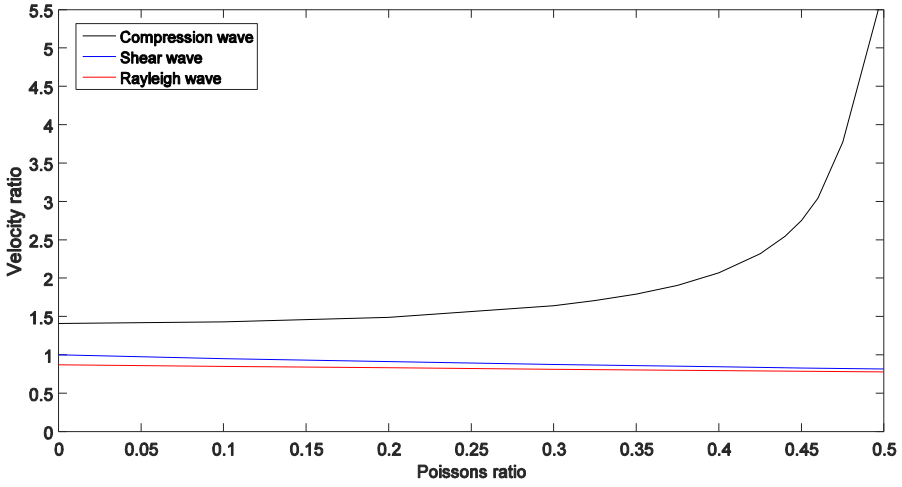

Figure 4.22 Saturation effects: effect of Poisson's ratio on normalised wave speeds

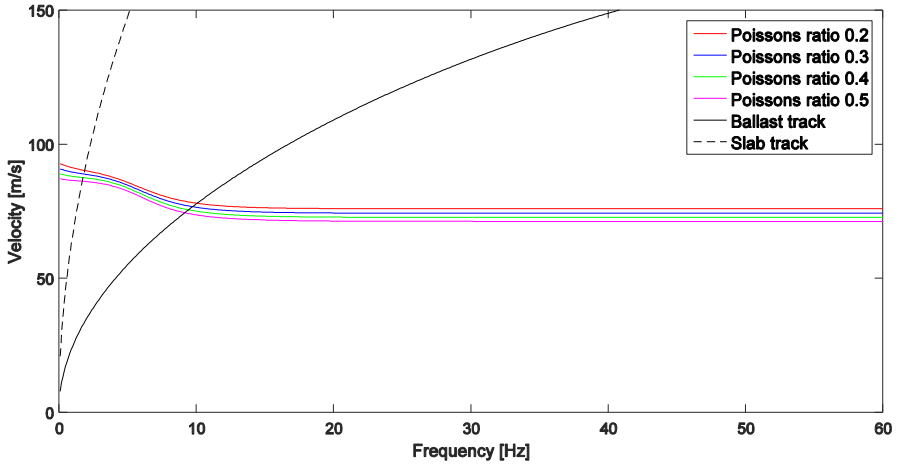

Figure 4.23 Saturation effect: effect of Poisson's ratio on dispersion characteristics of the ballasted and slab tracks

4.4.8 Other factors

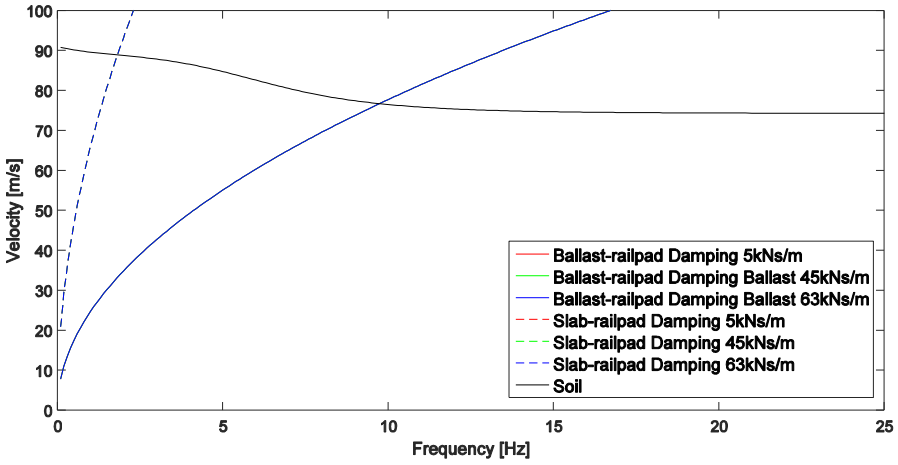

Figure 4.24 The effect of railpad damping on ballast and slab tracks on dispersion characteristics

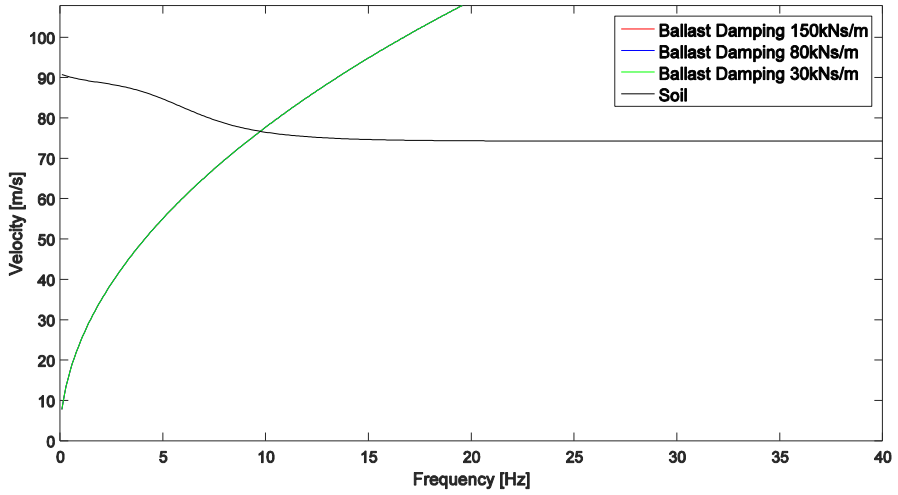

Figure 4.25 The effect of ballast damping on dispersion characteristics

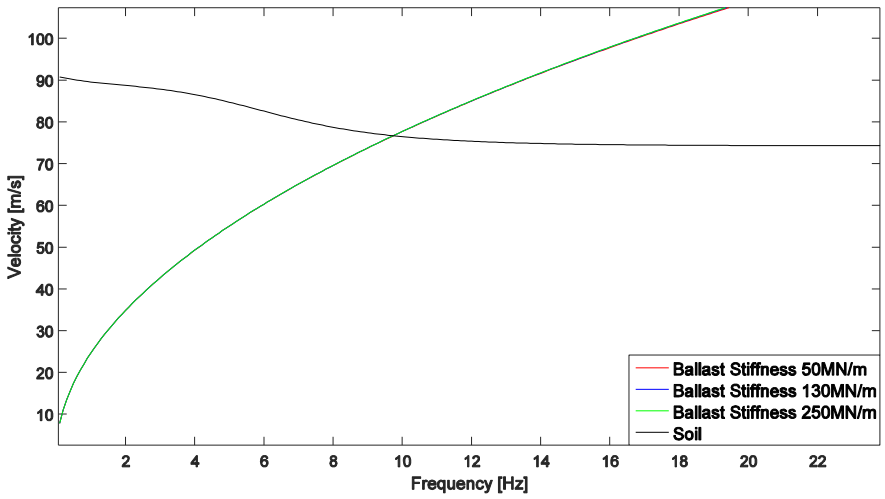

Figure 4.26 The effect of ballast Young's modulus on dispersion characteristics

Figure 4.24 shows the effect of changing railpad damping on both ballasted and slab tracks. The damping coefficient values range from 5 to 63 kNs/m. There was negligible effect on the critical velocities for both tracks. Similarly, the ballast damping had no significant effect on critical velocities as shown in Figure 4.25, where 30 to 160 kNs/m values were tested. The ballast stiffness was also tested (Figure 4.26), and the difference was small between 50 and 250 MN/m that it was negligible. The slab stiffness had already been tested in section 4.4.2 by changing the slab thickness.

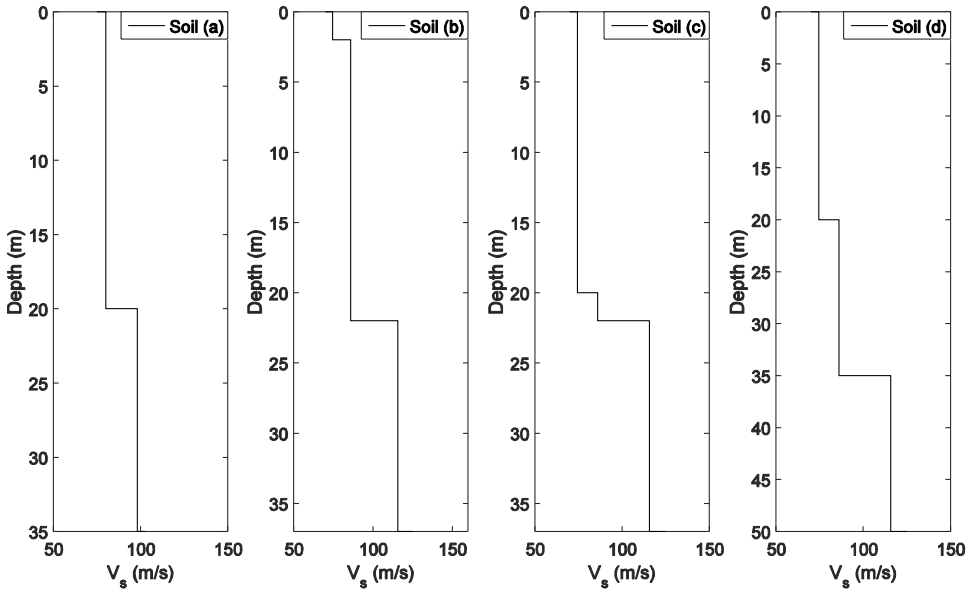

Figure 4.27 Shear wave velocity of soil profiles: Soil (a), Soil (b), Soil (c) and Soil (d)

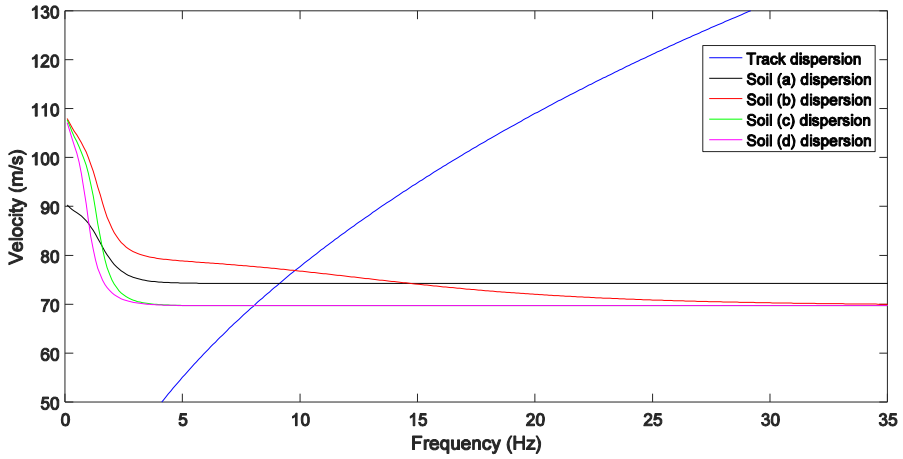

Figure 4.28 Deep soil layers effect on dispersion characteristics for four soil profiles: Soil (a), Soil (b), Soil (c) and Soil (d)

Deep soil layers were tested for their effect on dispersion relations. Figure 4.27 shows the shear wave velocity of the deep soil layers with depth. Figure 4.28 (a) shows the dispersion curve of a deep layer over a half-space. The densities were taken as 1800 kg/m^3 and

$2000\ kg/m^3$ and the Young's Modulus as $30\ MPa$ and $50\ MPa$, for both layers respectively. It was noticed that, if the top layer is a deep layer, then the critical velocity is determined by the top layer, as the intersection occurs with the shear velocity of the upper layer. Likewise, Figure 4.28 (c and d) shows the dispersion of very deep upper layers, on top of layers with thickness of $2\ m$ and $15\ m$, respectively, over the half-space, and both are dominated by the upper layer. The density is taken as $2000\ kg/m^3$ for the three layers, and Young's Modulus is $30\ MPa$, $40\ MPa$ and $75\ MPa$, respectively. Figure 4.28 (b) shows the results of a thin upper layer over a deep layer over half-space, and the intersection between the track and soil dispersion curves is at $78\ m/s$. In this case, the critical velocity is not determined by the shear wave velocity of the upper layer (which is $73\ m/s$); thus, the full dispersion relations of the system should be computed to determine the critical velocity.

4.5 Summary

Predicting the critical velocities of high speed trains is essential in order to increase safety and reduce maintenance costs. Therefore, it is necessary to be able to predict these effects in advance. The dispersion curve approach is beneficial for existing and new lines. The analytical approach includes calculation of dispersion curves for either a slab or ballasted track in a short run time and with minimal computational requirements. The analytical method was developed for both track and soil systems and the critical velocities were validated using a semi-analytical method with a 97% level of accuracy. The prediction of critical velocities is acceptable, since the maximum permissible train speed taken into consideration in practice is 70% of the critical velocity (National-Rail/standard, 2015).

An algorithm was then used to generate 1000 arbitrary soil profiles and a sensitivity analysis was undertaken to study the effects of different factors on critical velocities. The following points summarise the outcomes:

- Ballast height: the higher the ballast height, the less the critical speed since stiffness increases without an increase in bending stiffness.

- Slab height: the higher the slab height, the larger the critical speed because it results in a much stiffer track structure.
- Slab vs ballast tracks: slab tracks result in a higher critical velocity that occurs at a lower frequency (11%) than for ballasted tracks, the critical velocity of which occurs at higher frequencies. Nevertheless, this depends on the top soil layer properties.
- Rail bending stiffness: for ballasted tracks: the bending stiffness increases the critical velocity more than for the slab track because ballasted tracks have a lower bending stiffness. Thus, increasing the rail bending stiffness will result in a higher overall critical velocity.
- Railpad stiffness: this increases the critical velocity for ballasted track but the effect is minimal. For slab tracks, there is almost no effect.
- Soil saturation: for both tracks, the critical velocity decreased as Poisson's ratio is increased. This effects has more influence on ballasted tracks (5.4%) than slab tracks (2.5%).
- Damping: the damping has a negligible effect on critical velocities unless the site is highly nonlinear.
- Deep soil layers: if the top layer is deep, then it is the dominant layer and the critical velocity is equal to its shear velocity. This makes it easier to calculate critical velocities for deep soil layers rather than computing the full dispersion relations.

Chapter 5 Analytical Study

5.1 Introduction

In this chapter, another approach is proposed to simplify the computation of the Dynamic Amplification Factor (DAF) curves of the track in reduced computational time than that required for numerical analysis. DAF figures show the deflection of a structure due to the dynamic load that is applied to the structure and in relation to the deflection caused by a static load. DAF figures give an indication to determine the speed where the maximum deflection occurs. Numerical and semi-analytical approaches have been developed in the past to provide accurate and simple solutions to determine critical velocities using the factor figures. In this chapter, a semi-analytical approach, which was developed by modelling the track analytically and the soil numerically, is described.

The Thin Layer Method (TLM) was used for computing Green's functions of the ground. Green's function is an integral that allows differential equations within a domain to be solved for an impulse response. The method uses finite element methods to solve ground vibration problems for layered ground over half-space. The soil is semi-infinite and is discretised into finite layers in the vertical direction. The thin finite layers vary linearly. TLM has been used previously in combination with other methods (e.g. BEM) to calculate the ground response (Costa et al., 2012a; François et al., 2010; Tadeu & Kausel, 2000). Kausel (1981) presents a formulation of the method that allows for computation of 3D Green's functions.

In this chapter, the TLM formulation is explained briefly. The development of the model and the properties used are presented. The X2000 train at Ledsgård, Sweden, was used for validation of the results. The model allowed the train to run at different speeds in order to collect results for plotting the DAF figures. The field results from Ledsgård are compared to the deflections obtained from the semi-analytical approach in the time domain. In addition, tests of different factors were run to study their effect on deflection amplitudes, such as: slab

track instead of ballasted track and improving the properties of the organic clay layer (the layer which causes the nonlinearity issues at the Ledsgård site). Since it is applicable to modify parameters with the analytical approach, the results were also tested for effects when the train is running in the opposite direction (northbound and southbound at Ledsgård). Furthermore, the wheel spacing of the train was increased in order to study the effect on the resonance of soil layers.

5.2 Method Formulation

The dynamic analysis was linear and carried out in the wavenumber-frequency domain. For the track-ground dynamic formulation, the equation of motion (4.1) that is discussed in Chapter 4, was used. This allows for coupling between both domains. Similarly, the equivalent stiffness for the soil was computed from Equation (4.3) using Green's functions calculated using the TLM as described in this section. The relationship between the soil displacements and the pressure load was given by:

$$u(\alpha,\omega) = \int_{\sum} u^{G}(\alpha,\beta,\omega)p(\beta,\omega)d\Sigma \tag{5.1}$$

$u^{G}$is the Green's functions tensor of displacements used to calculate the displacement, u, when pressure, p_i, is applied along the surface. The surface is denoted by $\sum$ for $\alpha = \beta = x, y, z$ coordinates.

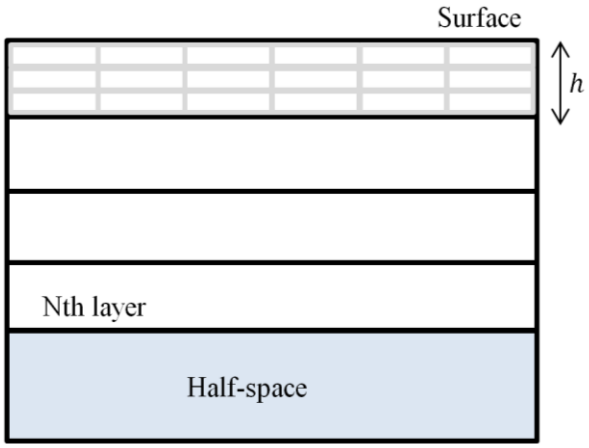

Figure 5.1 Finite layers on half-space

Figure 5.1 shows the TLM layout with half-space to prevent wave reflection at the base of the model. To allow for simulation of a vertically infinite domain, the half-space layer was not discretised while the layered region above was discretised vertically. The height of the thin layers was calculated to be small in comparison with the shear wavelength. The following relationship (5.2) was used, where Δh is the vertical discretisation and γ_s is the shear wavelength:

$$\Delta h = \frac{\gamma_s}{\Delta_\gamma} \tag{5.2}$$

Δ_γ varies between 4 and 20 (8 was taken for this model). The model was meshed and finite element methods were applied to determine the stiffness, K_t, of the system using the following relationship:

$$K_t = K_1^{global} - ik_1K_2^{global} - ik_2K_3^{global} + k_1^2K_4^{global} + k_2^2K_5^{global} + k_1k_2K_6^{global} - \omega^2M^{global} + K_r \tag{5.3}$$

K_1^{global} to K_6^{global} are stiffness matrices (the subscripts are related to the degrees of freedom) and M^{global} is the mass matrix. K_r stiffness matrix is related to the half-space, which follows the stiffness properties of the layer above in this model. Figure 5.2 shows the assembly and addition scheme of the global matrices including half-space. The last section is omitted in the case of rigid base.

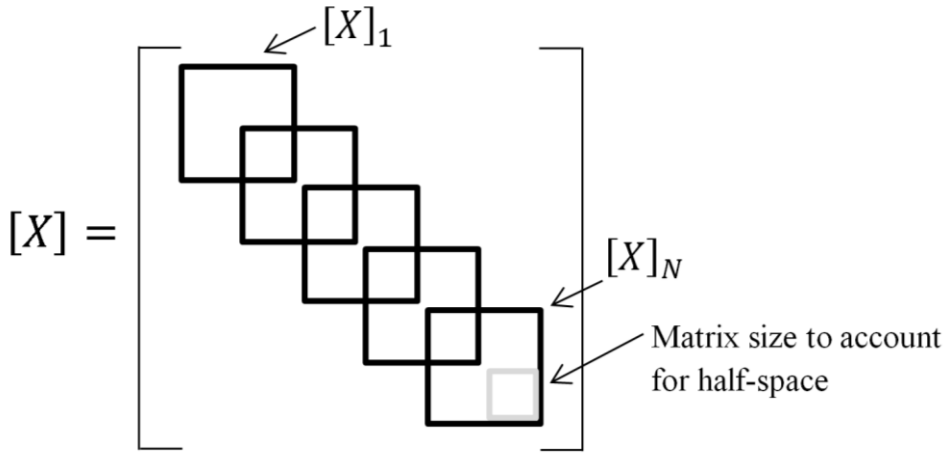

Figure 5.2 Matrix addition scheme including half-space

The global load and displacement vectors were assembled with the nodal vectors, and the displacements were solved using Equation (5.4). K is defined as $K_t + K_{dyn}$, where K_{dyn} is the dynamic stiffness matrix calculated using dynamic Lamé's constants (Equations (5.5) and (5.6), where the asterisk symbol indicates dynamic constants). The details of the dynamic stiffness matrix calculation are presented in the Appendix. ξ_s and ξ_p are damping of the shear and compression waves, respectively. Since the frequency may take complex values, the form $sgn(\omega)$ was taken, which represents the signum function.

$$P = KU \tag{5.4}$$

$$\lambda^* = \frac{Ev}{(1+v)(1-2v)}(1 + 2i\xi_p sgn(\omega)) \tag{5.5}$$

$$\mu^* = \frac{E}{2(1+v)}(1 + 2i\xi_s sgn(\omega)) \tag{5.6}$$

The wheels of the train were applied as moving point loads on the rail, without considering the multi-body vehicle system, for simplicity. The moving loads were simulated by including their effects considering the translational property of the Fourier transform. Because of this property, the following relationship was obtained between the frequency and the wavenumber relating to the speed, c, of the moving load (Ω is the driving frequency of the moving load):

$$\omega = \Omega - k_1 c \tag{5.7}$$

After obtaining Green's functions, the response was determined for a point in the ground surface with coordinate y in $(k_1, y, 0, \omega)$ domain, where the zero indicates the top of the upper soil layer. The response is described by Equation (5.8). The equivalent stiffness matrix was then calculated (Equation (4.3)) and added to the track system.

$$u(k_1, y, 0, \omega) = \frac{1}{2\pi}\int_{-\infty}^{+\infty} u^G(k_1, k_2, 0, \omega)\left(\frac{sin(k_2 b)^2}{(k_2 b)^2}\right) dk_2 \tag{5.8}$$

After solving Equation (4.1), inverse Fourier transform functions were then used to produce time histories of the displacements. It is important to note that the stiffness values of the ground material properties were manually reduced for the linear model as the speed increases to take into account the nonlinearity effect between the force and stiffness.

5.3 Development of the Model and Validation

The X2000 train has five carriages and 20 axle loads as shown in Table 5.2, which demonstrates the axle loads used in the model. Figure 5.3 shows the geometry and wheel spacing of the train. These loads were applied to the track system consisting of the rail, railpads, sleepers and ballast lying on top of the embankment and soil layers. The track width is $2.5\ m$ and the width of the rail base is $0.14\ m$. The parameters of the rail, railpads and sleepers are listed in Table 5.1. Hysteretic material damping is normally used for seismic responses and the damping coefficients for the track and soil are shown in Table 5.3.

Rail	
Mass per unit length (kg/m)	120
Young's modulus (MN/m^2)	210×10^3
Second moment of inertia (m^4)	6.11×10^{-5}
Resistant bending modulus (MNm^2)	12.89
Railpad	
Stiffness per unit length (MN/m^2)	600
Damping per unit length (MNs/m^2)	22.5
Sleepers	
Mass per unit length (kg/m)	490
Width (m)	0.25
Length (m)	2

Table 5.1 Properties of rail, railpads and sleepers

The average width of the ballast is $3.3\ m$, while the average width of the embankment is $4.1\ m$. The damping was calculated by multiplying the damping coefficients by the stiffness per unit length calculated from Equation (5.9):

$$k = \frac{E}{3(1-(2v))} \tag{5.9}$$

No. of wheels	1	2	3,4	5,6,7,8,13,14, 15,16	9,10,11,12	17,18	19	20
Axle load (kN)	188.5	183	185.7	122	125	143.2	119	167.5

Table 5.2 Axle loads for the X2000 train (Sheng, 2001)

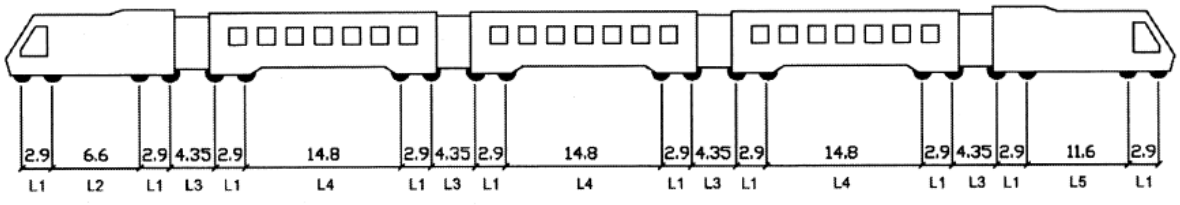

Figure 5.3 The geometry of the X2000 train (Paolucci et al., 2003)

Layer	**D (m)**	**E (MPa)**	**v**	**$\rho(kg/m^3)$**	**Damping Coefficient**
Top ballast	0.4	124	0.4	1800	0.061
Embankment	0.5	430	0.3	1900	0.061
Crust	1	20	0.491	1500	0.05
Organic clay	3	6	0.498	1250	0.05
Marine clay	Half-space	24.5	0.498	1470	0.05

Table 5.3 Track parameters for the X2000 track (Hall, 2000; Madshus & Kaynia, 2000; Takemiya, 2003)

The simulations were carried out for the semi-analytical approach and the results are shown in Figure 5.4 for different speeds. The stiffness of the soil layers is different for larger speeds due to soil nonlinearity; however, linear analysis type was carried out in this research. In order to take equivalent stiffness to account for nonlinearity, for the first three speeds, 19 m/s, 33 m/s and 38.9 m/s, the Young's modulus was taken as listed in Table 5.3, while for the remaining speeds, the modulus was reduced based on the calculated strains for the Swedish site that were carried out and are described in Chapter 6. There is a good agreement between the field results and the model outcomes; however, with higher speeds, the error ratio becomes bigger with larger peaks compared to the field results. This is still acceptable

considering the high uplift of speeds 51.1 m/s to 56.9 m/s for the field results; this indicates that the code is efficient for predicting the largest uplift at the site. Based on Figure 5.4, for lower speeds (up to speed 44.4 m/s), a quasi-static pattern was observed for the displacements, while the dynamic amplification governed the behaviour as the speed approached the Rayleigh wave velocity.

a) 19 m/s

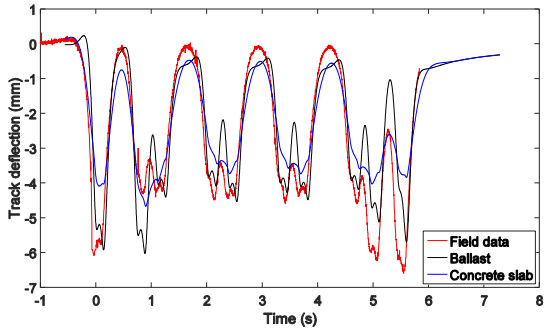

b) 33.3 m/s

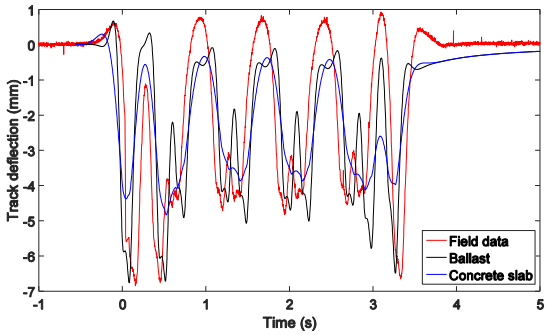

c) 38.9 m/s

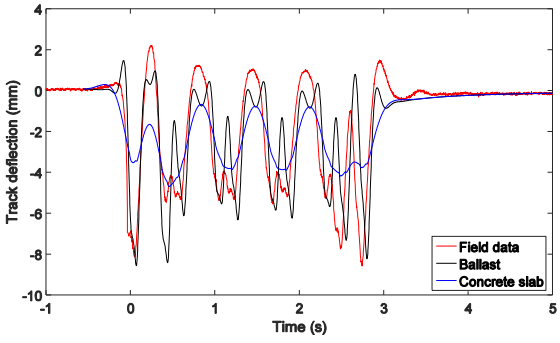

d) 44.4 m/s

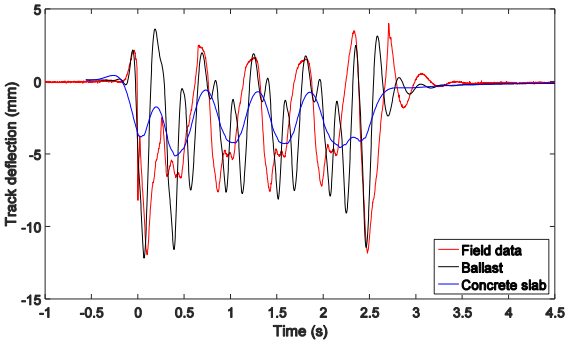

e) 49.4 m/s

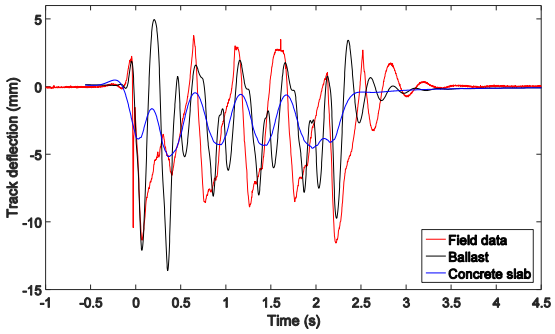

f) 49.7 m/s

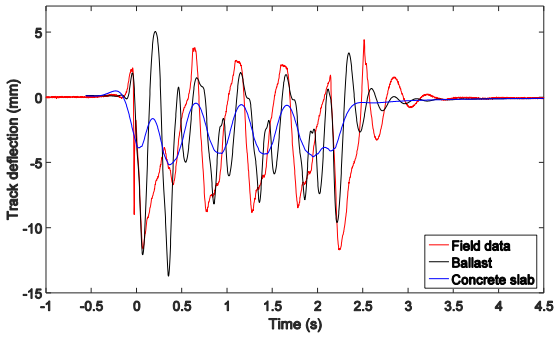

g) 50 m/s

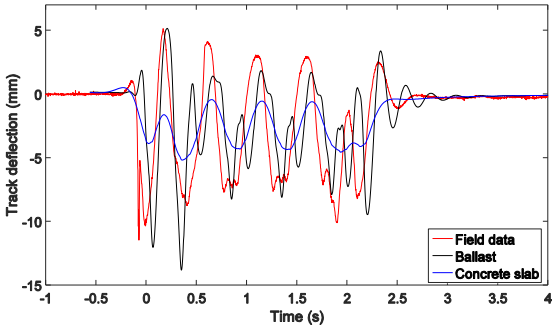

h) 50.3 m/s

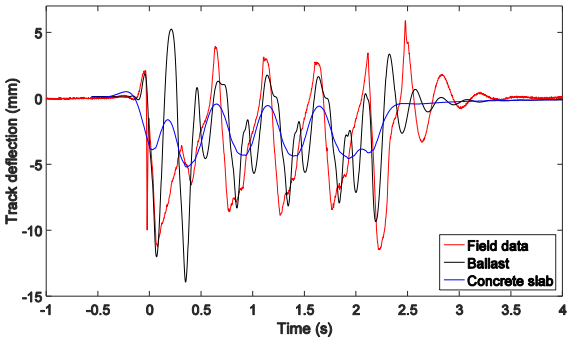

i) 51.1 m/s

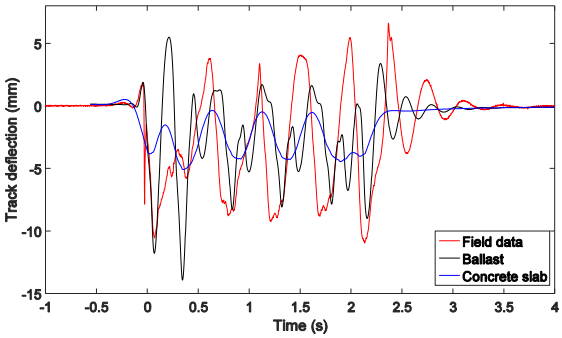

j) 51.4 m/s

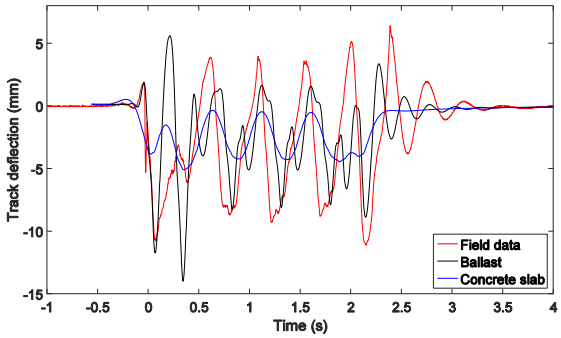

k) $56.7\ m/s$ l) $56.9\ m/s$

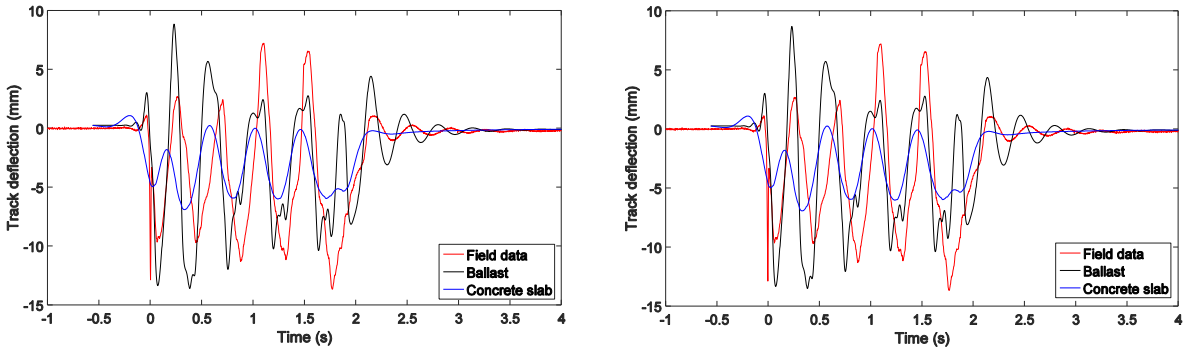

Figure 5.4 Measured and predicted time histories for the Ledsgård site for different speeds

Previous studies have investigated the ground response at the Ledsgård site if the speed is increased to $70\ m/s$ (Madshus & Kaynia, 2000). Figure 5.5 shows the vertical displacements obtained from the analytical approach in comparison with the data from a model developed by Madshus and Kaynia (2000) and another approach using DART3D software. Results of the analytical method developed in this research agree with Madshus and Kaynia's (2000) outcomes, while the predicted values from DART3D are slightly lower. Higher speeds are plotted in order to ensure the drop in deflection values in DAF curves in order to allow the critical velocity of the site to be determined. Figure 5.6 shows the peak deflection curves, where the positive values represent the uplift and the negative values represent the settlement, between the measured and predicted data for the semi-analytical approach. There is good agreement for the uplift; however, the level of accuracy is slightly lower for the downward deflections. For higher speeds, there is an over-estimation of peak values. Based on the peak deflections curve, the maximum uplift and displacement occur at a speed of $56\ m/s$; thus, this is referred to as the critical velocity of the site (Costa et al., 2010). The Rayleigh wave velocity for the Swedish track is calculated as $51\ m/s$ and it is approximately 91% of the critical velocity. The amplified effects start to increase

significantly as the site approaches the Rayleigh velocity until it reaches the critical velocity, then the deflections decrease as the speed is higher as observed at 70 m/s.

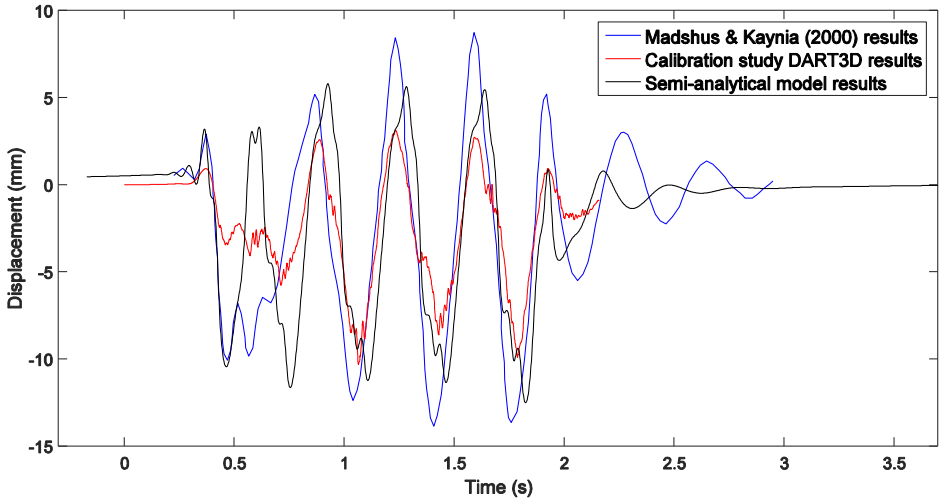

Figure 5.5 Time history comparison between the analytical approach results and previous approaches for speed 70 m/s (Madshus & Kaynia, 2000)

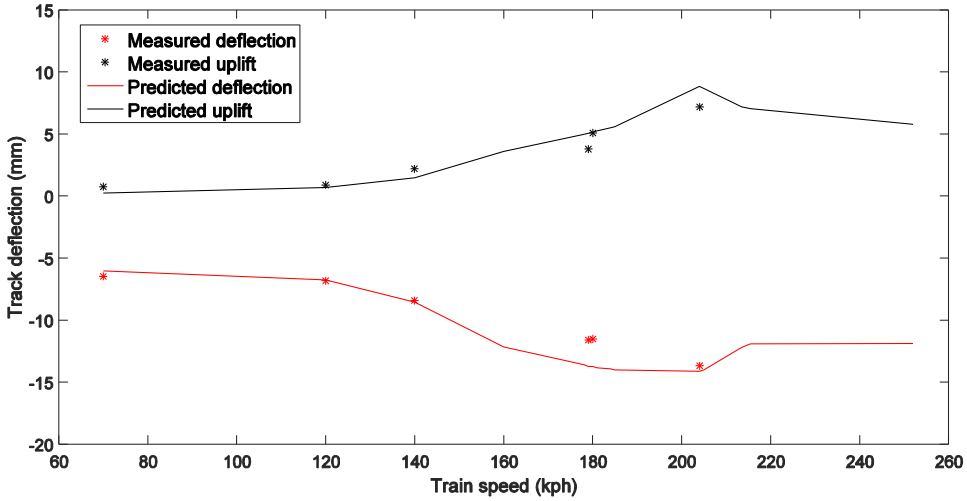

Figure 5.6 Peak deflection for the measured and predicted results

5.4 Soil Improvement and Factors Affecting Critical Velocities

After the validation of the code with actual field results, tests were carried out to study the effects of some factors on the behaviour of the Ledsgård site. First of all, a slab track model was developed. The slab results were then compared with the measured and predicted ballasted deflections. Secondly, the properties of the organic clay layer, which is the weak layer at the site, were improved. This section also shows the effect of wheel spacing and different axle load distribution on the ground response by making changes to the wheel spacing of the X2000 train, and also running the train specifications in opposite directions.

5.4.1 Slab tracks

The slab track was modelled instead of the ballasted track for the Ledsgård site to study the changes to ground response. The concrete slab layer was modelled on top of a Hydraulically Bonded Layer (HBL) and Frost Protection Layer (FPL). The parameters of the slab track were obtained from the SSF slab tracks (SSF-Ingenieure), and are presented in Table 5.4. The width of the slab, HBL and upper surface of the FPL layers was $2.5\,m$ and the FPL lower surface width was $2.94\,m$. The damping coefficient of the FPL layer was chosen to be 0.061. The comparison between the displacements of the slab and the ballasted tracks are shown in Figure 5.4. The slab track results show lower maximum deflections based on the outcomes from Figure 5.7, for maximum deflection and uplift. The uplift is reduced to almost zero. The effect of the slab is greater for the high speeds: the difference between the peaks is $2.6\,mm$ for speed $51.4\,m/s$, while it is $5.2\,mm$ for speed $56.9\,m/s$.

Layer	**D (m)**	**E (MPa)**	ν	$\rho(kg/m^3)$
Slab	0.54	34000	0.2	2400
HBL	0.33	5000	0.2	2400
FPL	0.22	126	0.3	2000

Table 5.4 Slab track parameters

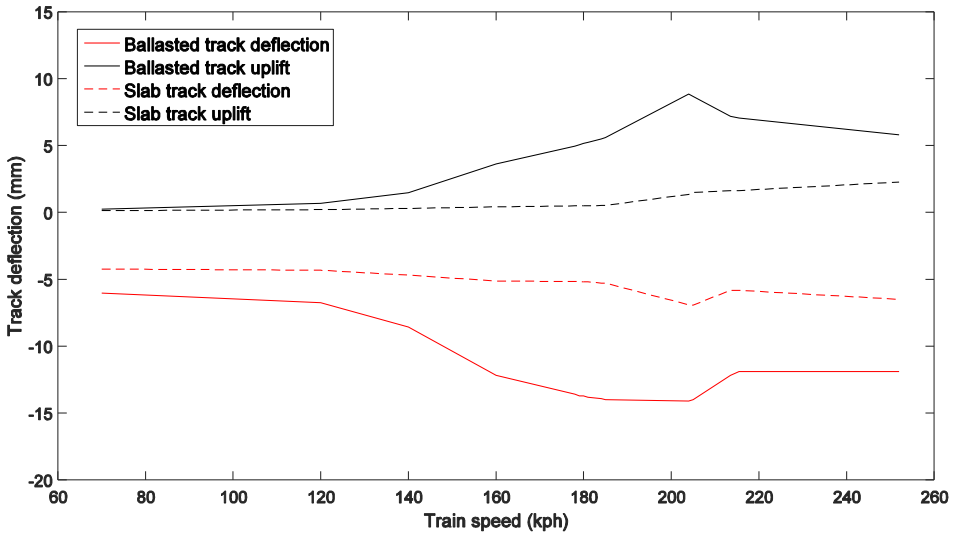

Figure 5.7 Peak deflection for ballasted and slab tracks

5.4.2 Improved soil layers properties

Figure 5.8 shows the soil layers with depth for the Ledsgård site. The organic layer, which is $3\,m$ in depth, has a Young's Modulus of $6\,MPa$. This layer is highly nonlinear and causes an amplified ground response. The properties for this layer were increased to $20\,MPa$ and the density to $1400\ kg/m^3$.

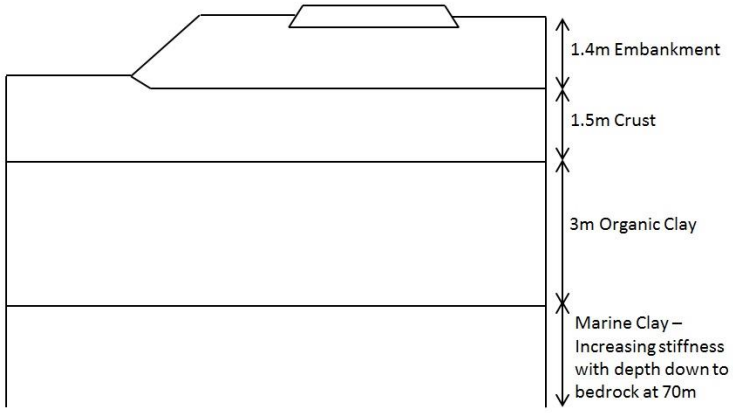

Figure 5.8 Soil layers with depth at the Ledsgård site

The time history results are shown in Figure 5.9 for speed $56.7\ m/s$ compared to the results for the unmodified predicted ballasted track. The effect has changed significantly as the maximum settlement is reduced by approximately $9\ mm$ and the uplift is almost zero. The peak is also $2.4\ mm$ smaller than the slab results for the same speed. Figure 5.10 shows the DAF curves comparison, where the uplift has decreased considerably for greater speeds. Comparing the DAF figures between slab tracks and organic clay soil improvement in Figure 5.11, the slab track shows major differences in reducing the effects of critical velocities for a track constructed on weak soil similar to that at Ledsgård site, since the organic clay is the main issue at the site. However, the reduction caused by replacing the ballast track with slab track is less than the reduction caused by the stone columns that were used to strengthen the soil at the site based on the numerical model results, which are discussed further in Chapter 7.

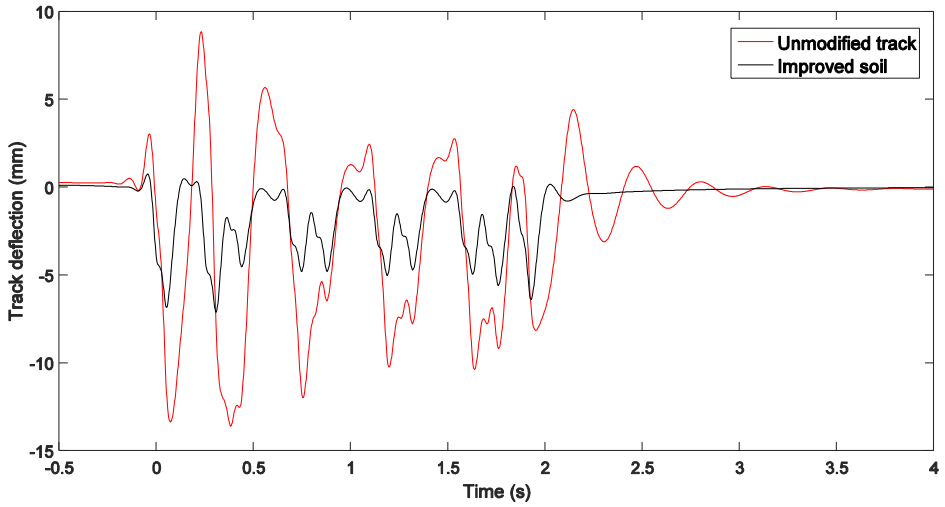

Figure 5.9 Time history for the Ledsgård site between the predicted results before and after soil improvement

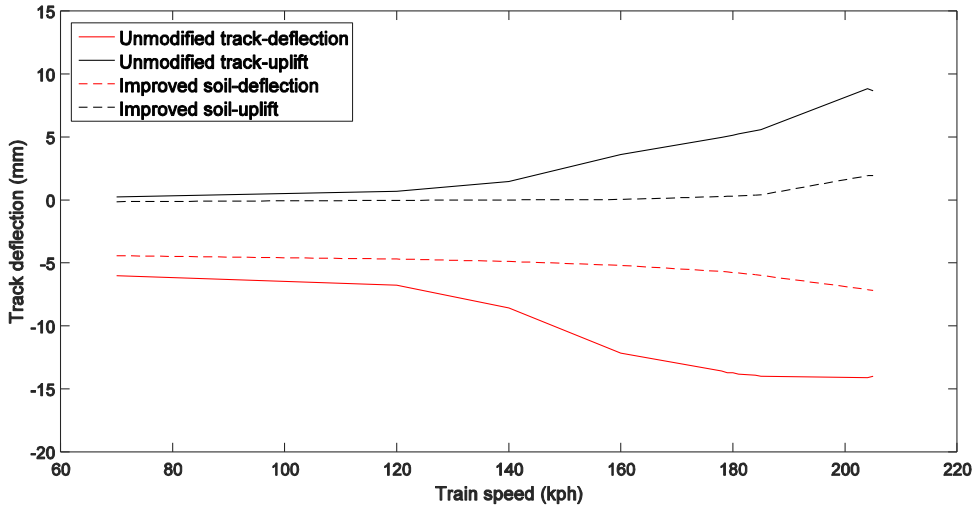

Figure 5.10 Maximum deflection and uplift for the unmodified track and predicted results after soil improvement

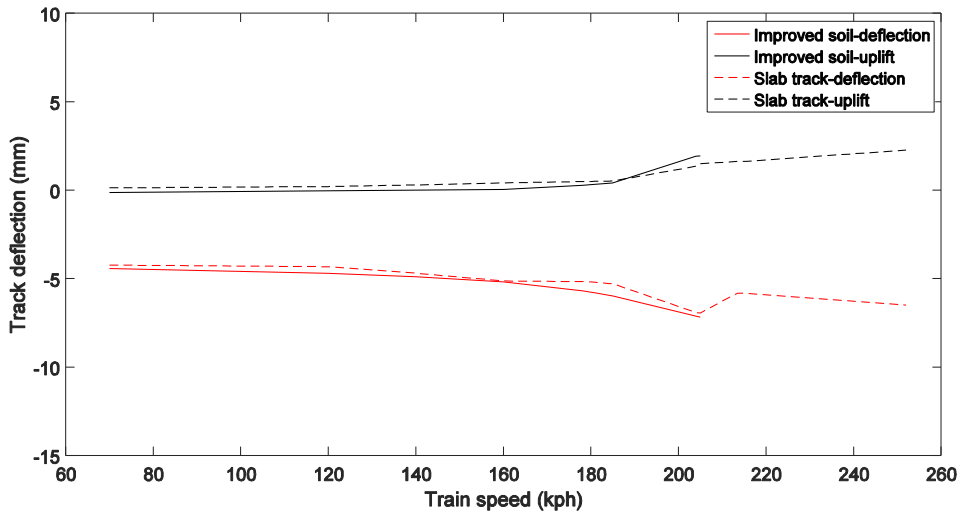

Figure 5.11 Maximum deflection and uplift for the slab track and predicted results after soil improvement

5.4.3 Increased wheel spacing effects

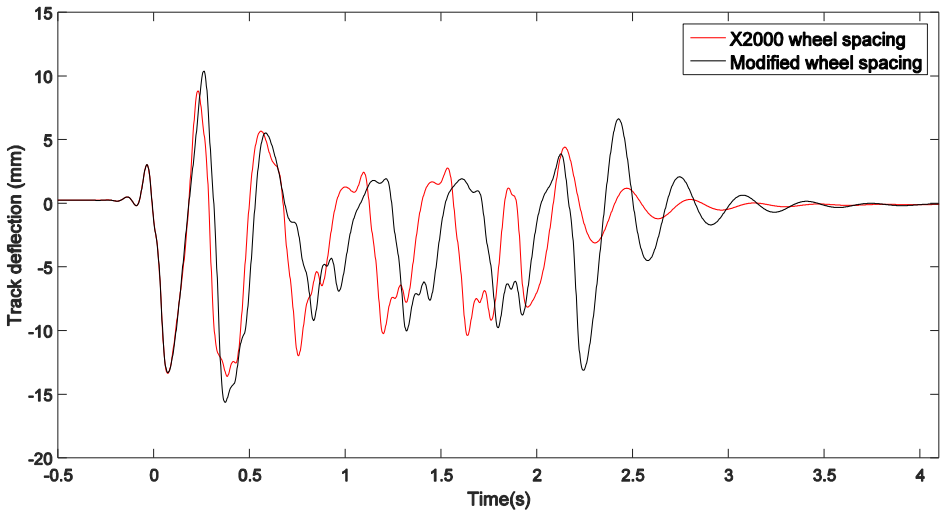

Figure 5.12 Time history for the Ledsgård site for the predicted results after increasing wheel spacing

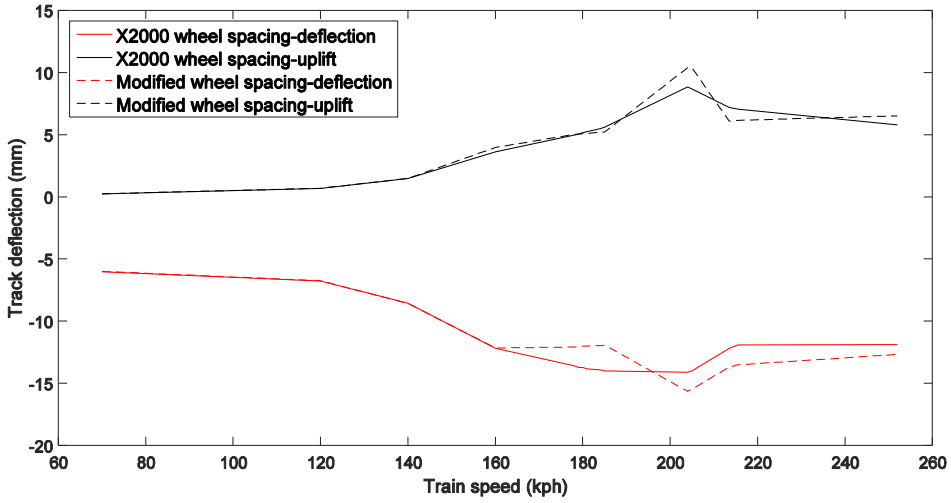

Figure 5.13 Maximum deflection and uplift for increased wheel spacing

The carriage length after increasing the wheel spacing was $27.3\,m$. The different wheel spacing did not have a major effect on critical velocity in terms of amplitude of deflections for certain speeds. Amplitudes are mostly affected by soil properties. However, the change of loading wavelength had an effect at greater speeds. Figure 5.13 shows the increase in deflection as the site reaches the critical velocity. The value of the critical velocity, $56\,m/s$, remains unchanged. It is important to note that the change of the loading frequency of the train in relation to the natural frequency of the ground affects the resonance (trail of displacements in Figure 5.12 for speed $56\,m/s$) and causes a change in deflection at critical speeds. Two major aspects that must be considered when analysing critical velocity effects: the speed when the train reaches the Rayleigh velocity of the soil, that is when the large deflections and uplifts start to occur, and the increase in loading frequency in relation to the natural frequency of the ground, which increases the critical velocity effects (Woodward et al., 2013).

5.4.4 Train running in both directions

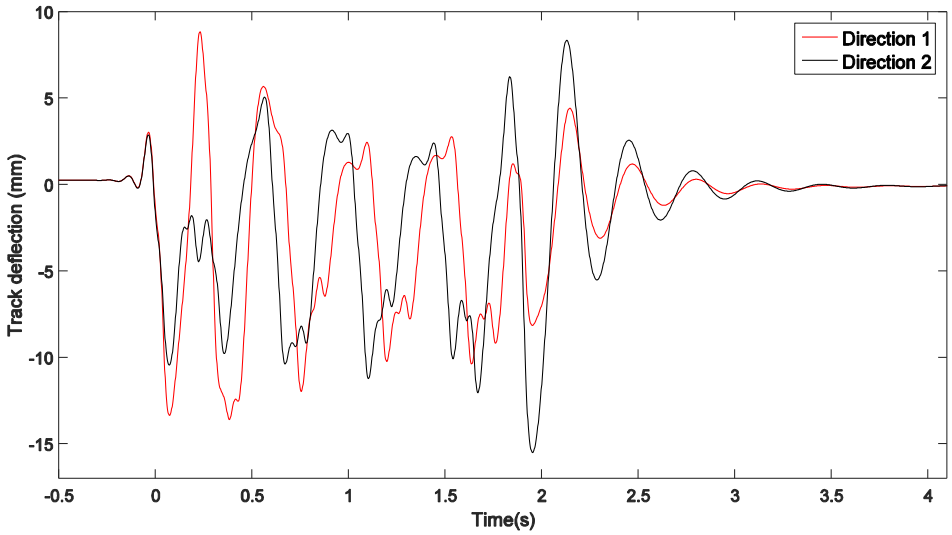

Figure 5.14 Time history for the Ledsgård site for predicted results for different train directions on the same track

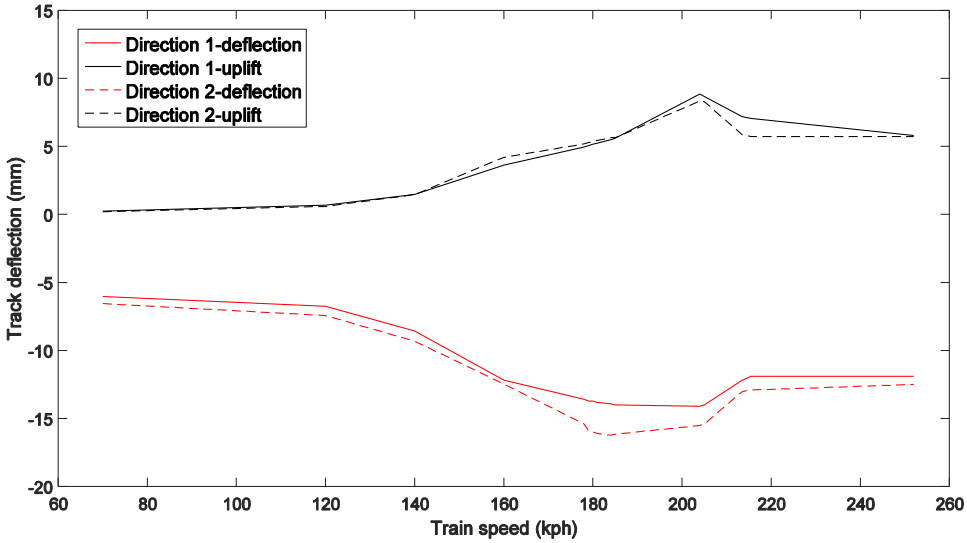

Figure 5.15 Maximum deflection and uplift for different train directions

The X2000 train was also run in both directions: northbound and southbound, for speed $56.7\,m/s$, since the spacing and axle loads are not symmetrical for the X2000 train. For Direction 1, the data used are shown in Table 5.2, while for Direction 2, the data were flipped. Since the axle load is larger at the end of the train and the wheel spacing was smaller for Direction 2, there was a larger deflection and uplift forming at the end based on Figure 5.14. The maximum peak deflection for Direction 2 in Figure 5.15, occurred at a speed of $51\,m/s$ while it occurred at a speed of $56\,m/s$ for Direction 1. The maximum uplift for both directions occurred at a speed of $56\,m/s$. This observation helps in understanding the effects of loading frequencies and superposition on the response of the ground.

5.5 Summary

A semi-analytical code was developed for DAF curves computation and production of deflection time histories. The Finite Element Thin Layer Method (FETLM) was implemented to compute Green's functions for the soil layers and the solution was computed in the frequency-domain. An inverse Fourier transform method was used to produce the time histories. The code proved to be accurate and it was validated with the field measurements from the Ledsgård site in Sweden. Extra tests were carried out using the code, which included testing different track types: slab track effects in comparison with ballasted track; soil type: strengthening the organic clay layer; and train properties: different axle spacing and loading. The following points are concluded:

- Slab tracks result in smaller deflection values than ballasted tracks for train tracks constructed over weak soil.
- Replacing the ballasted track with slab tracks reduces vibrations by 51.5%, mainly in terms of uplift reduction. This gives similar results as improving the weak organic clay layer in the ground, which reduces vibrations by 49.9% compared to the unmodified track.
- Altering the properties of an existing organic clay layer at the site has a major effect on the response. For reduction of the settlement and uplift, the organic clay layer must be treated and improved.
- The response depends on the axle loading and spacing; however the maximum deflection values are affected more significantly by soil properties than train properties.
- The increase in loading frequency of the train results in larger deflections at critical speeds; however, the value of the critical speed remains the same ($56\,m/s$ for the Swedish track).

Chapter 6 Three-Dimensional Numerical Approach

6.1 Introduction

This work has been divided into three sections, starting with the creation of a three-dimensional model of the track-ground system to investigate ground behaviour. The load was applied with user-defined subroutines, including the wheel-rail interaction forces in coupling the train to the track-ground system. Secondly, the models were developed for more than one train and compared to field results for validation. In order to analyse the critical velocity effects, the full 3D model, including the track-ground system and a full train system, were used to study the effects as well as studying different mitigation strategies, which are discussed in the following chapter.

The analysis in ABAQUS is explained in detail in the first section of this chapter, including the finite element implementation and moving load application. Linear analysis was carried out to avoid the computational effort of nonlinear analysis, and explicit time integration was carried out. An equivalent linear method, proposed by Costa et al. (2010), was used for this model in order to account for nonlinearity. Ballast and slab tracks are discussed in the fifth and sixth sections. The last section includes the validation of ballasted track models using two actual field results obtained from the Swedish track in Ledsgård for the X2000 train and the Portuguese track for the Alfa-Pendular train. The frequency plots for the Portuguese track are shown in order to check for dominant frequencies.

6.2 Three-Dimensional Track Modelling

This section includes tests and comparisons that were made for the initially developed model in order to obtain a less time consuming model for the soil model and track composition.

The use of a Euler-Bernoulli beam to represent the rail is efficient for models dedicated to the propagation of vibrations; it was stated by Knothe and Grassie (1993) that up to $500\ hz$, the rail can be modelled as a Euler-Bernoulli beam, while Timoshenko beams are more efficient for higher frequencies. However, Timoshenko beams were considered in this research in order to include shear deflections. Thus, Timoshenko beam elements were used for the rail in this model and concrete blocks were used for modelling the sleepers. Tests for the soil models by taking into account full and half-soil models under a point load that was applied at the same location were considered. Symmetry boundary conditions were applied to the half soil model along the track, in the x-direction for this model, thus only one rail and half the track were considered. The following Figure 6.1 shows the results of the full and half-soil models, clearly indicating the exact displacement values. A half-soil model was chosen to represent the ground beneath the track, to help reduce the computational requirements, and to allow longer tracks to be modelled. The boundary conditions are explained in Section 6.3.2.

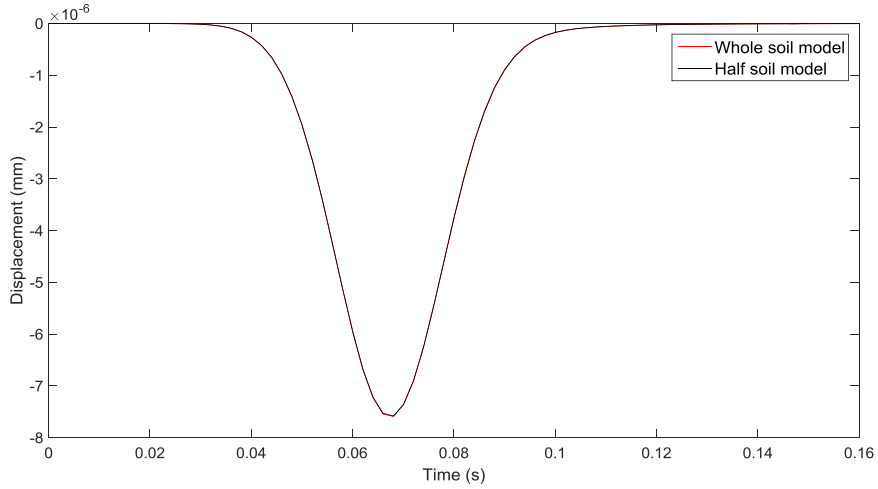

Figure 6.1 Rail displacements on the centre of the track for whole and half-soil models

In addition to soil models, another model considered different contact definitions between the rail and the sleepers, and also sleeper location in the 3D model. Table 6.1 shows the properties that were chosen for the test model. The load for one moving point load was

calculated by adding the masses of the wheel, bogie and car and multiplying the total by the gravitational force. Load application is more complicated as interaction forces between the wheel and the rail have to be considered; however, for a simple test, these forces are ignored. Sleepers were modelled on top of the ballast layer, and two rail-sleeper connections were tested: the regular tie contact and springs/dashpots provided by ABAQUS software. The use of springs/dashpots represents the railpads in the system.

Another model was developed whereby embedded sleepers were placed into the ballast and interaction was considered; however, in order to avoid contact issues between layers, it is better to model the whole track as one section. Therefore, to make it easier for the modelling process, embedded sleepers within the ballast layer, along with the other layers were considered to be one section. Figure 6.2 presents the results (close up view) of the four models. It can be noticed that the regular model, with the tie contact, and the embedded models produce a similar range of displacement values. The springs and dashpots model, on the other hand, provides slightly larger values. The railpad effect is important for highly dynamic models because of the high frequency vibrations that occur in such fields. The railpad effect will not be considered for the validation of the regular sites that do not experience resonance and large dynamic amplifications. The single part track with embedded sleepers model was adopted in the final model used for validation.

Layer	**D (m)**	**E (MPa)**	**ν**	**ρ (kg/m^3)**
Rail	-	210×10^3	0.3	7900
Sleepers	0.2	30×10^3	0.3	2400
Ballast	0.5	100	0.35	1800
Sub-ballast	0.2	300	0.35	2200
Subgrade	0.5	127	0.35	2100
Soil	8	227	0.3	2000

Table 6.1 Properties of the track and soil model

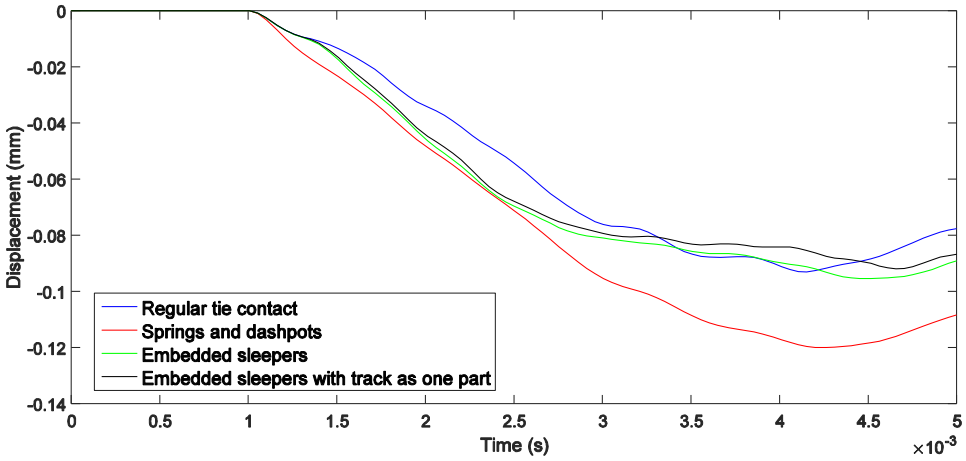

Figure 6.2 Comparison of rail and sleeper connection for different sleepers models (close up)

6.3 Finite Element Method Implementation

Since the finite element method has been proven to result in accurate prediction of the ground behaviour based on the literature review discussed in Chapter 3, it was also used for the development of this numerical approach. This section includes the time integration method chosen, material damping specifications and boundary conditions used for the soil and track systems. Then the wheel/rail interaction is discussed as it was modelled using the VDLOAD and VUFIELD subroutines provided by the ABAQUS software. The shape functions and other aspects were considered in the moving load application and added to the subroutines and explained further in the following section. Finally, this section includes initial testing of a single moving wheel application for validation purposes.

6.3.1 Explicit time integration

Time integration is widely used in wave propagation analysis using finite element approaches. The implicit time integration requires factorisation of the stiffness matrix; thus, requiring more computational effort than explicit time integration, which would use vector

computation only when using a diagonal mass matrix. For linear analysis, implicit time integration is sufficient for designing unconditional stability; however, explicit time integration is more efficient computationally for highly nonlinear and conditionally stable problems. For wave propagation analysis, the stability limit time step in the explicit analysis is related to the time required for a stress wave to cross the smallest element dimension in the model. In the case of having small elements in the material, the time increment can be very short, which makes it computationally expensive when the total response time is a few orders magnitude longer than the stability limit in dynamic problems. For this approach, explicit time integration was used. Results were obtained by executing the equation of motion (composed of C, K and M matrices) for a finite number of discrete time instants. The response (displacements and velocities) of the model at beginning and end of a time interval was obtained for multiple time instants. Once displacements and velocities at these points were obtained, initial conditions were applied to produce the acceleration results. The acceleration was calculated at time t and then used to calculate the velocity at $t + \frac{\Delta t}{2}$ and displacement at $t + \Delta t$. Explicit central-difference integration was used for the equation of motion (ABAQUS-Manual):

$$\dot{u}^n_{(i+\frac{1}{2})} = \dot{u}^n_{(i-\frac{1}{2})} + \frac{\Delta t_{(i+1)} + \Delta t_{(i)}}{2} \ddot{u}^n_{(i)} \tag{6.1}$$

$$u^n_{(i+1)} = u^n_{(i)} + \Delta t_{(i+1)} \dot{u}^n_{(i+\frac{1}{2})} \tag{6.2}$$

i is the increment number in the dynamic explicit step and u^n is the displacement where n is the degree of freedom. The values of velocity and acceleration, $\dot{u}^n_{(i-\frac{1}{2})}$ and $\ddot{u}^n_{(i)}$, are known from the previous increment. The acceleration was computed using the following formula at the beginning of the increment:

$$\ddot{u}^n_{(i)} = (M^{nJ})^{-1}(P^J_{(i)} - I^J_{(i)}) \tag{6.3}$$

For computational efficiency, a lumped mass matrix, M^{nJ} was used due to its simple inverse calculation, n is the degree of freedom. I^J is the vector of the internal force assembled from the individual elements to form a global stiffness matrix, and P^J is the vector of the applied load.

In order to ensure stability, a limit for the time increment was applied using the highest frequency, which is calculated automatically by the software. This was applied automatically in the ABAQUS software. Equations (6.4) shows the limit in case of no damping, and Equation (6.5) is the limit if damping is used, where ω_{max} is the maximum frequency and ξ_{max} is the fraction of critical damping in the mode of the highest frequency. The time increment was reduced when the damping was introduced. The time increment size is then approximated based on the smallest element dimension, L_{min}, and the dilatational wavespeed (P-wave), c_d, as presented in Equation (6.6).

$$\Delta t \leq \frac{2}{\omega_{max}} \quad \text{(Without damping)} \tag{6.4}$$

$$\Delta t \leq \frac{2}{\omega_{max}}\left(\sqrt{1+\xi_{max}^2}-\xi_{max}\right) \quad \text{(With damping)} \tag{6.5}$$

$$\Delta t \approx \frac{L_{min}}{c_d} \tag{6.6}$$

where the propagation wave speed is calculated using $c_d = \sqrt{\frac{\lambda_l+2\mu_l}{\rho}}$. For three-dimensional modelling, a factor between $\frac{1}{\sqrt{3}}$ and 1 is multiplied by the time increment to ensure a safe estimate.

6.3.2 Material damping and boundary conditions

Material damping was defined as well as boundary conditions to control the reflection of waves. Rayleigh damping was used for the material, defined as a linear combination of mass and stiffness matrices (Caughey, 1960). The parameters of Rayleigh damping are clarified as follows:

$$C = \alpha M + \beta K \tag{6.7}$$

$$\alpha_c = \frac{2\xi\omega_1\omega_2}{\omega_1+\omega_2} \tag{6.8}$$

$$\beta_c = \frac{2\xi}{\omega_1+\omega_2} \tag{6.9}$$

α_c and β_c are constants, $\omega_1$and ω_2 are the first natural frequency, and the highest value of natural frequency generated by the response vibration modes. The values chosen for the frequencies are discussed in Section 6.5.1. At lower frequencies, mass damping is considered to have a greater impact, while at higher frequencies, stiffness damping becomes the leading factor. The damping ratio is affected by the soil plasticity and that increases as the strain amplitude increases.

As the reflection of the propagating stress waves, which expand in the media of the three-dimensional model, is a source of error during the analysis stage, boundary conditions must be defined at the sides and bottom of the model to prevent this. Lysmer and Kuhlemeyer (1969) used viscous boundary conditions to ensure that radiation waves were not reflected. This technique is defined by using dashpots at the sides of the model in ABAQUS, and it has been followed in previous research (e.g. Hall (2000)).

In this research, symmetry boundary conditions were used since only half the soil model was built. The bottom of the model was fixed to allow the displacements to recover back to zero (ground level) when the load was released. For the sides, infinite elements were used instead of dashpots to prevent the reflection of waves and to control high frequency oscillations.

However, the addition of infinite elements can cause the analysis process to slow down; thus, the infinite elements were later removed and a deeper and wider soil model was used by increasing mesh size with depth (Shih et al., 2016a, 2016b). This had a similar effect to using infinite elements. Both soil models were tested and validated, as explained later in Section 6.7. The proposed boundary conditions were suitable for validating the model, even though they did not absorb all the Rayleigh waves, a small percentage of error was expected. It is important not to exceed the area of interest, because this would require a bigger mesh and more time to finalise the computational analysis (Hung & Yang, 2001).

6.3.3 Wheel-rail contact

Wheel-rail contact has been investigated in railway modelling practice, and simulations in this sector have seen rapid development and enhancements with different modifications and advancements (e.g. Kalker (2013)). The problems that are related to the modelling of wheel-rail interaction are discussed by Pombo and Ambrósio (2008) and they are classified into three categories: a) contact geometry, which relates to the contact location on the surface of the bodies, b) contact kinematics, which is related to the creepage or normalised relative velocities definition, c) contact mechanics, which is related to contact forces determination based on 3D rolling contact theories (Pombo & Ambrósio, 2004). To simplify the modelling procedure, wheel-rail contact was defined by a nonlinear Hertz's contact stress law for vertical loading forces, and the following equation demonstrates the nonlinearity between the material deformation, d, and the imposed load, N:

$$\mathrm{N} = \mathrm{K_{Hz}}\, \mathrm{d}^{3/2} \tag{6.10}$$

where the coefficient $\mathrm{K_{Hz}}$ is dependent on the radii of the arch between the rail and the wheel and the material elasticity of both bodies. A linearised model takes into account a small

variation in the deformation Δd around the nominal value of d_o. Equation (6.10) can be estimated by the following linear equation:

$$N = N_o + k_{Hz}\,\Delta d \tag{6.11}$$

With $K_{Hz} = 1\,GN/m$ in most of the studied cases, k_{Hz} is found from the nominal force N_o and the coefficient K_{Hz}

$$k_{Hz} = \left.\frac{\partial N}{\partial d}\right|_{d_o,N_o} = \frac{3}{2}\,K_{Hz}\,{d_o}^{1/2} = \frac{3N_o}{2d_o} \tag{6.12}$$

Kouroussis et al. (2014) mention that railway models are also able to use a linear alteration for this particular contact, at a certain moment in time, ignoring the dynamic behaviour of the contact for large values of wheel-rail force vibration. Equation (6.12) is frequently misused in some ground vibration models by removal of the force parameter, N_o, and applying a simpler $N - d$ law to verify the outcomes (Kouroussis et al., 2014).

6.3.4 Hermite shape functions

Hermite shape functions are generally used for calculating deflection and curvature at each element in beam analysis, and result in a higher degree of continuity than linear shape functions. For each node, the deflections and curvatures of adjacent elements must be similar to ensure a smooth transition. The derived shape functions are shown in Figure 6.3.

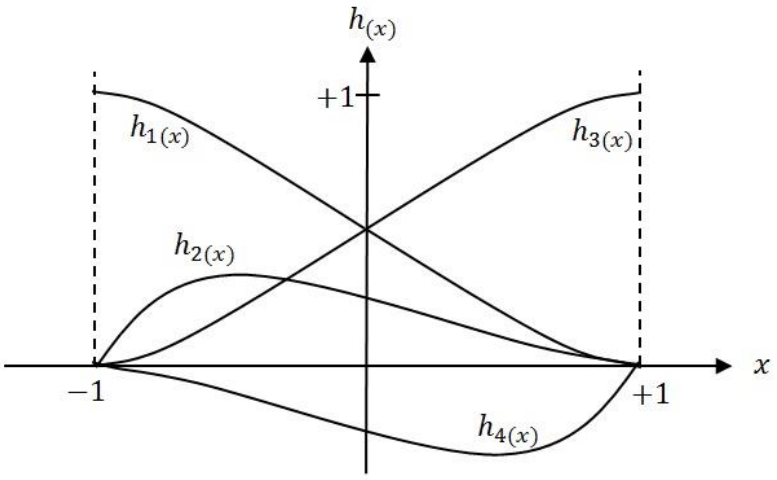

Figure 6.3 Hermite shape functions

$$H_1 = 1 - 3r^2 + 2r^3 \tag{6.13}$$

$$H_2 = L(r - 2r^2 + r^3) \tag{6.14}$$

$$H_3 = 3r^2 - 2r^3 \tag{6.15}$$

$$H_4 = L(-r^2 + r^3) \tag{6.16}$$

where L is the length of the element, $r = s/L$ and $s = x_2 - x_1$.

The software offers the usage of user-defined subroutines, which are programmed using the FORTRAN language. The VDLOAD subroutine was used to define moving, non-uniform, distributed loads. The VDLOAD code is called at every time step, providing values of nodal coordinates and solution-dependent nodal variables, such as displacements, velocities and accelerations at all defined degrees of freedom. For simplicity, element rotations can be eliminated from the code and only linear shape functions ($N_1 = 1 - r, N_2 = r$) were used in this research, as they have minimal effects on testing for high speed effects.

6.3.5 Initial testing simulations

A static point load simulation was carried out on a 3D model containing rail, track and soil models. Four point loads, representing axles of one car body, were applied to the middle of the rail element. Figure 6.4, showing the 3D model and the contour plot, presents the displacement. It is noted that the displacements develop at depth and at a distance from the rail presenting the transmission of ground waves. The purpose of testing stationary train inducing cyclic load is to assist in choosing adequate dimensions of the soil model based on transmission distance. For one car body, $4.4\,m$ depth and $3.6\,m$ width were sufficient; however, the dimensions were increased for full train systems as discussed in Section 6.5.1. In terms of track length, it was increased for moving loads depending on train speed.

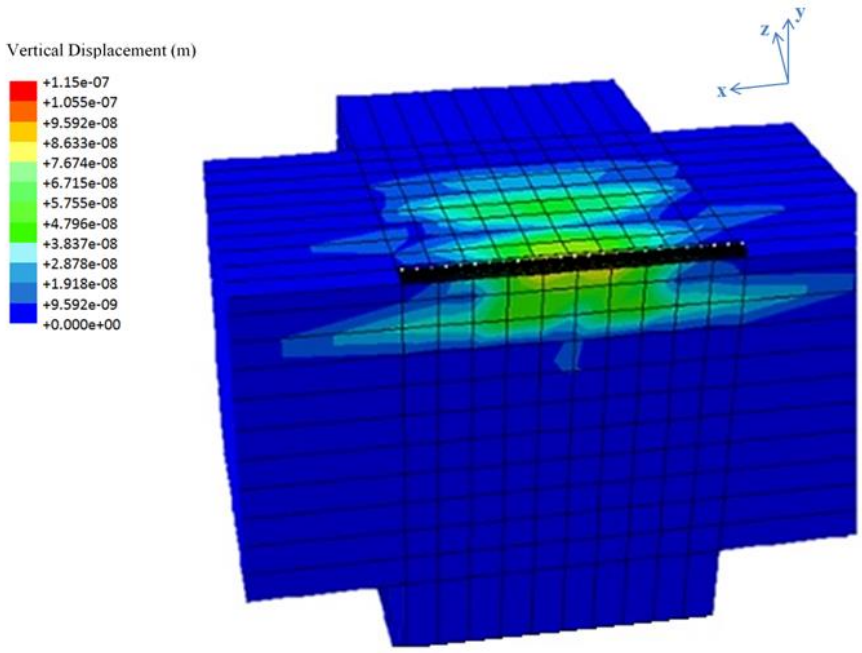

Figure 6.4 Contour plot of displacements for the initial testing model

6.4 Moving Load Application

The VDLOAD subroutine was used to define the loads for a full train system. The code allows the track length and the mesh size that is chosen for the three-dimensional model, along with the required speed and wheel numbers of the train to be inserted. A quarter-model was used to describe the dynamic loading on the vehicle. The bogie and the wheel were connected using a primary suspension system, and the bogie was connected to the vehicle body by a secondary suspension system. The interaction between the wheel and rail was modelled using a Hertzian contact spring, referring to Section 6.3.3. The interaction forces did not have a major effect on analysing for high speed effects, as the difference between maximum peak displacements was 1.04% after including contact forces for the validation cases in Section 6.7. However, to ensure a fully coupled and more accurate train system, the contact forces between the wheel and the rail were defined in the VDLOAD code. The mass, damping and stiffness values of the train system were inserted into the code, which assembled the matrices accordingly. Figure 6.5 explains the train quarter model.

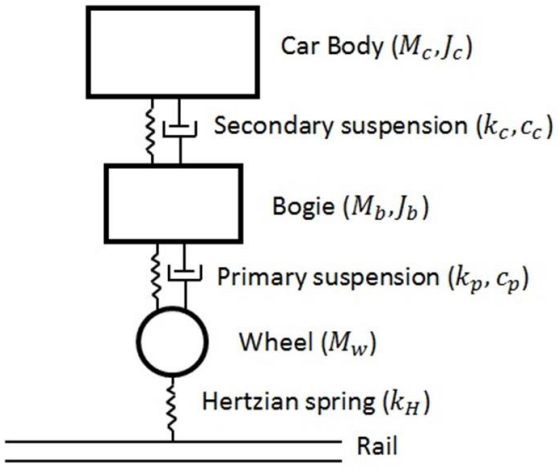

Figure 6.5 Diagram layout of the quarter-train model

The following equation of motion, Equation (6.17), was defined in the VDLOAD subroutine for the train system. The interaction force between the wheel and the rail was calculated as F_{wr}, shown in Equation (6.18).

$$\begin{pmatrix} k_c & -k_c & 0 \\ -k_c & k_c + k_b & -k_b \\ 0 & -k_b & k_b \end{pmatrix} \begin{pmatrix} u_c \\ u_b \\ u_w \end{pmatrix} + \begin{pmatrix} c_c & -c_c & 0 \\ -c_c & c_c + c_b & -c_b \\ 0 & -c_b & c_b \end{pmatrix} \begin{pmatrix} \dot{u_c} \\ \dot{u_b} \\ \dot{u_w} \end{pmatrix} +$$

$$\begin{pmatrix} \bar{m}_c & 0 & 0 \\ 0 & \bar{m}_b & 0 \\ 0 & 0 & \bar{m}_w \end{pmatrix} \begin{pmatrix} \ddot{u_c} \\ \ddot{u_b} \\ \ddot{u_w} \end{pmatrix} = \begin{pmatrix} \bar{m}_c g \\ \bar{m}_b g \\ m_w g + F_{wr} \end{pmatrix} \quad (6.17)$$

$$F_{wr} = K_{Hz}(u_w - u_r - r_{irr})^{3/2}, \quad \text{(if } u_w > u_r + r\text{, otherwise, } F_{wr} = 0) \quad (6.18)$$

k_c, k_b are the secondary and primary stiffness constants, respectively, c_c, c_b are the secondary and primary damping coefficients, respectively, u_r is the vertical displacement of the rail, r_{irr} is the rail surface irregularity, $\bar{m}_c$ is the mass of the car body and is equal to $\bar{m}_c = m_c/8$, $\bar{m}_b$ is the mass of the car body and is equal to $\bar{m}_b = m_b/4$, $\bar{m}_w$ is the mass of the wheel, and u_c, u_b and u_w are the vertical displacements of the car body, bogie and wheel, respectively. Rail surface irregularity was not considered in this research, thus, the value of r_{irr} was taken as zero. In order to test that the contact forces had been computed correctly, the interaction forces values were obtained from ABAQUS and plotted against time for the Alfa-Pendular train, in Portugal, as shown in Figure 6.6.

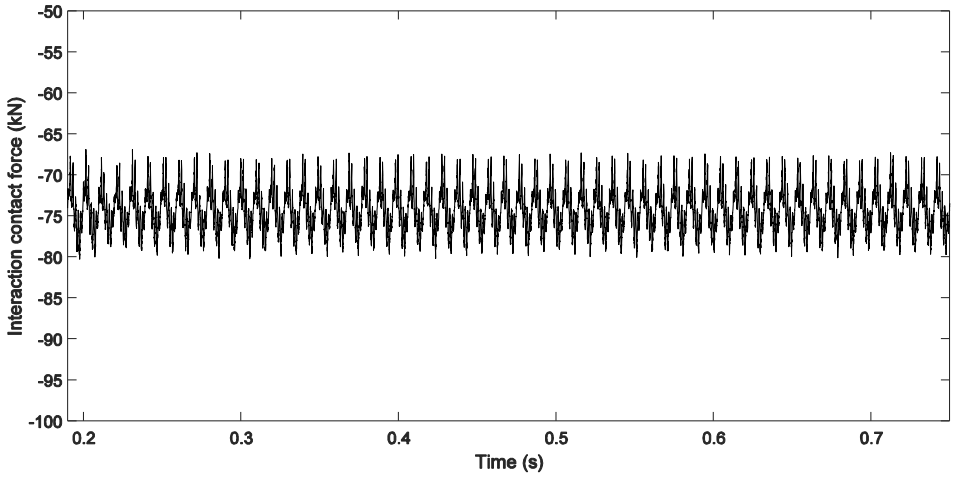

Figure 6.6 Wheel/rail contact forces (Alfa-Pendular train)

6.5 Ballasted Track Models

The trains that were used for the model validation were the Alfa-Pendular in Portugal, which operates at a maximum speed of $220\,km/h$ and the X2000 in Ledsgård, Sweden, which operates at a maximum speed of $200\,km/h$. The latter crosses organic clay and weak marine clay layers that are approximately $50\,m$ in depth. Because of these layers, the ground experienced a high response at the site, causing damage to the track during the initial testing (Costa et al., 2012b; Madshus & Kaynia, 2000). Previous research was carried out using ABAQUS for the X2000 train track, since the field test results for the site were collected for study purposes. A model by Hall (2000) was carried out to confirm the critical velocity effects with a model of $65\,m$ length and $50\,m$ depth. The analysis by Hall (2000) was performed using implicit time integration with a fixed time step of $0.001\,s$. In this research, the analysis of 3D model continued for both tracks to produce accurate results efficiently using an ABAQUS/Explicit analysis.

6.5.1 Track model

For both tracks models, the rail was modelled as a 2D Timoshenko beam that was $50\ m$ long, and the total number of beam elements was 500. The soil was modelled using two approaches: 1) $4\ m$ long infinite elements implementation on the sides, where the soil depth was $8\ m$, and the width was $12\ m$, and 2) increasing mesh size with depth, where the soil depth was $15\ m$, and the width was $20\ m$. Both approaches were tested in this research to help in preventing the reflection of waves within the model (Section 6.3.2). The results that are presented in this section are related to the latter method. 8-noded brick elements were used for the track and ground models.

The sleepers were embedded in the track model and the whole track section was modelled as one section. This helped to prevent any contact errors or discontinuities between the layers and reduced the computational requirements, which increased the efficiency of the analysis. The mesh size was $0.1\ m$, for the rail, $0.2\ m$, for the track, and $0.6\ m$, for the soil, and as mentioned earlier, the soil mesh size was increased with depth if no infinite elements were included, and the stretching factor was 1.2. For lower frequencies, the Rayleigh wavelength is large, while for higher frequencies, the Rayleigh wave does not penetrate to deeper layers, thus, small elements are only required for the upper layers. The spacing between sleepers was $0.6\ m$. Figure 6.7 shows the three-dimensional meshed models. Figure 6.8 shows the meshing increase of the models used, unlike Figure 6.7, which shows the regular meshing used when infinite elements were applied to the sides. Tie constraints were used between the bottom surface of the track and the top surface of the soil by setting master-slave formulations, which prevent the separation between the nodes; thus, there were no displacements between the surfaces. The coupling between the track and soil is governed by the finite element dynamic equilibrium formulation.

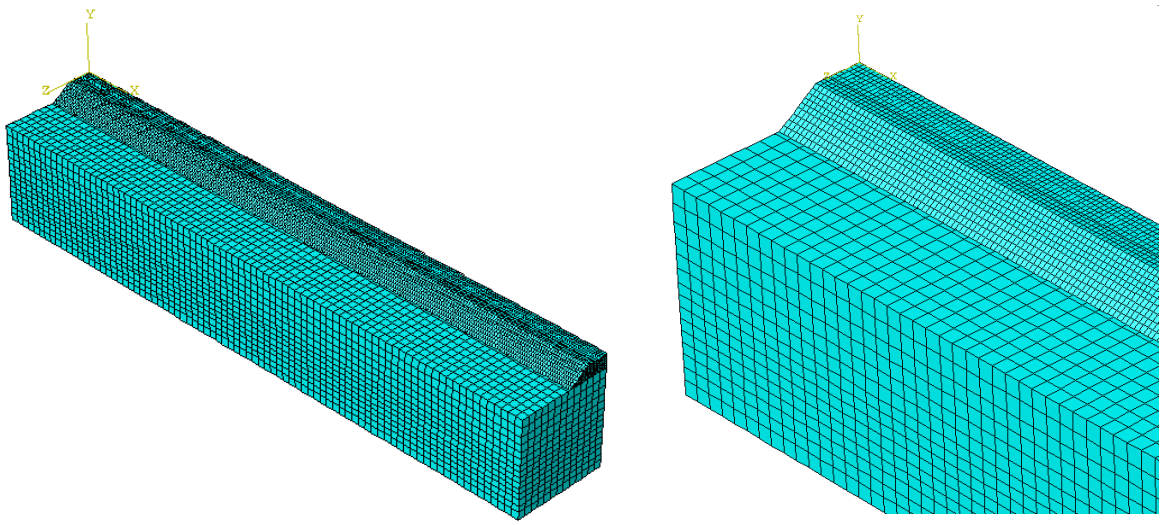

a) Whole mode

b) Close up view

Figure 6.7 3D mesh of the numerical model in ABAQUS

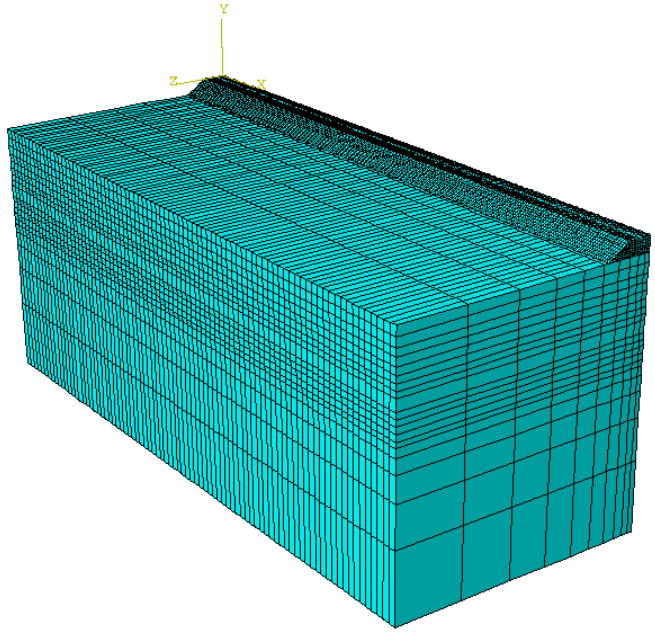

Figure 6.8 Meshing increase of the soil mode model in ABAQUS

The track and ground models for both train tracks were similarly modelled, the only differences were the depths of layers and the properties. The approximated parameters used for the track and ground are listed in Table 6.2, for the Swedish (Paolucci et al., 2003) and Portuguese tracks (Costa et al., 2012b), respectively. All the layers were considered homogeneous in this research for simplicity. For soil layers of the Portuguese track, field tests were used to collect the parameters of the soil layers by Costa et al. (2012b). In this model, soil layers up to $8\,m$ in depth were defined, only the top four soil layers were presented in Table 6.2. The parameters α and β for the Rayleigh damping are presented in Table 6.2, and they were calculated using Equations (6.8) and (6.9) (Section 6.3.2). The frequencies were taken as $\omega_1 = 5\,Hz$ and $\omega_2 = 20\,Hz$, which are in the range of the maximum vibration spectra that was measured (Costa et al., 2010; Hall, 2003). The damping ratios that are used in Rayleigh damping calculations for both sites are shown in Table 6.2 (Costa et al., 2012b; Hall, 2003).

Layer	**D (m)**	**E (MPa)**	**ν**	**$\rho(kg/m^3)$**	**ξ (%)**	**α**	**β**
X2000 track							
Top ballast	0.5	124	0.4	1800			
Embankment	0.5	430	0.3	1900			
Crust	1	20	0.491	1500	7	0.365	0.006
Organic clay	3	6	0.498	1250	4	0.209	0.0035
Marine clay	4	24.5	0.498	1470	7	0.365	0.006
Alfa-Pendular track							
Top ballast	0.57	97	0.12	1590			
Sub-ballast	0.55	212	0.2	1910			
Soil 1	1.4	93	0.488	2000	3	0.157	0.0026
Soil 2	1.2	85	0.493	2000	3	0.157	0.0026
Soil 3	1.1	143.3	0.491	2000	3	0.157	0.0026
Soil 4	0.9	109.1	0.494	2000	3	0.157	0.0026

Table 6.2 Properties of the Swedish and Portuguese track models (Costa et al., 2012b; Hall, 2000; Sheng et al., 2003)

Since the analysis was linear, the stiffness of the soil was altered for the Swedish site as the speed increased, in order to account for nonlinearity following the equivalent linear approach

proposed by Costa et al. (2010). The method suggests reduced shear modulus for sites with high strains (from $10^{-4}\ to\ 10^{-2}$). Figure 6.9 shows the shear modulus degradation curves with the increase in cyclic shear strain (Costa et al., 2010), where G_{sec} is determined at maximum stress and strain, and G_{max} corresponds to the reduced shear modulus as the loading increases. Figure 6.10 shows the stress-strain path under cyclic loading, where the slope of the stress-strain curve represents the shear modulus and the area of the loop represents the dissipation of energy in relation to the damping. In Figure 6.9, laboratory triaxial tests were carried out for the organic clay layer, and field measurements for the other layers. The embankment curve was provided by Costa et al. (2010) following Rollins et al. (1998) and Hardin and Kalinski's (2005) work for gravels properties.

After running the linear analysis for different speeds, the maximum octahedral shear strains were calculated for each element with depth for the three layers: crust, organic clay and marine clay. The maximum value in each layer was then selected. Effective octahedral shear strains, γ_{eff}, were calculated from Equation (6.19) (Halabian & Naggar, 2002; Lysmer et al., 1974) where ε and γ are the normal and shear strains, respectively, and R is a parameter between 0.5 and 0.7 and it is assumed to be equal to 0.65 in seismic analyses. The curves in Figure 6.9 were then used to obtain the new properties based on the maximum effective octahedral shear strain in each of the three soil layers. The procedure takes multiple iterations until a small percentage between the G_{sec}/G_{max} values is obtained from consecutive iterations. In this case, an average of 8.5% was obtained for the three layers. This method was only applied to the Swedish track model in this research since the site is highly nonlinear compared to the Portuguese site. In order to produce more accurate results, Costa et al. (2010) suggest following this procedure for every element in the cross section; however, this was not implemented in this research to reduce computational time.

$$\gamma_{eff} = R\frac{1}{3}\sqrt{(\varepsilon_{11}-\varepsilon_{22})^2+(\varepsilon_{11}-\varepsilon_{33})^2+(\varepsilon_{22}-\varepsilon_{33})^2+6(\gamma_{12}^2+\gamma_{13}^2+\gamma_{23}^2)} \qquad (6.19)$$

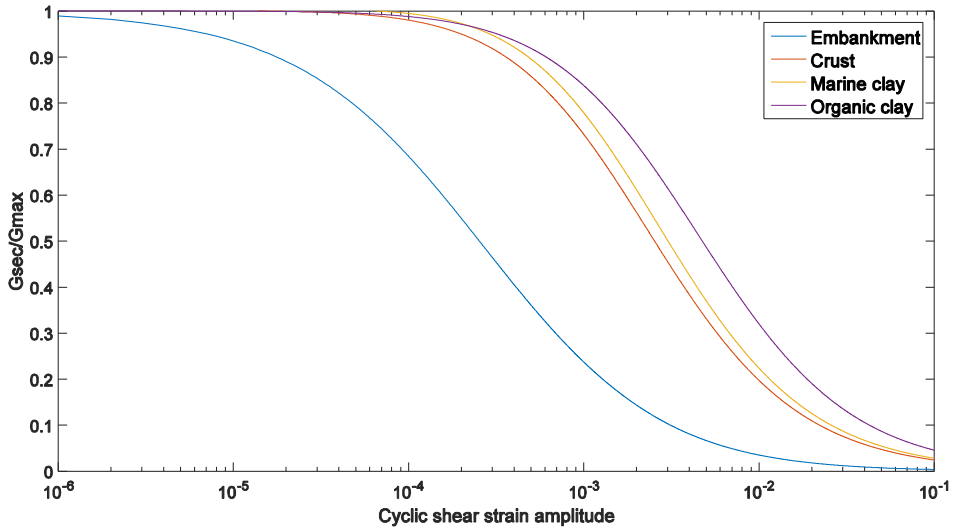

Figure 6.9 Shear modulus reduction curves (Costa et al., 2010)

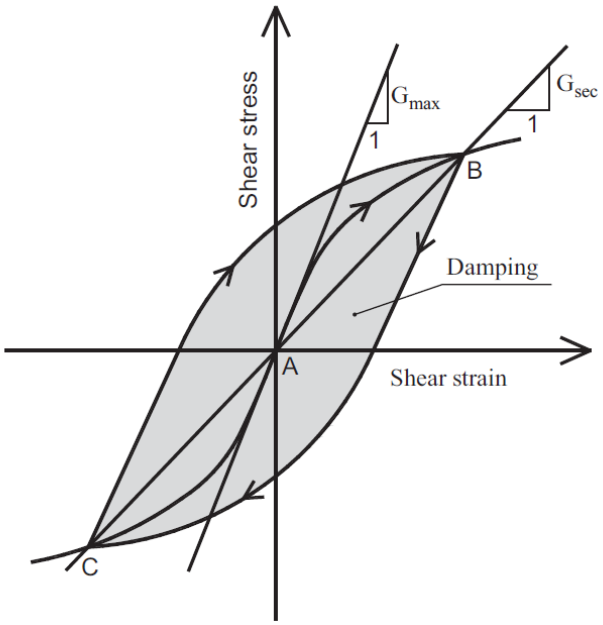

Figure 6.10 Shear-strain path during cyclic loading (Costa et al., 2010)

6.5.2 Train model

There are 20 axle loads in the X2000 train (5 carriages), and 24 axle loads in the Alfa-Pendular train (6 carriages). The axle loads of the X2000 train are shown in Table 5.2, from Chapter 5, Section 5.3. The load of the Alfa-Pendular is calculated from the average car, bogie and wheel masses, as shown in Table 6.3 (Costa et al., 2012b). Figure 6.11 shows the geometry and axle spacing of the train. Section 5.3 shows the geometry of the X2000 train.

Explicit time integration was carried out with a total time of $4\,s$, and the time steps were calculated automatically using ABAQUS as discussed in Section 6.3.1 based on Equations (6.4 to 6.6). The time increments were equal to 4.37×10^{-6} s and $8.38 \times 10^{-6}\,s$ for the Swedish and Portuguese tracks, respectively.

Component	**Mass (kg)**
Car body	$32900 - 35710$
Bogies	$4712 - 4932$
Axles	$1538 - 1884$

Table 6.3 Train properties of the Alfa-Pendular train (Costa et al., 2012b)

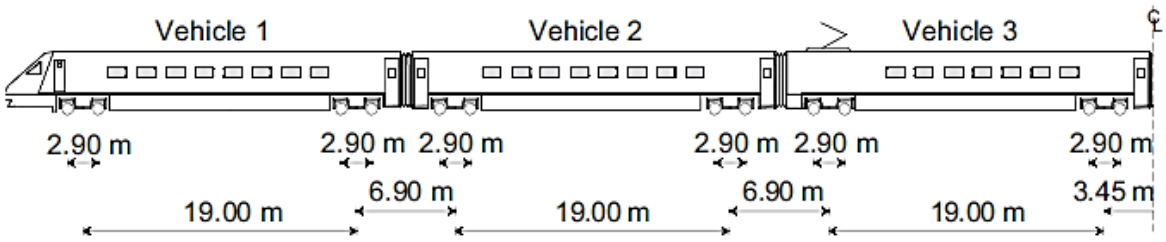

Figure 6.11 The geometry of the Alfa-Pendular train (Costa et al., 2012b)

6.6 Slab Track Models

Slab tracks were developed in ABAQUS in order to study the effect of track type on high speed effects. The properties chosen for the slab track are similar to the ones used in Section 5.4.1 from Chapter 5. Figure 6.12 shows the cross section of the slab track, including the Hydraulically Bonded Layer (HBL) and Frost Protection Layer (FPL). The X2000 train was run on the slab track model and the comparisons of the behaviour between the ballast and slab tracks is discussed in Chapter 7.

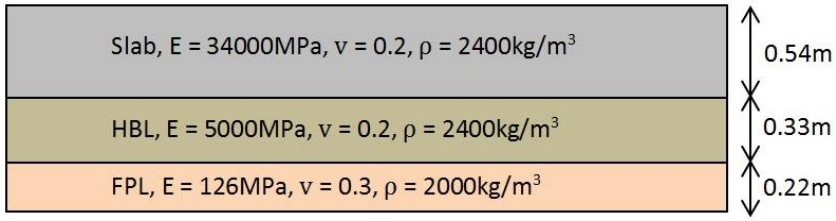

Figure 6.12 Cross section of the slab track

6.7 Ballasted Track Models Validation

It is important to validate the models before carrying on with the analysis and comparisons to ensure the ability to produce an accurate track response. This section includes the validation of the ballasted track models for both, the Swedish and Portuguese tracks, by comparing the numerical model results with the actual field. The results are mainly presented by plotting the rail displacements against time. Velocity results were also calculated for the Portuguese track model and compared to the ones processed from the site tests. The results have satisfactory outcomes in capturing the response as presented in this section.

6.7.1 Portuguese track validation

The two models, for the Swedish and Portuguese tracks were run for linear analysis. The approximate duration of the runs was six hours in ABAQUS for selected points on the rail, track and soil layers. The vertical displacement and velocity response of the Portuguese track were plotted against time in Figure 6.13 and Figure 6.14, respectively. For both figures, the simulation outcomes were compared to field results obtained from experimental tests (Costa et al., 2012b). Even though the vibrations before and after the passage of the train are not clearly identified, the deflections are in good agreement with the calculated results as shown in Figure 6.13. For the velocity response, Figure 6.14, the amplitudes of the computed model results were slightly lower than the field results; however, the outcomes were almost identical. The positive values in the displacement figures indicate the track uplift, showing peaks ranging from $0.09\ mm$ to $0.12\ mm$.

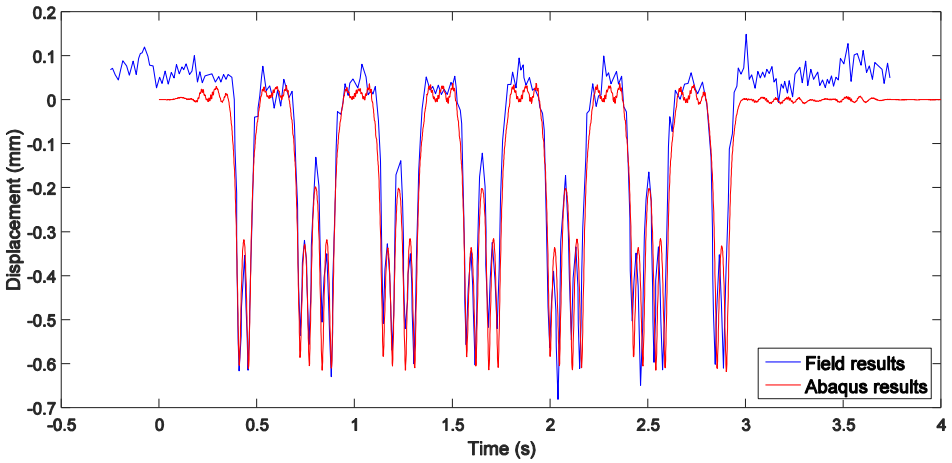

Figure 6.13 Vertical displacement response (Portuguese track)

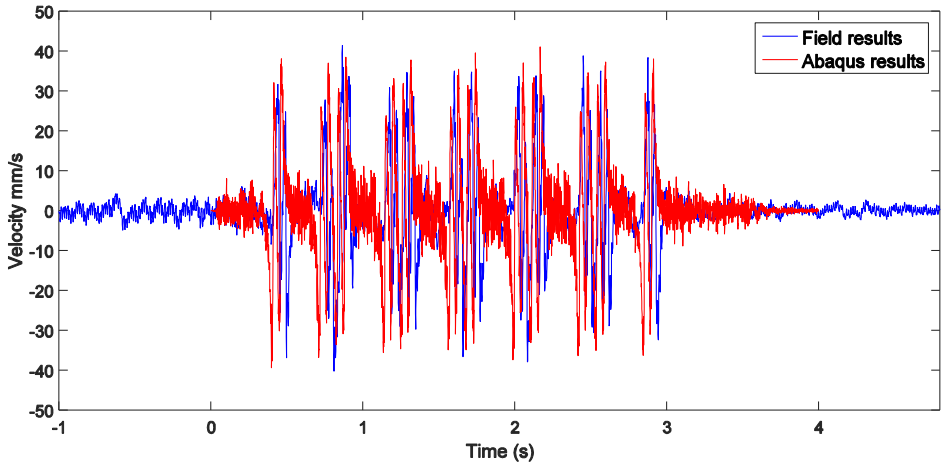

Figure 6.14 Vertical velocity response (Portuguese track)

The displacement and velocity responses of the Portuguese track were plotted in the frequency domain. In order to convert the time domain results obtained from ABAQUS, Fourier transform was applied using MATLAB. The values of the signals were then plotted in absolute values against the frequency. Figure 6.15 and Figure 6.16 show the displacement and velocity frequency plots, respectively.

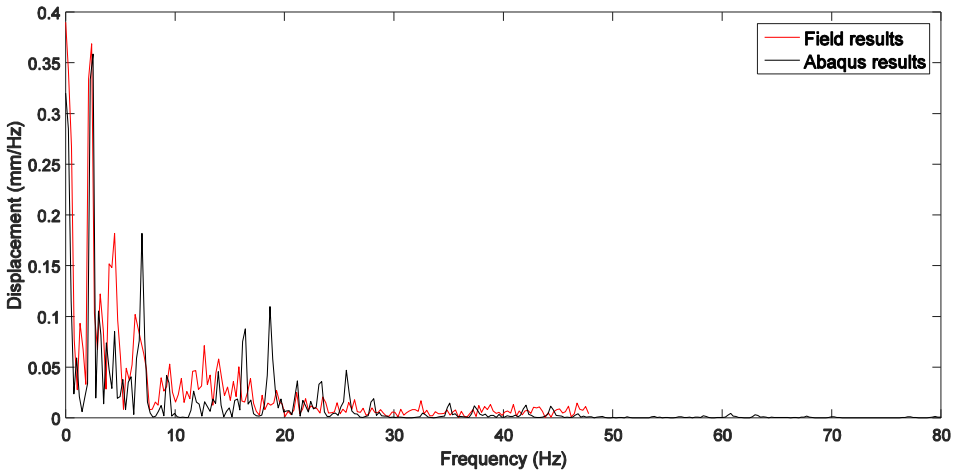

Figure 6.15 Displacement response in the frequency domain (Portuguese track)

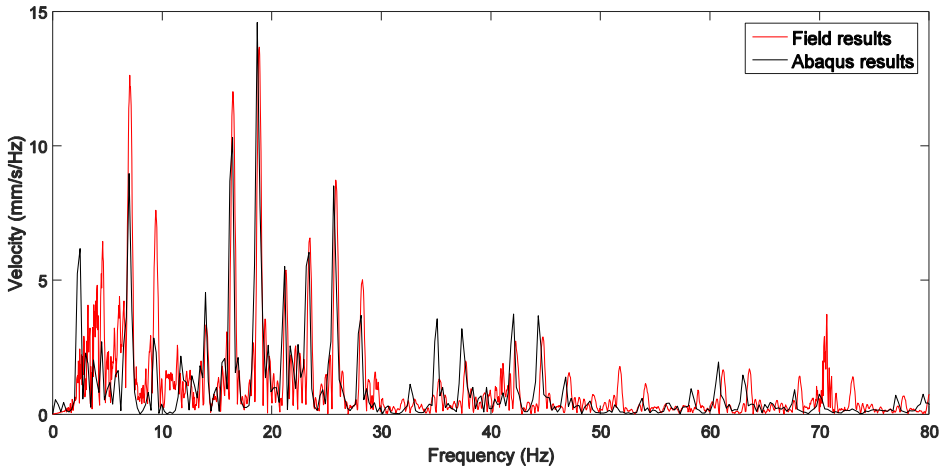

Figure 6.16 Velocity response in the frequency domain (Portuguese track)

There is a good agreement between the frequency response for both displacement and velocities values; however, the frequency contents are not fully reliable as differences in peak values are observed in the range $8-30$ Hz, for the displacement response, and the range $3-10$ Hz, for the velocity response. Even though the magnitudes are different for higher frequencies, dominant frequencies agree for the displacement and velocity frequency contents. The differences in results are related to the excitation method, irregularities and track nonlinearity.

6.7.2 Swedish track validation

The Swedish National Rail Administration (Banverket) provided the field tests results for the Ledsgård site for the X2000 train (Madshus & Kaynia, 2000). The model was run at a speed of $19\,m/s$ (not the maximum speed of the train) for validation purposes, and the vertical response was compared to the field results in Figure 6.17. The deflections show a good agreement with the field results, even though the site is known for high dynamic amplifications and low stiffness of soil layers. This proves that the model can achieve good

results without a deep soil model for lower speeds as modelled previously (Hall, 2000), thus making it more time efficient.

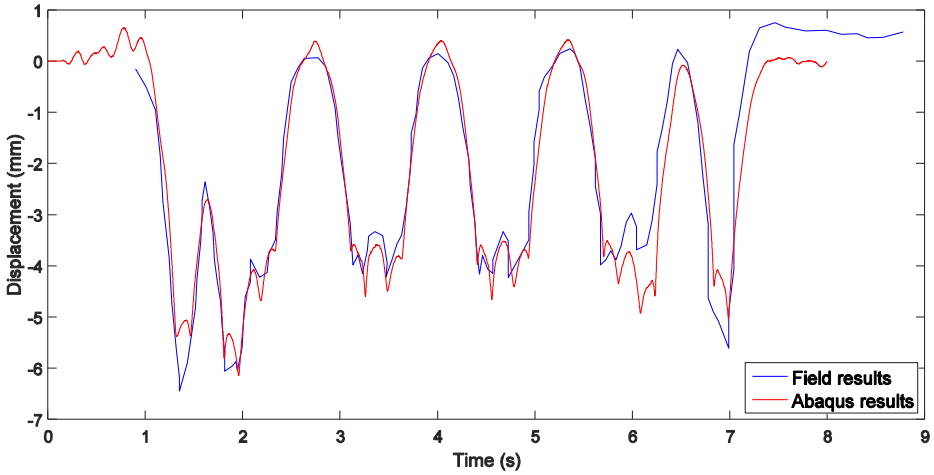

Figure 6.17 Vertical displacement response for 19 m/s speed (Swedish track)

Figure 6.18 shows the results of a linear analysis for a higher speed for the Ledsgård site (speed 51 m/s). It is important to note the track uplift is larger than the ones obtained from the Portuguese track (approximately 5.1 mm from the actual field results). Since it is a linear mode, the differences between the results are higher than the results for the lower speed. The pattern shows agreement between the calculated results and the field test results, considering the site is highly dynamic. For the Swedish track, the site is approaching critical velocity, unlike the Portuguese site, which has stiffer soil.

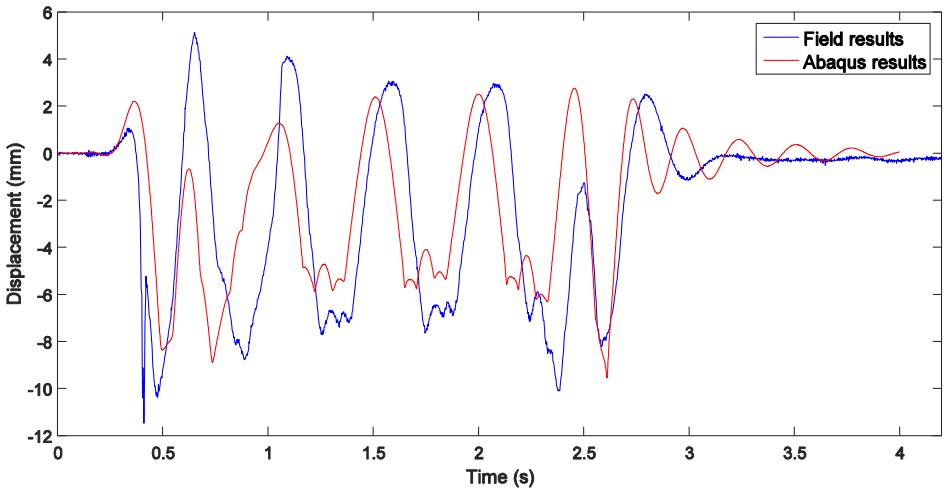

Figure 6.18 Vertical displacement response for 50 m/s speed (Swedish track)

Since the track at this speed is producing large vibrations and uplifts, it was modelled with springs between the rail and sleepers for consideration of the railpads effects. The springs had a stiffness of 3.8 Mpa. Figure 6.19 shows a comparison between the models: with and without the railpads. It can be noticed that the behaviour of the first part improved after introducing the railpads as the difference in displacement values between the actual field results and the numerical model was 2.1 mm at 0.6 s (5.8 mm without the railpads). However, the last section resulted in higher amplifications compared to actual field results with a difference in the results, namely 6.7 mm at 2.53 s (4.1 mm without the railpads). Due to the improvement in the pattern of the results, the railpad definition was considered in any model relating to the Swedish track in Chapter 7. Figure 6.20 shows the DAF curve for the Ledsgård site for different speeds. The DAF curve shows that the equivalent linear method is able to predict the behaviour of the ground at different speeds with high accuracy. The maximum speed of the train in the numerical models was extended to investigate the behaviour after passing the critical speed. The displacements began to decrease after passing the critical velocity of 56 m/s, as expected. Figure 6.20 also shows the results of the semi-analytical approach developed in Chapter 5 in comparison with the numerical approach results. At a speed of 56 m/s, the semi-analytical model results in an overestimation of the uplift value by 20%. Similarly, at a speed of 44 m/s, an overestimation is noticeable

between the semi-analytical and numerical models results for the deflection and uplift. However, both models are in agreement with the field results.

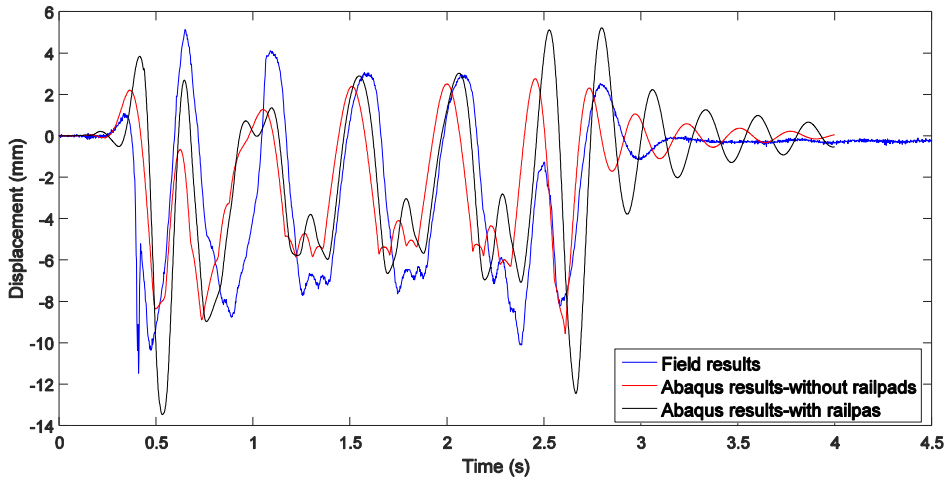

Figure 6.19 The effect of railpads modelling on the vertical displacement response for speed $50\ m/s$ (Swedish track)

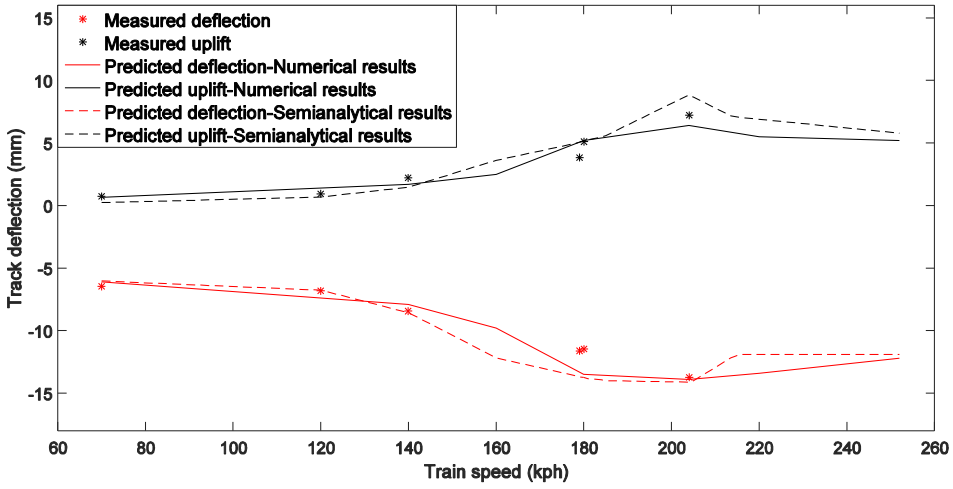

Figure 6.20 Peak deflection for the measured and predicted results from the numerical and semi-analytical approaches (Swedish track)

6.8 Summary

The main objective of this chapter was to create a 3D numerical model of the track that results in an accurate ground response in order to study critical velocity effects. The finite element analysis was carried out using ABAQUS. Different types of track were modelled: ballasted and slab tracks. The ballasted track models for the X2000 train in Sweden, and the Alfa-Pendular train in Portugal were validated against experimental field results. The following points were considered during the modelling process:

- Explicit time integration was followed since it is more accurate for nonlinear problems, and it also requires less computational effort than implicit analysis that requires factorisation of stiffness matrices.
- A half-soil model with symmetrical boundary conditions was used to reduce the computational effort.
- Infinite elements or increased mesh size with depth were used to prevent the reflection of the waves.
- The train model and the application of loads were implemented using subroutines VDLOAD and VUFIELD provided by ABAQUS.
- Contact forces between the rail and the track were also considered in the subroutine to produce more accurate results.
- Equivalent linear analysis was sufficient to predict high velocity effects based on validation outcomes.
- The effects of railpads were considered in modelling highly nonlinear sites as they affect the response when critical velocities of the site are reached.

The computed response outcomes of the models are in good agreement with the field results. Displacement and velocity responses were tested, which proves that the method is efficient for predicting the ground behaviour under critical velocities. The analysis of different types of tracks and other effects will be discussed further in Chapter 7.

Chapter 7 Analysis of Simulations

7.1 Introduction

Fully coupled 3D numerical approach was developed in Chapter 6 in order to predict critical velocity effects and analyse them. After validating the models successfully, this chapter includes stress analysis of ground behaviour and comparisons between different modifications to the models. For the Swedish track, the Mach cone phenomenon is discussed further since it is noted clearly at the Ledsgård site. Furthermore, the stresses in the ground levels beneath the track are checked for the organic clay layer.

The following sections discuss the mitigation strategies to be followed at the sites to reduce the critical velocity effects. Being able to model the mitigation strategies is extremely important for the industry as the information gleaned can be used for future projects in order to reduce costs and maintenance. The Swedish track has already been improved by installing stone columns beneath the ground, which have worked to greatly reduce the vibrations (Holm et al., 2002; Madshus et al., 2004), so the Swedish track model is used in this section. To begin with, there is a discussion of how these stone columns were introduced into the 3D model for the X2000 train track in ABAQUS. After that, a description of how the properties and depth of these stone columns were changed to study the effect of the change on the site is included.

In addition, the chapter also includes consideration of slab track models. The slab tracks replace the regular ballasted track at the Ledsgård site model in order to allow the effect on ground vibrations to be studied. Additionally, the chapter includes how the asphalt models were applied to the same site and conclusions were drawn for the most effective mitigation methods for a highly nonlinear railway track. Furthermore, how asphalt models were developed with various asphalt layer depths to study the effect on the ground behaviour is considered. This chapter also considers the displacement response of various points on an

asphalt track before and after weak soil transition area, and on the transition areas. There are other different mitigation strategies and track improvement methods that can be applied to railway tracks (e.g. reinforcement using polymer geocomposites); however, for highly nonlinear sites, it is concluded that treating the ground layers (e.g. stone columns) is more effective for vibration reduction than track improvement alternatives (e.g. slab tracks or asphalt layers) based on the outcomes of this chapter.

7.2 Analysis

Critical velocities result in different effects including ground Mach cone and surface vibrations, and track uplift. The displacement plots are shown in Section 6.7 (Figure 6.17 and Figure 6.19). For the Swedish track, the stresses are analysed underneath the rail at different elements. Furthermore, observations of the ground Mach cone and surface vibrations are presented on a contour plot of the 3D model.

7.2.1 Stress analysis for the Swedish track

Studying stresses in elements is important for understanding how the soil deforms. The normal and shear stresses are obtained from ABAQUS software for two elements of the Swedish railway track model. The elements are located beneath a sleeper in the middle of the track: the first element is 1 m deep (top of the crust layer) and the second element is at a depth of 2.6 m (in the organic clay layer). The elements beneath the sleepers have higher stresses than the ones located between sleepers due to load transmission. Figure 7.1 and Figure 7.3 show the normal stresses, and Figure 7.2 and Figure 7.4 show the shear stresses, for Elements 1 and 2 at a speed of $56\ \mathrm{m/s}$, respectively. In ABAQUS, the positive stress values indicate tension and the negative values indicate compression. The subscripts of σ: 11, 22 and 33 refer to the x-direction, y-direction and z-direction, and 12, 13 and 23 refer to the xy-plane, xz-plane and yz-plane as explained in Figure 2.5.

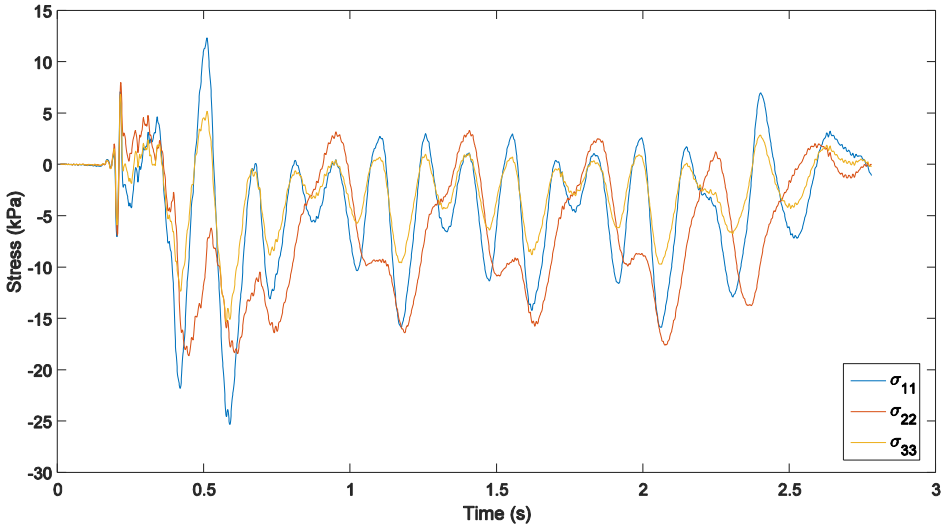

Figure 7.1 Normal stresses of Element 1

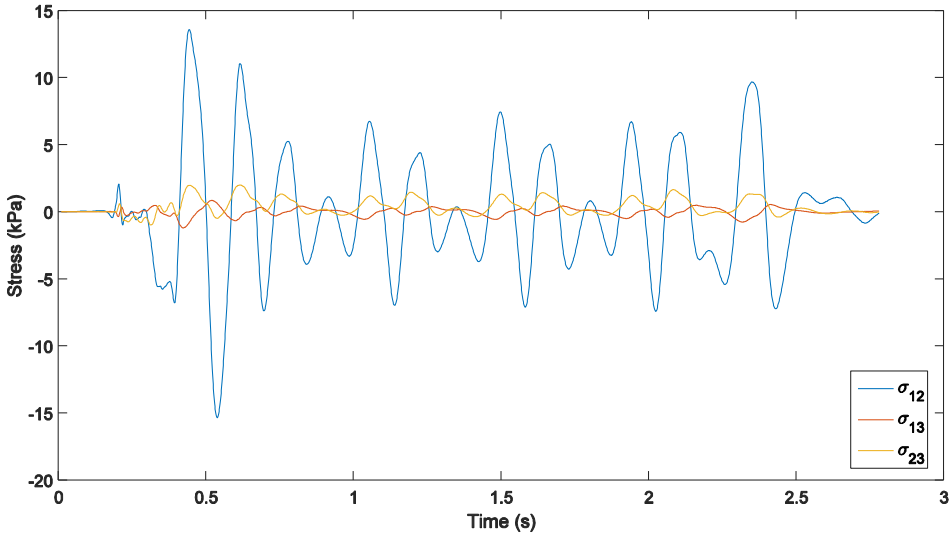

Figure 7.2 Shear stresses of Element 1

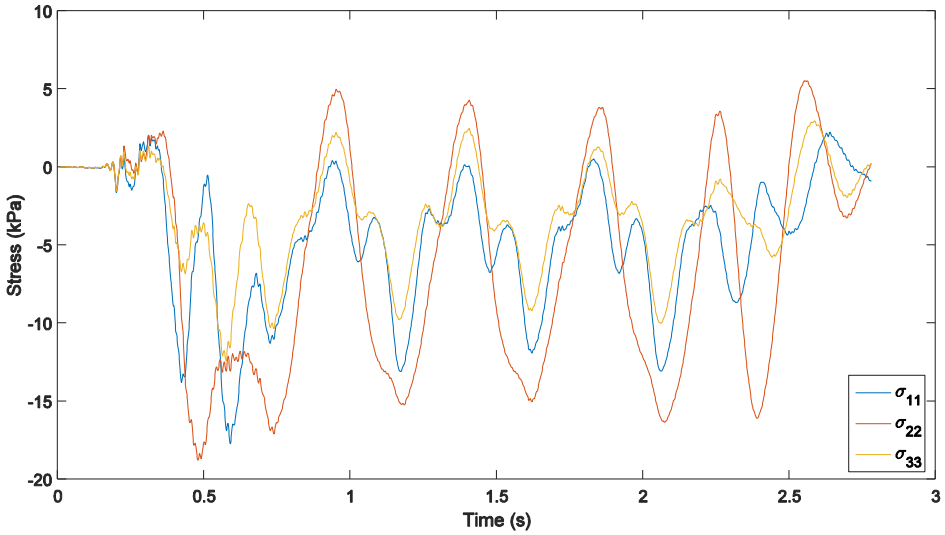

Figure 7.3 Normal stresses of Element 2

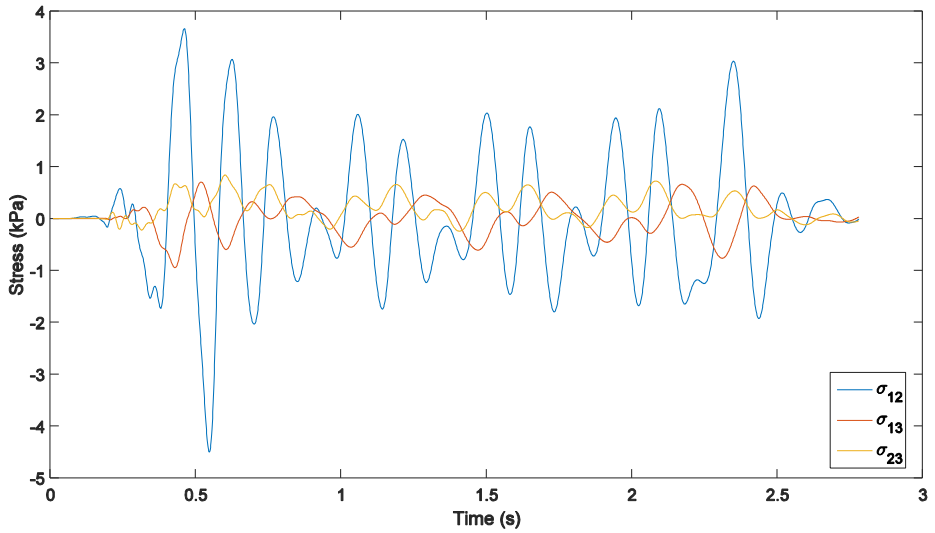

Figure 7.4 Shear stresses of Element 2

From Figure 7.1 to Figure 7.4, the normal stresses were more significant than shear stresses, with σ_{11} being the dominant normal stress for Element 1. For Element 2, the three normal stresses gave similar values, as this element is deeper in the soil than Element 1 which was

located in the embankment. Thus, the dominant normal stress for Element 1 was in the same direction as the train passage (x-direction for this model). It was also noted that the dominant shear stress is σ_{12}, which was also due to the train passage and occurred vertically in the direction of the applied load. The stress values, in general, decrease when the depth of the element increases.

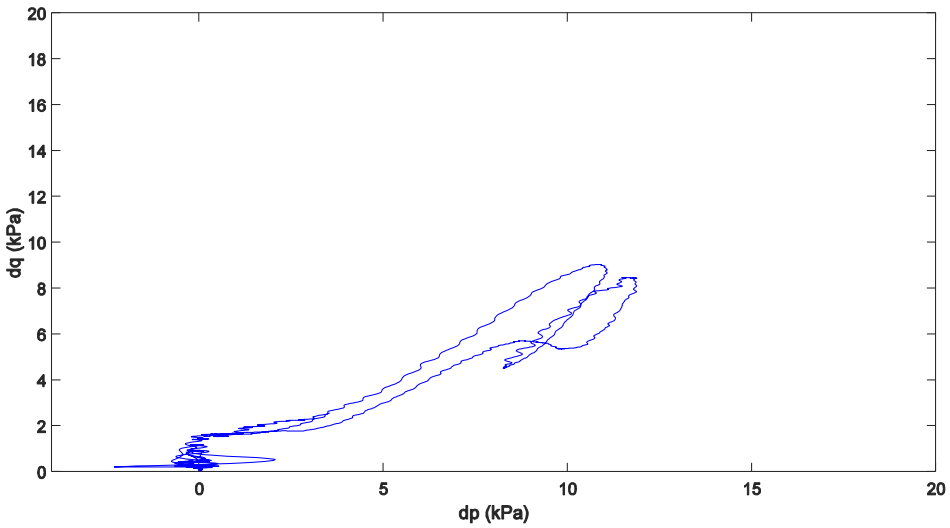

a) Speed 19 m/s

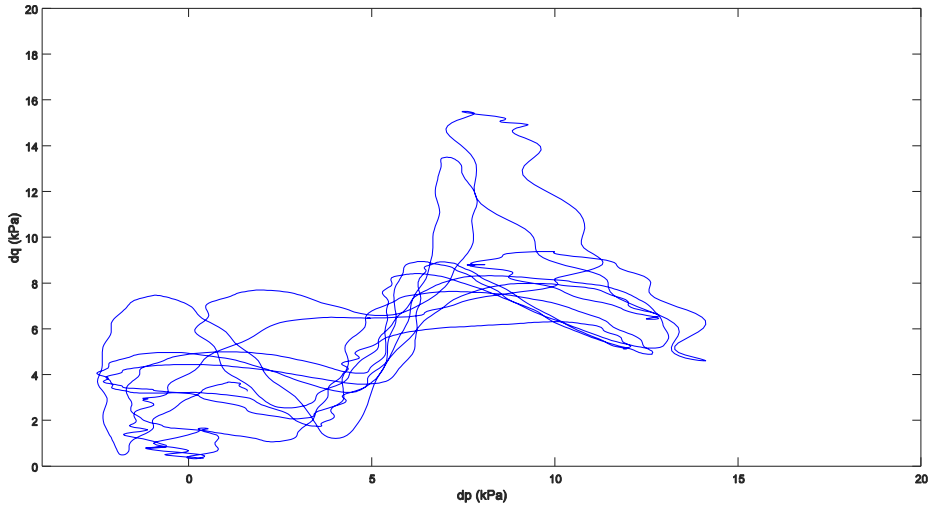

b) Speed 56 m/s

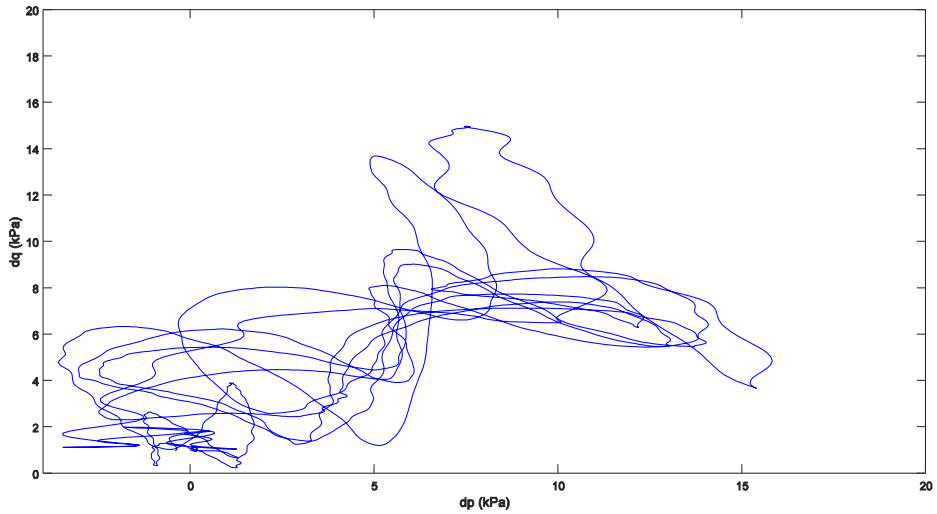

c) Speed 61 m/s

Figure 7.5 Stress path at depth 2.6 m in the organic clay layer during train passage for speeds

In addition, the stress paths are plotted for Element 2 (depth 2.6 m) in the organic clay layer (Figure 7.5). The stress paths are presented using Equation (2.9) for the mean stress (dp), and Equation (2.13) for the shear stress (dq) referred to in Chapter 2. Figure 7.5 shows the changes in the stress path between speeds (a) 19 m/s and the critical speed of (b) 56 m/s, in addition to an extra speed of (c) 61 m/s. The figures show that the stress path is dependent on the train speed, as the mean and shear stress increased with the increase in train speed. For speed 19 m/s, the loading and un-loading which follows the wheel passage can be clearly identified. However, the stress distribution shows a dynamic response rather than a quasi-static stress pattern (the loading and un-loading cannot be identified) as the train speed reaches the critical velocity. This is due to the dynamic effects and change of stress state in the soil due to the train passage at higher speeds. It is noted that the shear stress increment is slightly reduced as the train speed increases from 56 m/s to 61 m/s. The outcomes agree with the discussions of Costa et al. (2010) and Yang et al. (2009). It is important to note that these stress paths follow the theory of elasticity (Costa et al., 2010).

The stress values would be different if a nonlinear analysis was used, due to the varying properties of the soil depending on deviatoric stresses and atmospheric pressure (Varandas et al., 2016).

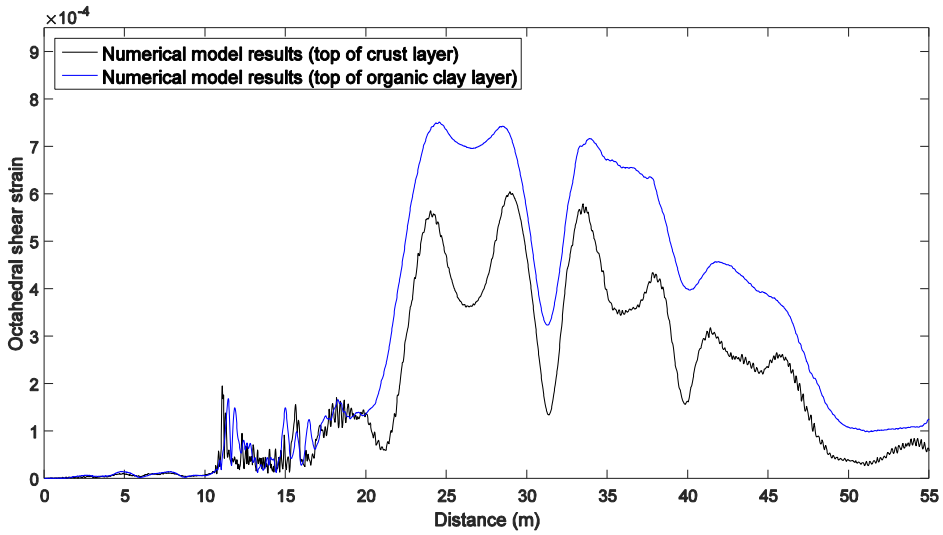

a) Speed 19 m/s

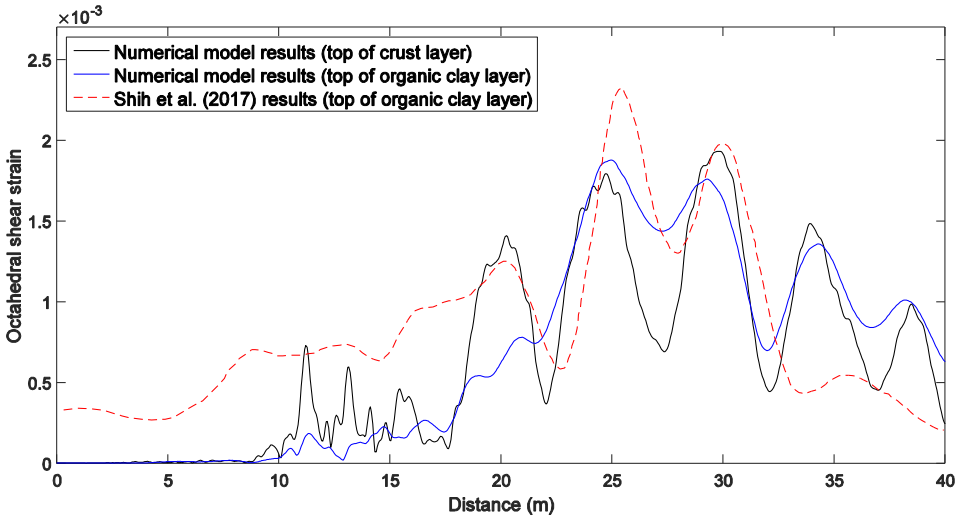

b) Speed 51 m/s (Shih et al., 2017)

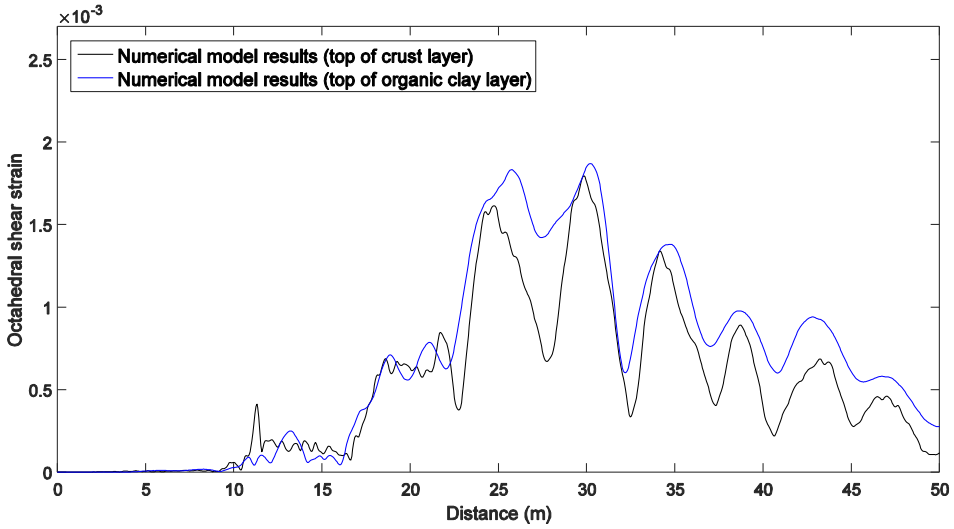

c) Speed 56 m/s

Figure 7.6 Octahedral shear strain variation over distance below the rail on top of the crust and organic clay layers for speeds

Figure 7.6 shows the octahedral shear strains calculated from Equation (6.19) for speeds 19 m/s, 51 m/s and 56 m/s along the track length for the ground surface and top of the organic clay layer. The maximum amplitudes occur at the passage of the first car, as presented in the figures. The strain level is compared against the results of an equivalent nonlinear model obtained by numerical analysis by Shih et al. (2017) for speed 51 m/s (Figure 7.6 (b)) at the top of the organic clay layer. The maximum amplitude produced in this research was 24% lower than the nonlinear model for a speed of 51 m/s. The difference in results occurred as the equivalent linear method in this research was implemented based on the maximum effective octahedral shear strain of the entire layer. This can be minimised by reducing the stiffness of every element in the cross section (Section 6.5.1). The maximum octahedral shear strains were plotted with depth in Figure 7.7 for the same three speeds. It was observed that the maximum values occurred in the organic clay layer dropping from 2.29×10^{-3} to 0.65×10^{-3} at the bottom of the organic clay layer, indicating the increase of shear strain levels according to soil softness. The results of the nonlinear model by Shih et al. (2017) are also compared in Figure 7.7 for speed 56 m/s. For

this speed, the maximum results produced in this research were 34.1% and 16.5% less than the nonlinear model for the top and bottom of the organic clay layer, respectively. The outcomes show that the equivalent linear models are capable of producing good results with slight differences in comparison to nonlinear models.

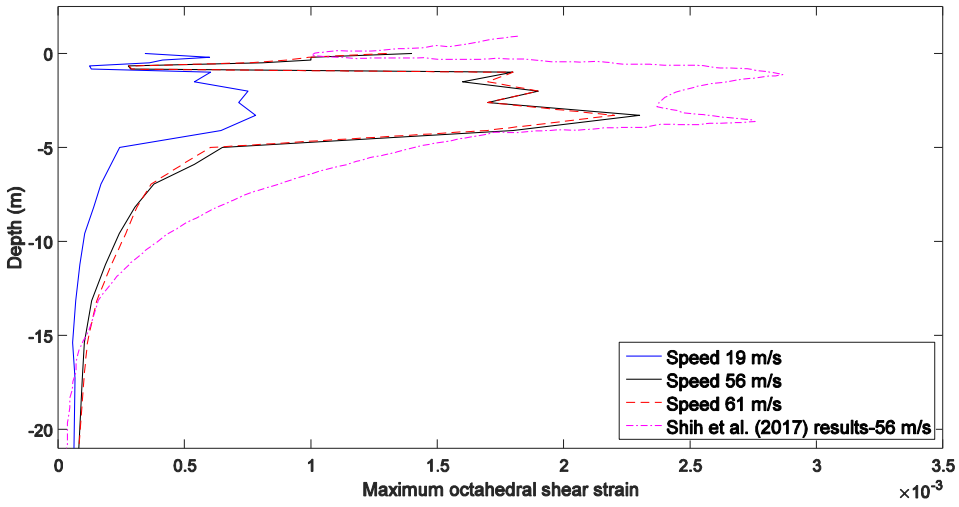

Figure 7.7 Maximum octahedral shear strain variation over depth for three speeds: 19 m/s, 56 m/s (Shih et al., 2017) and 61 m/s

7.2.2 Ground Mach cone

As mentioned, the critical velocity effects include track vibrations, track uplift and wave transmission. Figure 7.8 shows a 3D contour plot of the Swedish track model running at critical velocity, presenting the wave transmission away from the track (up to 7 m away from track centre) and at depth (up to 9.5 m in depth). The figure shows the amplified response for running a train at critical velocities over weak soil, as the soil deflections extend to 9.5 m depth with an average displacement of 2.36 mm. Referring to the ground Mach cone phenomenon (Section 2.5.1), Figure 7.9 shows a contour plot from an overhead perspective, indicating the surface Rayleigh wave transmissions and Mach cones forming as the train

passes by. Figure 7.9 indicates the Mach cone angle, which is approximately 45° for critical conditions (Equation 2.16).

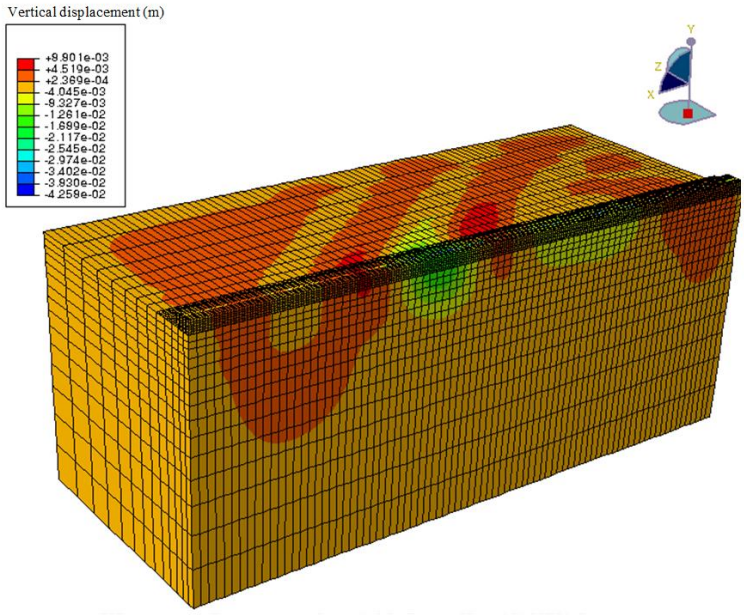

Figure 7.8 3D contour plot at a speed of $50\ m/s$ (X2000 train on the Ledsgård track)

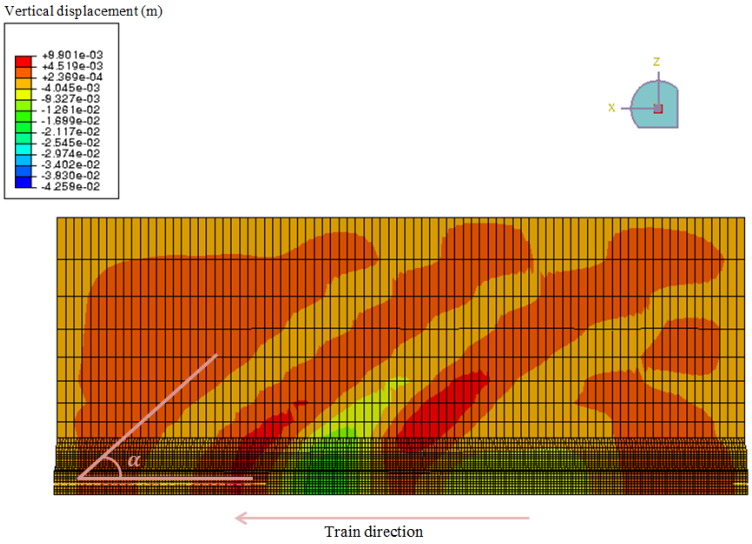

Figure 7.9 Plan view of the contour plot

7.3 Mitigation Strategies

This section includes three mitigation methods that could be applied to reduce vibrations. They were applied to the numerical model in ABAQUS for the Swedish track in order to compare their effect on the displacement response at a speed of $51\ m/s$.

- Stone columns: this method was followed in the actual field at Ledsgård. Changes were applied to the model in terms of different column properties and depths. This method is considered cheap in terms of the materials used; however, it is highly time consuming to install the columns in the ground beneath the track.
- Slab track: the slab track which was modelled in ABAQUS in Section 6.6 of Chapter 6 was compared with the ballasted numerical and actual data to analyse the difference in response. Even though the concrete slab is stiffer than ballast, it is more expensive to use in track construction.
- Asphalt track: the track was analysed in terms of ground stiffness transitions with chosen points before and after the transition. This method is generally cheap in terms of materials and installation.

7.3.1 Stone columns

The Swedish National Rail Administration (Banverket) supervised the ground vibration measurement in the field at Gothenburg, Sweden. The purpose of the project was to understand the high vibration levels of an embankment for a high speed train, whereby Ledsgård was subjected to extensive measurements to study the ground vibration levels (Hall, 2000). This section includes the soil investigations performed at the site in order to measure the soil properties, and train-induced vibration investigations using extensometers and geophones. The 3D model of the piles is also explained in this section, and the results are compared with the actual field results that were obtained after the pile installation.

Deep Mixing Method (DMM) is an in-situ technique, which strengthens weak soils by mechanically mixing them with a cementitious binder. DMM was used for installing Lime Cement Columns (LCC) beneath the track in order to increase its stiffness. The procedure is

beneficial for improving the characteristics of the soil: it increases strength and reduces compressibility. There are different treatment patterns that can be used for DMM and a grid pattern was used for the site. Holm et al. (2002), Takemiya (2003) and Madshus et al. (2004) estimated the parameters of the columns after performing un-drained shear and compression tests. Young's modulus is $300\,MPa$ for stabilised gyttja and $500\,MPa$ for stabilised clay. The shear modulus is $150\,MPa$ for stabilised gyttja and $200\,MPa$ for clay. In terms of depth, the columns were installed in a ladder-type configuration with two longitudinal walls extending to $7\,m$ depth, and transverse walls extending to $6\,m$ depth below the rail. Every second column in the longitudinal walls extended to $13\,m$ depth. Details are presented in Figure 7.10. These parameters were used in the mitigation technique modelling for this research.

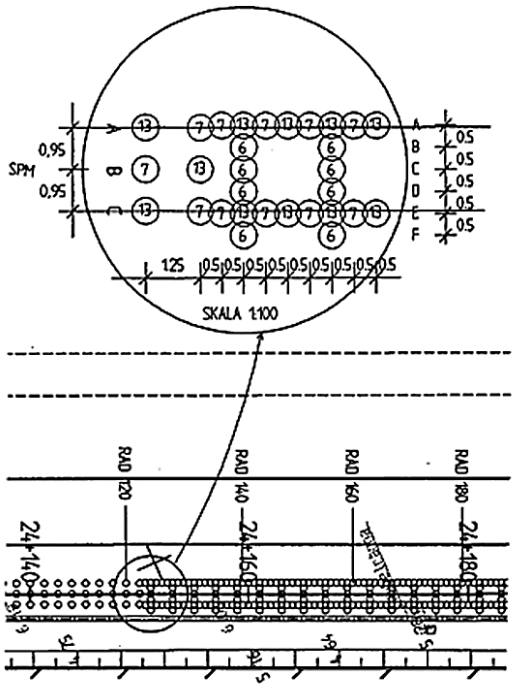

Figure 7.10 Overhead view of the DMM columns (numbers in circles show the depth of the columns) (Holm et al., 2002)

a- Soil investigation:

The material properties and geometrical characteristics were estimated for the finite element model, where some parameters were calculated from the compressive and shear waves' mathematical relationships (E and ν), and other parameters were obtained directly from measurements (ρ and ξ). The geometry was estimated from the boring tests and from the changes in soil properties; moreover, the dynamic soil properties (low-strain) were measured in laboratory and field soil investigations. The field investigation was divided into down-hole, cross-hole and dynamic surface tests; however, the most useful test was found to be the cross-hole test. A cross-hole test is used to measure the material damping value and the soil stiffness. On the other hand, laboratory tests help find the density, static and dynamic triaxial values, and dynamic bender element (Hall, 2000).

b- Measurements of train-induced ground vibrations:

The high speed train X2000 was used to identify the measurements of ground vibration for a passing train, wherein it was tested at various speeds, back and forth, to determine different types of ground dynamic movements along the embankment of the railway and the surroundings. Tests were performed to measure the ground vibration induced by the train, where extensometers were used to identify the vertical deflections and measure the particle acceleration in the railway embankment. The static deflection was measured first, as the train stood stationary for 20 minutes, and this was then followed by increasing the train speed from $10,\ 70,\ 120,\ 140,\ 160, 180$ to $200\ km/h$ (Hall, 2000).

It was necessary to integrate the signals from the accelerometer to identify the particle velocity, which was accomplished using a trapezoidal rule. Also, the signals coming from the geophones were integrated to measure the particle displacement; however, the extensometer signals were also used to calculate particle velocities. A $25\ Hz$ low-pass filter was applied in order to eliminate any disturbances and noise, where it was chosen due to the value of ground vibration energy being found to be less than 5 Hz (Hall, 2000).

7.3.2 Stone column 3D models in ABAQUS

The developed 3D numerical model of the Swedish railway track was used with a different soil model that included the stone columns, which were installed at the site to reduce the vibrations. Changes to properties and depth of the columns were applied in ABAQUS, which facilitated the analysis. The model was validated with actual field results before any changes were applied to the columns in the model. The changes were then compared to the results of the unmodified columns properties and depths used to study the different effects.

a- Model development:

The columns were designed in ABAQUS as shown in Figure 7.11. All the other properties for the Swedish track remained unchanged. The Young's modulus used for the stabilised clay was $500\ MPa$, Poisson's ratio was 0.49 and the density was $1900\ kg/m^3$. Based on Figure 7.10, the depth of the columns varied: $6\ m$, $7\ m$ and $13\ m$ deep columns were used.

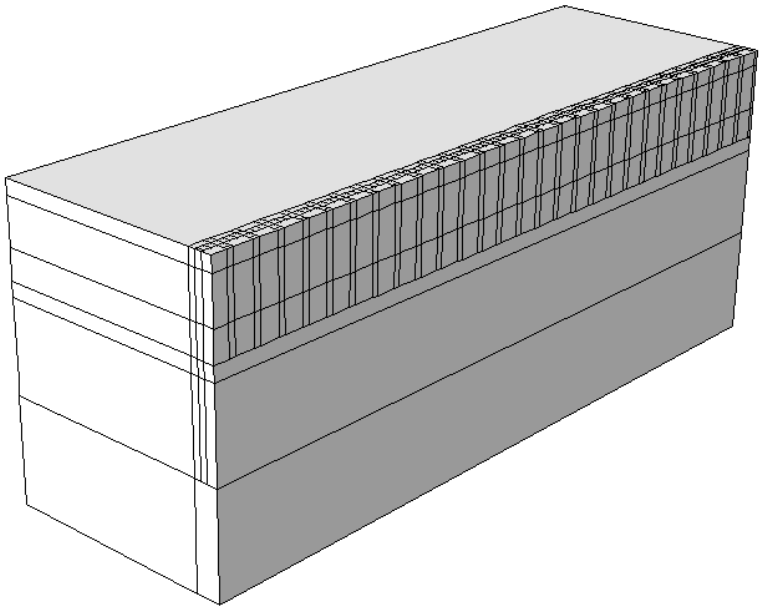

Figure 7.11 3D model of the soil showing the lime/cement columns design in ABAQUS

b- Validation of stone columns models:

The simulation was carried out in ABAQUS implementing the same load application used for the X2000 train (VDLOAD subroutine). The displacements were plotted against time as shown in Figure 7.12, comparing the displacements before and after the treatment. Major improvement was noticed as the track uplifts were approximately $0.02\ mm$ and the vibration at the end was significantly reduced. The maximum deflection of peaks was reduced from approximately $8\ mm$ to $1.5\ mm$ under passenger cars and $13.5\ mm$ to $2\ mm$ under the locomotive car. A similar range of results was obtained by Madshus et al. (2004).

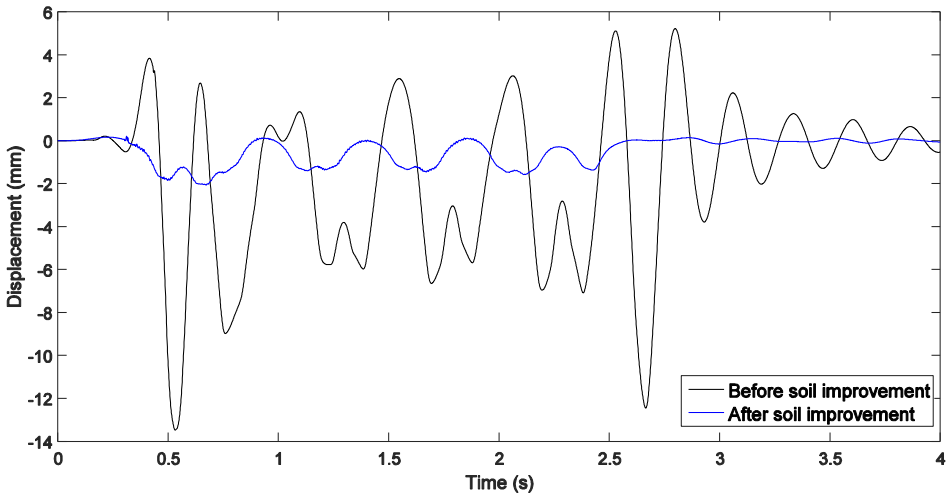

Figure 7.12 Displacement response for the Swedish track before and after soil stabilisation

Various changes were made to the piles properties to study their effects. As $13\ m$ deep lime/cement columns are expensive to construct, the depth of these columns was reduced to $7\ m$. The remaining $6\ m$ and $7\ m$ deep columns were unchanged. Since the depth of the weak organic clay layer is approximately $4\ m$ from the soil surface, $7\ m$ deep piles were considered sufficient to cover the weak area, and thus reduce vibrations. Figure 7.13 shows that, considering $7\ m$ as the maximum depth of the piles used was enough as the maximum

deflection obtained was $2.4\,mm$ ($0.4\,mm$ difference from the actual piles model). In addition, the material properties were changed for a Young's Modulus of $5{,}000\ MPa$ for the $7\,m$ piles, and the results were almost equal to the ones obtained by the actual piles properties used in the site. In conclusion, the behaviour does not change dramatically as long as the weak layer is covered, and any depth beyond that just increases construction cost and time.

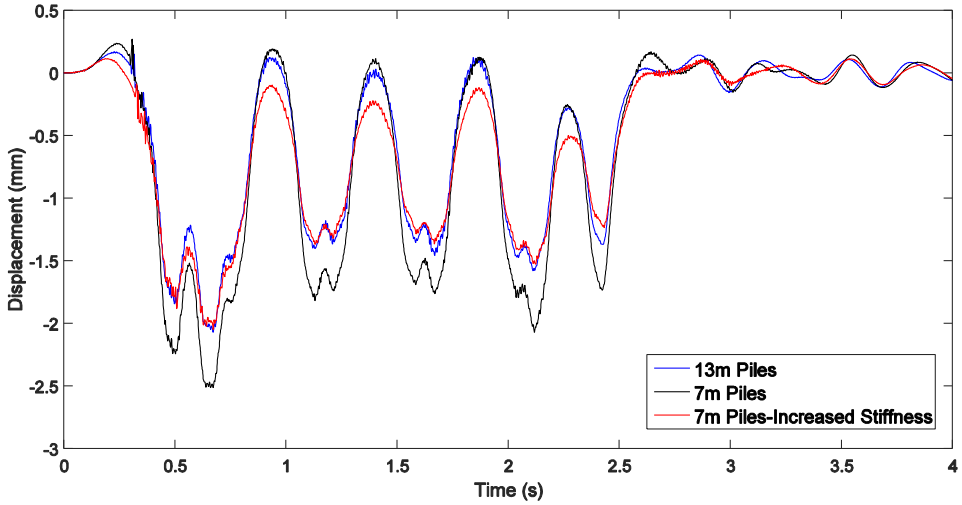

Figure 7.13 Displacement response for the Swedish track comparing different pile properties

7.3.3 Slab models

Slab tracks were modelled for the Swedish track in Section 6.6. The results were compared with the ballasted model for the same track and the actual field results in Figure 7.14. The slab tracks are stiffer, thus the maximum deflection was reduced from $13.5\,mm$ to approximately $8\,mm$ between the ballasted and the slab models in ABAQUS. The track uplift was also reduced by approximately 79.3%. For a critical case, as for the Swedish track, the slab track represents an improvement; however, the deflections are still high because the soil is not treated. The lime/cement columns represent a better solution for this site.

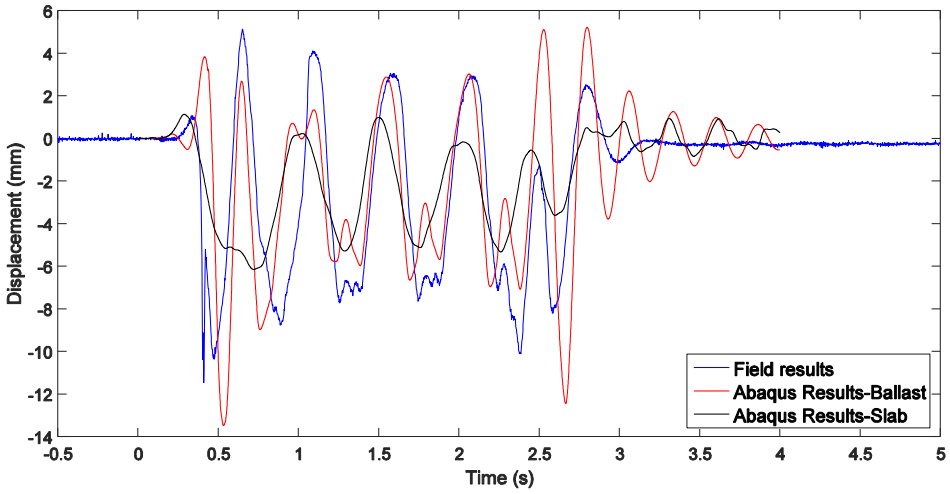

Figure 7.14 Displacement response for the Swedish track comparing the ballasted and slab track models with the actual field results

7.3.4 Asphalt models

Three asphalt models were considered to test the difference made by including an asphalt layer in the ballast on ground behaviour and track displacements. The properties and dimensions that were considered for these models are presented in Table 7.1. The asphalt models were tested for three different depths to study the effect of the layer thickness on the response, $0.1\,m, 0.15\,m$, and $0.2\,m$. The sleepers were embedded in the ballast and the asphalt layer was also located in the ballast as shown in the cross section in Figure 7.15. The rail was $50\,m$ long and the sleepers were $0.24\,m$ in width.

Layer	D (m)	E (MPa)	v	$\rho(kg/m^3)$
Rail	0.153	210,000	0.3	7800
Sleepers	0.2	30,000	0.3	2400
Ballast	0.55	150	0.25	1800
Asphalt	0.1, 0.15, 0.2	5000	0.35	2400
Sub-ballast	0.1	100	0.3	2200
Subgrade	Infinite	20.8	0.35	2000

Table 7.1 Properties of the asphalt-ballasted track models

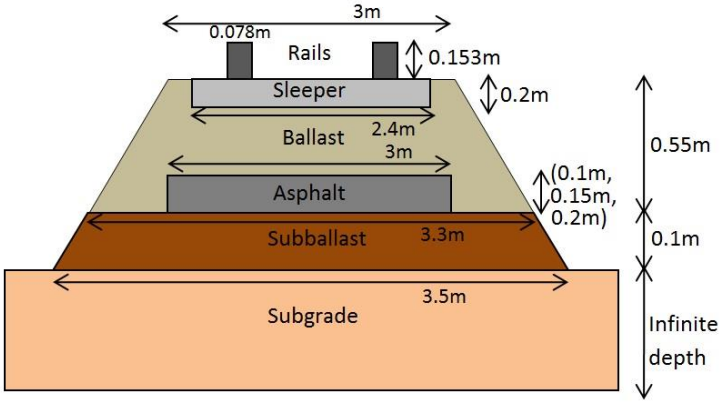

Figure 7.15 Ballasted track model with asphalt layers

A single moving load was applied on the track. The asphalt layer reduced the displacement values, as noticeable in Figure 7.16. The increase in the layer thickness reduced the values even further. In addition, the values of the uplift were also reduced; however, the difference is minimal. The effect on the Swedish track is tested throughout this section.

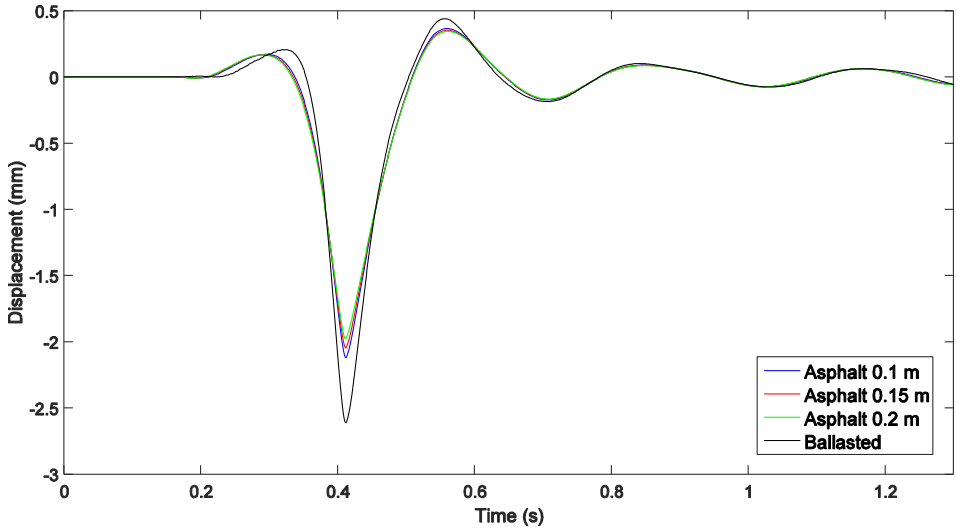

Figure 7.16 The displacements of 1 moving load on asphalt models of different depths ($0.1\ m, 0.15\ m,$ and $0.2\ m$)

For this section, a low stiffness soil transition to represent a track wet spot was added to the model and the behaviour was analysed to test the difference in peak deflections for the rail, asphalt layer, and ground surface as the train passed the weak transition. The weak section was $1\ m$ long and the Young's Modulus was $10\ MPa$. The deflections were collected for the rail, top of the asphalt layer and top of the soil model. Five different points were tested as shown in Figure 7.17, with two points located before and after the transition, one point located in the middle and two points located on the edge of the transition zone.

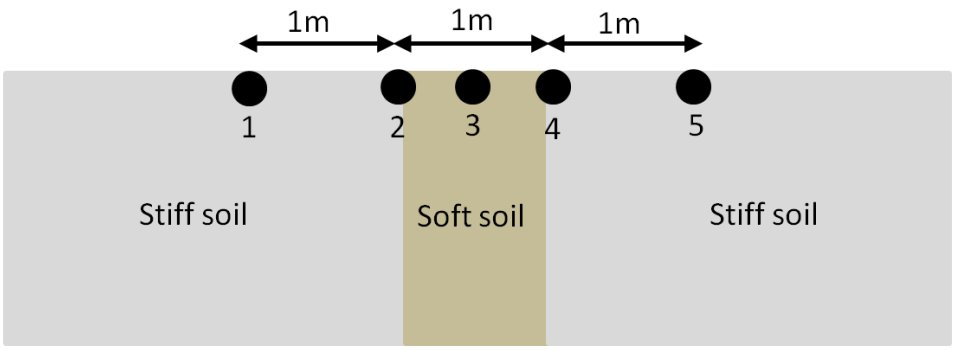

Figure 7.17 Layout of the tested points for the transition model

Figure 7.18 shows the displacement results plotted against time for Point 1 after running one point load. The displacement of the rail was the largest as expected since the displacement was reduced with depth. Table 7.2 shows a summary of the maximum deflections and time of occurrence for the five points. The maximum deflection of the rail increased from 1.78 mm at Point 1 to 1.97 mm at Point 3, then it decreased as it passed the transition zone back to approximately 1.8 mm. The asphalt layer displacement was not affected greatly at Points 2, 3 and 4, but it slightly decreased, by 0.13 mm, at Point 5. For the soil displacement, the value increased gradually from 1.41 mm at Point 1 to 1.66 mm at Point 5. Unlike the rail displacement, the values increased even after passing the soft soil, which was due to vehicle dynamics. The dynamic wheel force distribution is larger at transition zones, as the train travels from soft to stiff material (Kerr et al., 2001; Sañudo et al., 2016). Nevertheless, this case needs further investigation in the future before drawing conclusions. It is interesting to note the change in pattern in terms of time occurrence between the displacement of the rail, asphalt and soil layers for before and after passing the soft soil area. The three occurred at a similar time for Point 3, which is located in the centre of the soft soil. The difference between peak values for the asphalt layer and ground layers underneath the track was minimal between the stiff and soft soils when the asphalt layer was added. This minimal change occurred since the asphalt layer increased the overall stiffness of the track. In reality, asphalt functions as an adhesive material mixed with aggregates to strengthen the

connectivity in the layer, which reduced the penetration of the particles in the ground layers beneath it; however, this effect was not considered in this model.

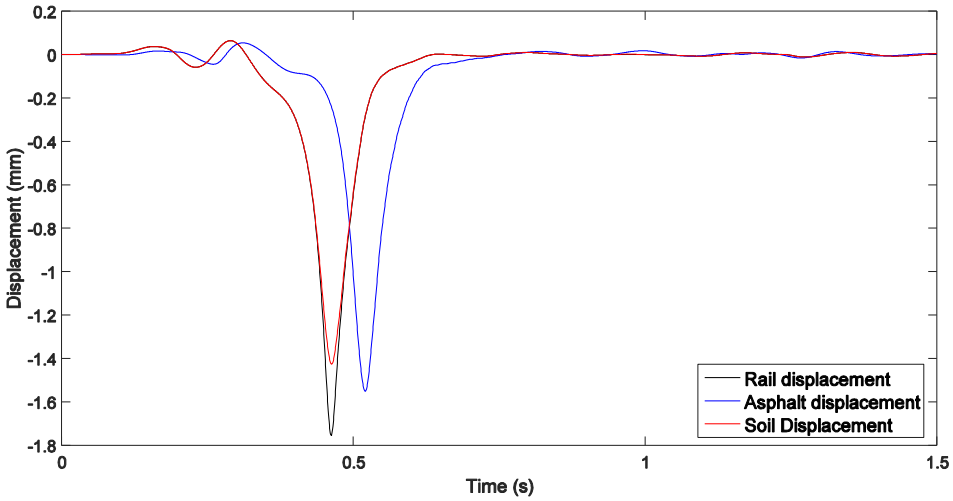

Figure 7.18 Displacement response of the asphalt models under a moving point load over a soil transition zone (Point 1)

Point	Layer	Maximum Deflection (mm)	Time of Maximum Deflection (s)
Point 1	Rail	1.78	0.46
	Asphalt	1.59	0.51
	Soil	1.41	0.46
Point 2	Rail	1.83	0.47
	Asphalt	1.64	0.50
	Soil	1.49	0.52
Point 3	Rail	1.97	0.48
	Asphalt	1.65	0.48
	Soil	1.53	0.47
Point 4	Rail	1.95	0.50
	Asphalt	1.63	0.47
	Soil	1.62	0.50
Point 5	Rail	1.80	0.51
	Asphalt	1.50	0.46
	Soil	1.66	0.48

Table 7.2 Maximum deflections and time of occurrence of the five points

To test the effect of an asphalt layer on critical velocity effects, the layer was added to the Swedish track model. The model was run at a low speed of $15\ m/s$. Figure 7.19 compares the displacements between the unmodified ballasted and asphalt tracks. The change between the values was minimal, as the asphalt track resulted in a $0.31\ mm$ reduction in maximum displacement. The previously mentioned 5 points were also checked for the Swedish site in the case of a soft soil transition zone. The differences in maximum deflection values were $2.42\ mm$, $2.33\ mm$ and $2.51\ mm$ for Points 1, 3 and 5, respectively. The difference in this case was larger due to the soft soil. Figure 7.20 shows the response for speed $51\ m/s$. The difference between the ballasted and asphalt tracks was larger than the outcomes for $15\ m/s$ speed. The maximum uplift increased by $1.21\ mm$, while the asphalt layer caused a reduction in the deflection by $1.52\ mm$. This demonstrates that the asphalt layer is not sufficient to reduce the vibrations for a weak site, in comparison to slab tracks and stone columns.

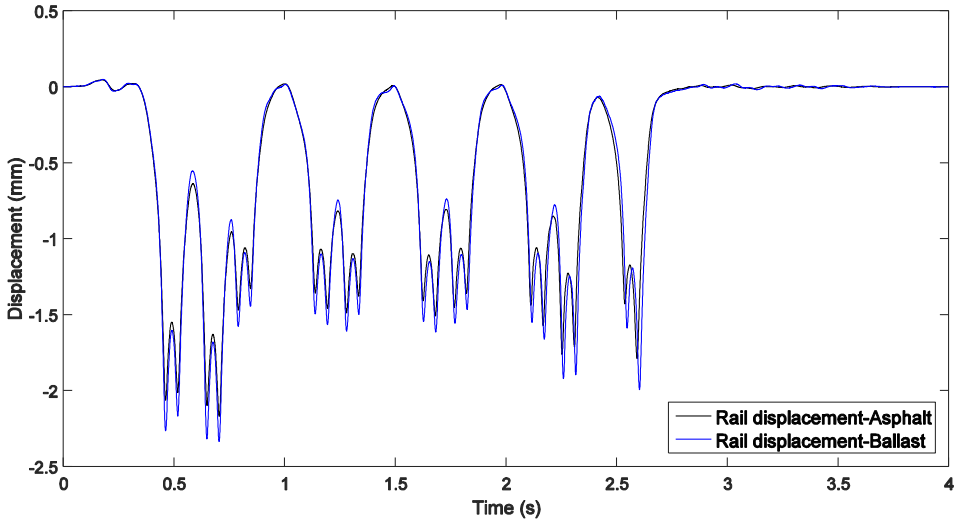

Figure 7.19 Displacement response for the Swedish track for the regular ballasted and asphalt models for speed $15\ m/s$

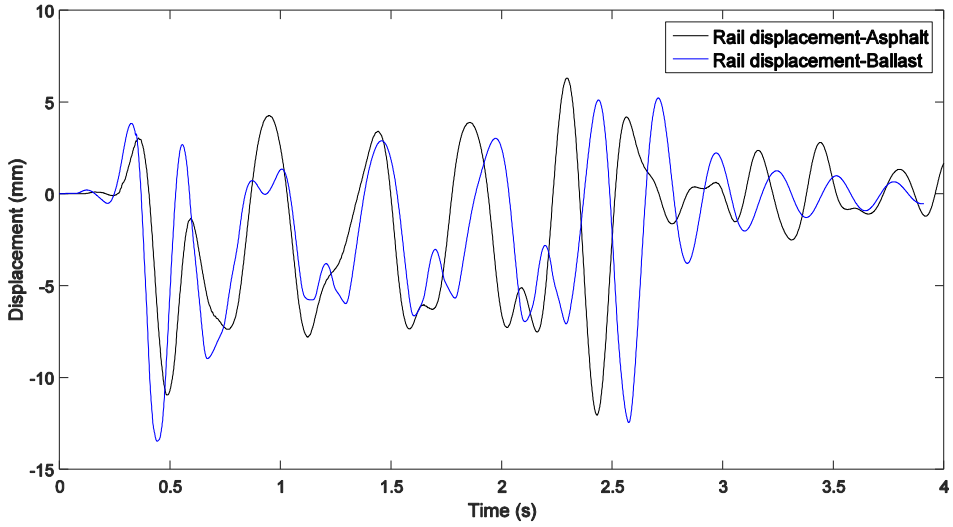

Figure 7.20 Displacement response for the Swedish track for the regular ballasted and asphalt models for speed $51\ m/s$

7.4 Summary

After development of the 3D numerical models, general comments and analysis were carried out for the results. The Swedish site model results clearly show the critical velocity effects: track uplift, ground resonance and surface vibrations. Stresses were collected for two elements at depth below a chosen sleeper. One element was located in the embankment, while the second element was located on top of the organic clay layer. The stress paths were analysed for critical speeds and octahedral shear strain variation with depth were plotted for different speeds. The following conclusions were drawn:

- The maximum normal stresses in the track and soil elements occur in the same direction as the passing train. The dominant shear stresses occur vertically in the same direction as the applied vertical load.
- The stresses depend on train speed, as the shear and mean stresses increase when the train speed approaches critical velocity. However, the shear stress begins to decrease as the train speed becomes larger than the critical velocity.

- The stress paths show clear configuration for loading and un-loading of the axle loads for lower speeds ($19\ m/s$). The configuration shows dynamic behaviour and it becomes difficult to identify the loading and un-loading effects as the train speed approaches critical velocity ($56\ m/s$).
- The maximum octahedral shear strain occurs for the first two axles, as their mass is larger than the other axles. The value of octahedral shear strain reduces with depth. It is also observed that it is at its maximum in the organic clay layer in comparison to other layers, due to the low stiffness.

In addition, this chapter included models of three mitigation strategies:

1) Deep Mixing Method was used to stabilise the Swedish track and this method was modelled and tested in ABAQUS in this chapter. Stone columns result in significant reduction in vibrations. Changes to material properties and depth of the piles were made. Decreasing the pile depth to $7\ m$ with an increased stiffness results in similar results as the actual piles used. When considering the depth of the piles, covering the weak layer at the site is sufficient to significantly reduce deflections and uplifts.
2) Slab tracks reduce vibrations and track uplift, but they are not sufficient to be used as a solution for weak sites since the soil is the major issue. The reduction in vibration is less than the reduction caused by stone columns.
3) The asphalt layer does not provide a good solution for highly nonlinear sites, as the differences in results were minimal in comparison to the other two methods modelled in this chapter. A weak soil transition for the asphalt models does not affect the magnitude greatly; however, the deflection pattern changes for the rail, asphalt layer and soil before and after the transition.

Chapter 8 Conclusions and Recommendations

8.1 Background

Train speeds have been increasing rapidly to facilitate means of transportation and reduce travel time. Amplified ground response can occur due to the construction of high-speed rail lines over weak sites with soft soil. The "critical speed" occurs when the train speed approaches the ground Rayleigh wave speed, leading to wave propagation and large ground vibrations. However, due to the complexity and nonlinearity of the soil, it is hard to accurately predict the ground behaviour and critical velocity values. The amplified vibrations affect passengers safety, as they cause damage to the rail and track components.

To meet these challenges, one key aspect is to improve the predictive tools for track dynamic investigations, including: development of modelling methods adapted for describing track response, assessment of materials and the influence of different track/train properties on ground behaviour, and evaluation of the stabilisation techniques in order to reduce critical velocity effects. Whilst researchers have developed different approaches, from 2D, 2.5D to 3D modelling methods, there are still limitations in modelling, especially for train-track interactions. This research aim was to provide new approaches of predicting critical velocity effects and investigating mitigation strategies.

8.2 Description of the Developed Methods

Carrying on from previous research, analytical and numerical approaches have been improved and developed throughout this research in order to fulfil the main objectives. Three main methods were developed:

1) Analytical dispersion analysis:

Dispersion curves were produced for a track-soil system. Apparent velocity calculations are used for soil dispersions. The method takes account of multi-layered soil on top of half-space homogeneous soil. Using inverse Fourier transform functions, the dispersion characteristics for track and soil are plotted in velocity-frequency plots. These plots allow for determination of the critical velocity at the intersection point between the dispersion curves of the track and the soil. The model is validated for critical velocity calculations and the method provides a high level of accuracy. Sensitivity analysis was carried out using the dispersion analysis to study the effects of different factors on critical velocity. 1000 arbitrary soil profiles were generated.

2) Semi-analytical approach for producing DAF curves:

The developed semi-analytical approach provides a prediction of 3D ground response and Dynamic Amplification Factors of a certain railway track in a shorter simulation run time than numerical methods. The track is modelled analytically and the ground response is calculated using finite element methods in the implementation of TLM to calculate Green's functions. The semi-analytical model was validated against the Swedish track.

3) Numerical approach using finite element methods in ABAQUS:

The 3D numerical approach provides a fully coupled finite element model in ABAQUS for track-ground systems. In addition, the lumped mass train system and applied loads are coded using FORTRAN programming language to produce a more realistic vehicle model. The train-track interaction forces are also included in the code, as this was a challenge in modelling faced by previous researchers for modelling the train system in ABAQUS. Explicit time integration is carried out due to its efficiency in dealing with conditionally stable problems. There are two tested methods that are applied to the sides of the model in order to prevent wave reflection: a) using infinite elements and b) increasing the mesh size with increased depth and width of the soil model. Both methods resulted in a similar

response in this research. In order to account for the nonlinearity of the Swedish site, an equivalent linear method proposed by Costa et al. (2010) was followed in this research. The method recommends reducing the shear modulus values based on the maximum effective octahedral shear strains obtained from the linear analysis. The method was applied to the Swedish track and DAF curves were obtained for various speeds and compared against field results. The DAF curve also included extended speeds above the maximum speed of the X2000 train in order to investigate the behaviour after passing the critical velocity. In comparison to the semi-analytical approach, the fully numerical method produces more accurate outcomes, including displacements, velocities, accelerations, stresses, strains etc. at any point along the track, with depth, and away from the track.

The numerical model was validated against actual field results for two main sites: the X2000 train track in Sweden and the Alfa-Pendular train track in Portugal. The mitigation model of stone columns was also validated against the results of the Swedish site before and after ground improvement.

8.3 Key Conclusions

The following conclusions were drawn:

- Concrete slab tracks typically have a higher critical velocity and track displacements than ballasted tracks due to their increased stiffness. Also, the critical speed typically occurs at a lower frequency for slab track. Increasing ballast depth has a low effect on the critical velocity; however increasing slab depth has a large increase, because it acts to improve bending stiffness.
- Increasing railpad stiffness can increase the critical velocity of ballasted tracks, however is insignificant for concrete slab tracks. The same is true for rail bending stiffness, also due to ballasted track having low bending stiffness.
- Regarding soil effects, soil saturation was found to have a negative impact on the critical speed particularly for ballast tracks, and soil damping has a negligible effect

for all track types. If the soil consists of a deep uppermost layer then this will govern the critical speed, however if thinner layers exist close to the surface then they must also be considered.

- Close to critical velocity, track deflections are affected by train axle configuration and direction of train passage as the superposition characteristics of axle loads changes.
- Regarding a case study of Ledsgard, Sweden, it was observed that the mean stress and shear stresses in the soil increased as the train speed approached critical velocity. The shear stress increased by 72.2%, as the speed was increased from $19\ m/s$ to $56\ m/s$. Also, the loading pattern changed dramatically with the loading/un-loading regimes unclear at the higher speed. Regarding octahedral strains, large strains were found in the softest soil layer and were comparable in magnitude to nonlinear models such as Shih et al. (2017).
- For the case of Ledsgard, Sweden, simulations showed that stone columns offer significant improvements in track deflections. However it was found that column construction depth should only cover the weakest organic clay layer and that additional depth is unnecessary. The use of stone columns compared to concrete and asphalt slab tracks was compared and it was found that stone columns offer strongest performance.

8.4 Limitations

Limitations related to the numerical modelling approaches considered in this thesis include:

1- Due to the nonlinearity of the ballast and subgrade materials, which results in a reduction in stiffness and increase in damping under cyclic loading, nonlinear models provide more realistic results than linear analysis. Nonlinearity analysis in ABAQUS can be simulated using several approaches; however, the run time of analysis is increased and the computational effort is large; thus, only equivalent linear analysis was considered in this research.

2- The vehicle system in the numerical approach was developed with a simplified approach using springs and dampers to account for primary and secondary suspensions. The configuration of the train system, in reality, is more complicated and it is different depending on train type.
3- The ballast, in reality, is composed of particles, while it is modelled as solid block elements in the 3D numerical model. This causes tension in the ballast elements.

Other limitations are related to the analytical approaches. For the dispersion analysis, the developed code that produces velocity-frequency dispersion relations is only applicable for multi-soil layers with increased stiffness with depth. Thus, it cannot be used for calculating soil layers with a greater stiffness on top of a layer with a lower stiffness.

8.5 Recommendations for Future Work

The following points are recommended for future research:

1- Other mitigation strategies, in addition to the ones considered in this research, could be considered for modelling, such as geosynthetics.
2- Nonlinearity modelling in ABAQUS could be considered, as well as other boundary condition methods for the soil models to improve them to allow more accurate results for the Swedish track case to be produced. This also affects the stress values obtained from the simulations, as the stress obtained from a linear analysis is less than those obtained from a nonlinear analysis for track and soil (Varandas et al., 2016). Additionally, the equivalent linear models carried out in this research consider 0.65 for the parameter of the effective octahedral shear strain calculations (Chapter 6) in order to produce the reduced shear modulus values. This parameter could be changed and investigated further for more accurate results.

3- The interaction force between the wheel and rail was added in the modelling process; however, the irregularities were assumed to be zero. A further modification would be required to consider the irregularities.

4- As for the dispersion analysis in a velocity-frequency approach, the analysis could be improved further to produce solutions for multi-layered soil with decreasing stiffness with depth. This would help in implementing real-life cases similar to that at the Swedish site where there is a crust layer on top of an organic clay layer.

5- Sub-modelling using co-simulation could be considered for future work, which is favourable for benefitting from other specialised modelling software in combination with ABAQUS. Subsystems are modelled and simulated separately, as the coupling is carried out at a later stage. ABAQUS software offers co-simulation with a variety of other programs, for example: ANSYS, SIMPACK etc. (ABAQUS-Manual).

Appendix

The dynamic stiffness matrix, which is used in FETLM in Chapter 5, is explained by Sheng (2001) in the wave-number domain, and presented in the following equation, as $\emptyset = \frac{\pi}{2}$ if k_1 is zero, otherwise $\emptyset = \tan^{-1}\frac{k_2}{k_1}$.

$$K_{dyn} = \begin{bmatrix} \sin(\emptyset).sgn(k_2) & \cos(\emptyset).sgn(k_1) & 0 \\ -\cos(\emptyset).sgn(k_1) & \sin(\emptyset).sgn(k_2) & 0 \\ 0 & 0 & 1 \end{bmatrix} RS^{-1}$$

$$\begin{bmatrix} \sin(\emptyset).sgn(k_2) & -\cos(\emptyset).sgn(k_1) & 0 \\ \cos(\emptyset).sgn(k_1) & \sin(\emptyset).sgn(k_2) & 0 \\ 0 & 0 & 1 \end{bmatrix} \quad \text{(A.1)}$$

If $\omega \neq 0$, the matrices R and S are computed as follows:

$$R = \begin{bmatrix} 0 & 1 & 0 \\ -\frac{i\gamma}{b_p^2} & 0 & 1 \\ \frac{a_p}{b_p^2} & 0 & \frac{i\gamma}{a_s} \end{bmatrix} \quad \text{(A.2)}$$

$$S = \begin{bmatrix} 0 & -\mu^* a_s & 0 \\ \frac{2i\mu^* a_p \gamma}{b_p^2} & 0 & -\frac{\mu^*(\gamma^2 + a_s^2)}{a_s} \\ \lambda^* - 2\mu^* \frac{a_p^2}{b_p^2} & 0 & -2i\mu^*\gamma \end{bmatrix} \quad \text{(A.3)}$$

while for $\omega = 0$:

$$R = \begin{bmatrix} 0 & 1 & 0 \\ 0 & 0 & 1 \\ -\frac{\lambda^*+3\mu^*}{2a_p\mu^*} & 0 & \frac{i\gamma}{a_s} \end{bmatrix} \tag{A.4}$$

$$S = \begin{bmatrix} 0 & -\mu^* a_s & 0 \\ -\frac{i\gamma\mu^*}{a_p} & 0 & -\frac{\mu^*(\gamma^2+a_s^2)}{a_s} \\ \lambda^* + 2\mu^* & 0 & -2i\mu^*\gamma \end{bmatrix} \tag{A.5}$$

where:

$$\gamma = \sqrt{k_1^2 + k_2^2} \tag{A.6}$$

$$a_p = \sqrt{\frac{\gamma^2-\omega^2}{c_p^2}} \tag{A.7}$$

$$a_s = \sqrt{\frac{\gamma^2-\omega^2}{c_s^2}} \tag{A.8}$$

$$b_l = \frac{\omega^2}{c_p^2} \tag{A.9}$$

The phase velocities of the compression and shear waves are calculated as $c_p = \sqrt{\frac{\lambda^*+2\mu^*}{\rho}}$ and $c_s = \sqrt{\frac{\mu^*}{\rho}}$, respectively.

References

ABAQUS-Manual. Documentations and user's manual.

Andersen, L., Nielsen, S. R., & Krenk, S. (2007). Numerical methods for analysis of structure and ground vibration from moving loads. Computers & structures, 85(1), 43-58.

AREA. (1996). Manual for railway engineering, American Railway Engineering Association (AREA).

Arlaud, E., Costa, S., & Balmes, E. (2014). Validation of a reduced model of railway track allowing long 3D dynamic calculation of train-track interaction. Proceedings of conference: Computer Methods and Recent Advances in Geomechanics, Japan.

Auersch, L. (1996). Dynamic plate-soil interaction—finite and infinite, flexible and rigid plates on homogeneous, layered or Winkler soil. Soil Dynamics and Earthquake Engineering, 15(1), 51-59.

Auersch, L. (2005). Simplified methods for wave propagation and soil-structure interaction: The dispersion of layered soil and the approximation of FEBEM results. Proceedings of the 6th International Conference on Structural Dynamics.

Auersch, L. (2014). The Use and Validation of Measured, Theoretical, and Approximate Point-Load Solutions for the Pre-diction of Train-Induced Vibration in Homogeneous and Inhomogeneous Soils. International Journal of Acoustics and Vibrations, 19(1), 52-64.

Balendra, T., Chua, K., Lo, K., & Lee, S. (1989). Steady-state vibration of subway-soil-building system. Journal of engineering mechanics, 115(1), 145-162.

Banimahd, M. (2008). Advanced finite element modelling of coupled train-track systems: a geotechnical perspective. PhD thesis, Heriot-Watt University.

Bian, X., Cheng, C., Jiang, J., Chen, R., & Chen, Y. (2016). Numerical analysis of soil vibrations due to trains moving at critical speed. Acta Geotechnica, 11(2), 281-294.

Cao, Z., Cai, Y., Sun, H., & Xu, C. (2011). Dynamic responses of a poroelastic half-space from moving trains caused by vertical track irregularities. International Journal for Numerical and Analytical Methods in Geomechanics, 35(7), 761-786.

Caughey, T. (1960). Classical normal modes in damped linear dynamic systems. Journal of Applied Mechanics, 27(2), 269-271.

Chahour, K., Lefeuve-Mesgouez, G., & Mesgouez, A. (2014). Spectral analysis of a railway track in contact with a multilayered poroviscoelastic soil subjected to a harmonic moving load. Soil Dynamics and Earthquake Engineering, 64, 24-37.

Chen, Y. H., Huang, Y. H., & Shih, C. T. (2001). Response of an infinite Timoshenko beam on a viscoelastic foundation to a harmonic moving load. Journal of Sound and Vibration, 241(5), 809-824.

Claisse, P., & Calla, C. (1992). Rail ballast: conclusions from a historical perspective. Proceedings of the Institution of Civil Engineers-Transport . (Vol. 159): London: Published for the Institution of Civil Engineers by Thomas Telford Services.

Clark, C. (1957). Track Loading Fundamentals–Parts 1-7. Railway Gazette, 106.

Clark, R. A., Dean, P. A., Elkins, J. A., & Newton, S. G. (1982). An investigation into the dynamic effects of railway vehicles running on corrugated rails. Journal of Mechanical Engineering Science, 24(1), 65-76.

Colaço, A., Costa, P. A., & Connolly, D. P. (2016). The influence of train properties on railway ground vibrations. Structure and Infrastructure Engineering, 12(5), 517-534.

Connolly, D., Giannopoulos, A., & Forde, M. (2013). Numerical modelling of ground borne vibrations from high speed rail lines on embankments. Soil Dynamics and Earthquake Engineering, 46, 13-19.

Connolly, D., Kouroussis, G., Woodward, P., Costa, P., Verlinden, O., & Forde, M. (2014). Field testing and analysis of high speed rail vibrations. Soil Dynamics and Earthquake Engineering, 67, 102-118.

Costa, P., Calçada, R., & Cardoso, A. (2012a). Ballast mats for the reduction of railway traffic vibrations. Numerical study. Soil Dynamics and Earthquake Engineering, 42, 137-150.

Costa, P., Calçada, R., & Cardoso, A. (2012b). Track–ground vibrations induced by railway traffic: In-situ measurements and validation of a 2.5 D FEM-BEM model. Soil Dynamics and Earthquake Engineering, 32(1), 111-128.

Costa, P., Calçada, R., Cardoso, A., & Bodare, A. (2010). Influence of soil non-linearity on the dynamic response of high-speed railway tracks. Soil Dynamics and Earthquake Engineering, 30(4), 221-235.

Costa, P., Colaço, A., Calçada, R., & Cardoso, A. (2015). Critical speed of railway tracks. Detailed and simplified approaches. Transportation Geotechnics, 2, 30-46.

Dahlberg, T. (2006). Track issues. Handbook of railway vehicle dynamics, 143-179.

De Barros, F., & Luco, J. (1995). Stresses and displacements in a layered half-space for a moving line load. Applied Mathematics and Computation, 67(1), 103-134.

Degrande, G., & Lombaert, G. (2001). An efficient formulation of Krylov's prediction model for train induced vibrations based on the dynamic reciprocity theorem. The Journal of the Acoustical Society of America, 110(3), 1379-1390.

DFT. (2010). High Speed Rail. UK.

Dieterman, H., & Metrikine, A. (1996). The equivalent stiffness of a half-space interacting with a beam. Critical velocities of a moving load along the beam. European journal of mechanics, series A: solids, 15, 67-90.

Edward, D. (2007). Reservoir engineering and petrophysics (Volume V). Society of Petroleum Engineers.

Ekevid, T., & Wiberg, N. E. (2002). Wave propagation related to high-speed train: a scaled boundary FE-approach for unbounded domains. Computer methods in applied mechanics and engineering, 191(36), 3947-3964.

El Kacimi, A., Woodward, P., Laghrouche, O., & Medero, G. (2013). Time domain 3D finite element modelling of train-induced vibration at high speed. Computers & structures, 118, 66-73.

Elfino, M. K., & Davidson, J. L. (1989). Modeling field moisture in resilient moduli testing. Paper presented at the Resilient moduli of soils: laboratory conditions, pp 31-51, ASCE.

Esveld, C. (2001). Modern railway track (Vol. 385): MRT-productions Zaltbommel, The Netherlands.

Esveld, C., & Markine, V. (1998). Slab track design for high speed. Rail Engineering International.

Ferrara, R., Leonardi, G., & Jourdan, F. (2013). A Two-Dimensional Numerical Model to Analyze the Critical Velocity of High Speed Infrastructure. Paper presented at the Fourteenth International Conference on Civil, Structural and Environmental Engineering Computing.

Ferreira, A., & Lopez-Pita, A. (2015). Numerical modelling of high speed train/track system for the reduction of vibration levels and maintenance needs of railway tracks. Construction and Building Materials, 79, 14-21.

Foti, S. (2000). Multistation methods for geotechnical characterization using surface waves. Politecnico di Torino.

Foti, S., Lai, C. G., Rix, G. J., & Strobbia, C. (2014). Surface wave methods for near-surface site characterization: CRC Press.

François, S., Schevenels, M., Galvín, P., Lombaert, G., & Degrande, G. (2010). A 2.5 D coupled FE–BE methodology for the dynamic interaction between longitudinally invariant structures and a layered halfspace. Computer methods in applied mechanics and engineering, 199(23), 1536-1548.

François, S., Schevenels, M., Thyssen, B., Borgions, J., & Degrande, G. (2012). Design and efficiency of a composite vibration isolating screen in soil. Soil Dynamics and Earthquake Engineering, 39, 113-127.

Frýba, L. (1972). Vibration of Solids and Structures under Moving Loads. Springer Netherlands, The Netherlands.

Galvín, P., Romero, A., & Domínguez, J. (2010). Fully three-dimensional analysis of high-speed train–track–soil-structure dynamic interaction. Journal of Sound and Vibration, 329(24), 5147-5163.

Gandoza3DModels. Retrieved from http://www.gandoza.com/ (accessed 3rd March, 2017).

Halabian, A. M., & Naggar, M. (2002). Effect of non-linear soil–structure interaction on seismic response of tall slender structures. Soil Dynamics and Earthquake Engineering, 22(8), 639-658.

Hall, L. (2000). Simulations and analyses of train-induced ground vibrations: A comparative study of two-and three-dimensional calculations with actual measurements: PhD thesis, Royal Institute of Technology, Division of Soil & Rock Mechanics.

Hall, L. (2003). Simulations and analyses of train-induced ground vibrations in finite element models. Soil Dynamics and Earthquake Engineering, 23(5), 403-413.

Hanazato, T., Ugai, K., Mori, M., & Sakaguchi, R. (1991). Three-dimensional analysis of traffic-induced ground vibrations. Journal of geotechnical engineering, 117(8), 1133-1151.

Hardin, B., & Kalinski, E. (2005). Estimating the shear modulus of gravelly soils. Journal of Geotechnical and Geoenvironmental Engineering, 131(7), 867-875.

Haynes, J. G., & Yoder, E. J. (1963). Effect of repeated loading on gravel and crushed stone base course materials used in the AASHO (American Association of State Highway Officials) road test: Highway Research Record 39.

Hicks, G. (1970). Factors Influencing the resilient properties of granular materials. PhD thesis, University of California, Berkeley, Calif.

Hicks, G., & Monismith, L. (1971). Factors influencing the resilient response of granular materials. Highway research record(345).

Hills, D. A., Nowell, D., & Sackfield, A. (1993). Mechanics of elastic contacts. Butterworth-Heinemann Ltd., Oxford.

Holm, G., Andréasson, B., Bengtsson, P.-E., Bodare, A., & Eriksson, H. (2002). Mitigation of track and ground vibrations by high speed trains at Ledsgard, Sweden. Swedish Deep Stabilization Research Centre, Report, 10, 58.

Huang, H., & Chrismer, S. (2013). Discrete element modeling of ballast settlement under trains moving at "Critical Speeds". Construction and Building Materials, 38, 994-1000.

Hung, H. H., & Yang, Y. B. (2001). A review of researches on ground-borne vibrations with emphasis on those induced by trains. In proceedings of the National Science Council, Part A: Physics, Science & Engineering., 25(1), 1-16.

Hussein, M., & Hunt, H. (2007). A numerical model for calculating vibration from a railway tunnel embedded in a full-space. Journal of Sound and Vibration, 305(3), 401-431.

Jethro, M. (2015). 10 killed after French high-speed train derails and crashes into canal. Retrieved from http://edition.cnn.com/2015/11/14/europe/france-tgv-train-derailment/ (accessed 20th Dec, 2016).

Jones, D. V. (1987). The surface propagation of ground vibration. PhD thesis, University of Southampton.

Jones, S. (2010). Ground vibration from underground railways: how simplifying assumptions limit prediction accuracy. PhD thesis, University of Cambridge.

Kalker, J. J. (2013). Three-dimensional elastic bodies in rolling contact (Vol. 2): Springer Science & Business Media.

Kausel, E. (1981). An explicit solution for the Green functions for dynamic loads in layered media: Department of Civil Engineering, School of Engineering, Massachusetts Institute of Technology.

Kaynia, A. M., Madshus, C., & Zackrisson, P. (2000). Ground vibration from high-speed trains: prediction and countermeasure. Journal of Geotechnical and Geoenvironmental Engineering, 126(6), 531-537.

Kenney, J. (1954). Steady-state vibrations of beam on elastic foundation for moving load. Journal of Applied Mechanics-Transactions of the ASME, 21(4), 359-364.

Kerr, A. D., Lucas, A., & Bathurst, A. (2001). A Method for Upgrading the Performance at Track Transitions for High-Speed Service. National Technical Information Service.

Knothe, K., & Grassie, S. (1993). Modelling of railway track and vehicle/track interaction at high frequencies. Vehicle system dynamics, 22(3-4), 209-262.

Knothe, K., & Wu, Y. (1998). Receptance behaviour of railway track and subgrade. Archive of Applied Mechanics, 68(7), 457-470.

Knutson, R. M., & Thompson, M. R. (1977). Resilient response of railway ballast. Transportation Research Record(651).

Kouroussis, G., Connolly, D. P., Alexandrou, G., & Vogiatzis, K. (2015). The effect of railway local irregularities on ground vibration. Transportation Research Part D: Transport and Environment, 39, 17-30.

Kouroussis, G., Connolly, D. P., & Verlinden, O. (2014). Railway-induced ground vibrations–a review of vehicle effects. International Journal of Rail Transportation, 2(2), 69-110.

Kouroussis, G., Gazetas, G., Anastasopoulos, I., Conti, C., & Verlinden, O. (2011). Discrete modelling of vertical track–soil coupling for vehicle–track dynamics. Soil Dynamics and Earthquake Engineering, 31(12), 1711-1723.

Kouroussis, G., Verlinden, O., & Conti, C. (2009). Ground propagation of vibrations from railway vehicles using a finite/infinite-element model of the soil. Proceedings of the Institution of Mechanical Engineers, Part F: Journal of Rail and Rapid Transit, 223(4), 405-413.

Kramer, S. L. (1996). Geotechnical Earthquake Engineering. Prentice Hall, New York.

Krylov, V. V. (1995). Generation of ground vibrations by superfast trains. Applied Acoustics, 44(2), 149-164.

Krylov, V. V., Dawson, A., Heelis, M., & Collop, A. (2000). Rail movement and ground waves caused by high-speed trains approaching track-soil critical velocities. Proceedings of the Institution of Mechanical Engineers, Part F: Journal of Rail and Rapid Transit, 214(2), 107-116.

Kumar, B., Anbazhagan, P., & Sitharam, T. (2006). Development of theoretical dispersion curves and comparison with Multichannel Analysis of Surface Waves (MASW). 13th Symposiom on Earthquake Engineering.

Lamb, H. (1904). On the propagation of tremors over the surface of an elastic solid. Philosophical Transactions of the Royal Society of London. Series A, Containing papers of a mathematical or physical character, 203, 1-42.

Law, E. H. (1974). Nonlinear Wheelset Dynamic Response to Random Lateral Rail Irregularities. Journal of Engineering for Industry, 96(4), 1168-1176.

Liu, T. (2010). Efficient reformulation of the Thomson–Haskell method for computation of surface waves in layered half-space. Bulletin of the Seismological Society of America, 100(5A), 2310-2316.

Lysmer, J., & Kuhlemeyer, R. L. (1969). Finite dynamic model for infinite media. Journal of the Engineering Mechanics Division, 95(4), 859-878.

Lysmer, J., Udaka, T., Tsai, C., & Seed, H. B. (1974). FLUSH - a computer program for approximate 3-D analysis of soil-structure interaction problems. No. PB-259332; EERC-75-30. California University.

Madshus, C., & Kaynia, A. (2000). High-speed railway lines on soft ground: dynamic behaviour at critical train speed. Journal of Sound and Vibration, 231(3), 689-701.

Madshus, C., Lacasse, S., Kaynia, A., & Hårvik, L. (2004). Geodynamic challenges in high speed railway projects Geotechnical Engineering for Transportation Projects (pp. 192-215).

Mauer, L. (1995). Determination of track irregularities and stiffness parameters with inverse transfer functions of track recording vehicles. Vehicle system dynamics, 24(1), 117-132.

Mead, D. J. (1970). Free wave propagation in periodically supported, infinite beams. Journal of Sound and Vibration, 11(2), 181-197.

Metrikine, A., & Popp, K. (2000). Steady-state vibrations of an elastic beam on a visco-elastic layer under moving load. Archive of Applied Mechanics, 70(6), 399-408.

Miller, G., & Pursey, H. (1955). On the partition of energy between elastic waves in a semi-infinite solid. Paper presented at the Proceedings of the Royal Society of London: mathematical, physical and engineering sciences, 233(1192), 55-69.

Monismith, C. L., Seed, H. B., Mitry, F., & Chan, C. (1967). Predictions of pavement deflections from laboratory tests. Paper presented at the Second International Conference on the Structural Design of Asphalt Pavements.

National-Rail/standard. (2015). Track bed investigation, design and installation NR/L2/TRK/4239. (Issue: 1).

Nsabimana, E., & Jung, Y.-H. (2015). Dynamic subsoil responses of a stiff concrete slab track subjected to various train speeds: A critical velocity perspective. Computers and Geotechnics, 69, 7-21.

ORR-Data. National Rail Trends and Office of Rail and Road data portals, retrieved from http://dataportal.orr.gov.uk/browsereports/2 (accessed 18th October. 2017).

Paixão, A., Fortunato, E., & Calçada, R. (2015). The effect of differential settlements on the dynamic response of the train–track system: A numerical study. Engineering structures, 88, 216-224.

Paolucci, R., Maffeis, A., Scandella, L., Stupazzini, M., & Vanini, M. (2003). Numerical prediction of low-frequency ground vibrations induced by high-speed trains at Ledsgaard, Sweden. Soil Dynamics and Earthquake Engineering, 23(6), 425-433.

Pombo, J., & Ambrósio, J. (2004). A multibody methodology for railway dynamics applications. Instituto Superior Tecnico, Lisbon, Portugal.

Pombo, J., & Ambrósio, J. (2008). Application of a wheel–rail contact model to railway dynamics in small radius curved tracks. Multibody System Dynamics, 19(1), 91-114.

RailOne. (2011). Rheda 2000 Ballastless Track System.

Remennikov, A. M., & Kaewunruen, S. (2008). A review of loading conditions for railway track structures due to train and track vertical interaction. Structural control and Health monitoring, 15(2), 207-234.

Remington, P., & Webb, J. (1996). Estimation of wheel/rail interaction forces in the contact area due to roughness. Journal of Sound and Vibration, 193(1), 83-102.

Rollins, M., Evans, D., Diehl, B., & William, D. (1998). Shear modulus and damping relationships for gravels. Journal of Geotechnical and Geoenvironmental Engineering, 124(5), 396-405.

Sañudo, R., Dell'Olio, L., Casado, J. A., Carrascal, I. A., & Diego, S. (2016). Track transitions in railways: A review. Construction and Building Materials, 112, 140-157.

Scheffel, H., Fröhling, R. D., & Heyns, P. S. (1994). Curving and stability analysis of self-steering bogies having a variable yaw constraint. Vehicle system dynamics, 23(S1), 425-436.

Seed, H. B., Chan, C. K., & Lee, C. E. (1962). Resilience characteristics of subgrade soils and their relation to fatigue failures in asphalt pavements. Paper presented at the International Conference on the Structural Design of Asphalt Pavements. Supplement.

Seed, H. B., & Idriss, I. M. (1970). Soil moduli and damping factors for dynamic response analyses. Earthquake Engineering Research Center, University of California, USA.

Selig, E. T., & Waters, J. M. (1994). Track geotechnology and substructure management: Thomas Telford.

Serdelová, K., & Vičan, J. (2015). Analysis and design of steel bridges with ballastless track. Procedia Engineering, 111, 702-708.

Shearer, P. M. (2009). Introduction to seismology: Cambridge University Press.

Sheng, X. (2001). Ground vibrations generated from trains. University of Southampton.

Sheng, X., Jones, C., & Petyt, M. (1999). Ground vibration generated by a load moving along a railway track. Journal of Sound and Vibration, 228(1), 129-156.

Sheng, X., Jones, C., & Thompson, D. (2003). A comparison of a theoretical model for quasi-statically and dynamically induced environmental vibration from trains with measurements. Journal of Sound and Vibration, 267(3), 621-635.

Sheng, X., Jones, C., & Thompson, D. (2004). A theoretical model for ground vibration from trains generated by vertical track irregularities. Journal of Sound and Vibration, 272(3), 937-965.

Shih, J. Y., Thompson, D. J., & Zervos, A. (2014). Assessment of track-ground coupled vibration induced by high-speed trains. The 21st International Congress on Sound and Vibration, China.

Shih, J. Y., Thompson, D. J., & Zervos, A. (2016a). The effect of boundary conditions, model size and damping models in the finite element modeling of moving load on a track/ground system. Soil Dynamics and Earthquake Engineering, 89, 12-27.

Shih, J. Y., Thompson, D. J., & Zervos, A. (2016b). Modelling moving loads on a track/ground system by using the finite element method. Soil Dynamics and Earthquake Engineering.

Shih, J. Y., Thompson, D. J., & Zervos, A. (2017). The influence of soil nonlinear properties on the track/ground vibration induced by trains running on soft ground. Transportation Geotechnics, 11, 1-16.

Smith, A., Wheat, P., & Nixon, H. (2008). International benchmarking of Network Rail's maintenance and renewal costs. Institute for Transport Studies (ITS) and Office of Rail and Road (ORR).

Srinivasan, M. (1969). Modern permanent way. Somaiya Publications PVT Limited, India.

SSF-Ingenieure. Slab track systems on different substructures, retrieved from www.ssf-ing.de (accessed 28th July, 2017).

Steenbergen, M. J., & Metrikine, A. V. (2007). The effect of the interface conditions on the dynamic response of a beam on a half-space to a moving load. European Journal of Mechanics-A/Solids, 26(1), 33-54.

Stewart, H. E., & O'Rourke, T. D. (1988). Load factor method for dynamic track loadings. Journal of transportation engineering, 114(1), 21-39.

Suiker, A. S. J., De Borst, R., & Esveld, C. (1998). Critical behaviour of a Timoshenko beam-half plane system under a moving load. Archive of Applied Mechanics, 68(3), 158-168.

Sweere, G. T. H. (1990). Unbound granular bases for roads. PhD thesis, Technische Universitiet Delft, Netherlands.

Tadeu, A. J., & Kausel, E. (2000). Green's functions for two-and-a-half-dimensional elastodynamic problems. Journal of engineering mechanics, 126(10), 1093-1097.

Takemiya, H. (2003). Simulation of track–ground vibrations due to a high-speed train: the case of X-2000 at Ledsgard. Journal of Sound and Vibration, 261(3), 503-526.

Takemiya, H., & Bian, X. (2005). Substructure simulation of inhomogeneous track and layered ground dynamic interaction under train passage. Journal of engineering mechanics, 131(7), 699-711.

Thompson, D. (2008). Railway noise and vibration: mechanisms, modelling and means of control. Elsevier, UK.

Thompson, M. R., & Robnett, Q. (1979). Resilient properties of subgrade soil. Journal of transportation engineering, 105(1), 71-89.

Timoshenko, S. (1954). The collected papers of Stephen P. Timoshenko. Science Magazine, 120(3113), 339-340.

Triepaischajonsak, N., & Thompson, D. (2015). A hybrid modelling approach for predicting ground vibration from trains. Journal of Sound and Vibration, 335, 147-173.

Triepaischajonsak, N., Thompson, D., Jones, C., Ryue, J., & Priest, J. (2011). Ground vibration from trains: experimental parameter characterization and validation of a numerical model. Proceedings of the Institution of Mechanical Engineers, Part F: Journal of Rail and Rapid Transit, 225(2), 140-153.

UIC. High Speed. Retrieved from http://www.uic.org/highspeed#General-definitions-of-highspeed (accessed 19th June, 2017).

Uzan, J. (1985). Characterization of granular material. Transportation Research Record, 1022(1), 52-59.

Uzan, J. (1992). Resilient characterization of pavement materials. International Journal for Numerical and Analytical Methods in Geomechanics, 16(6), 453-459.

Varandas, J. N., Hölscher, P., & Silva, M. A. (2011). Dynamic behaviour of railway tracks on transitions zones. Computers & structures, 89(13), 1468-1479.

Varandas, J. N., Paixão, A., Fortunato, E., & Hölscher, P. (2016). A Numerical Study on the Stress Changes in the Ballast Due to Train Passages. Procedia Engineering, 143, 1169-1176.

Verbraken, H., Lombaert, G., & Degrande, G. (2011). Verification of an empirical prediction method for railway induced vibrations by means of numerical simulations. Journal of Sound and Vibration, 330(8), 1692-1703.

Woodward, P., El Kacimi, A., Laghrouche, O., Medero, G., & Banimahd, M. (2012a). Application of polyurethane geocomposites to help maintain track geometry for high-speed ballasted railway tracks. Journal of Zhejiang University SCIENCE A, 13(11), 836-849.

Woodward, P., Kacimi, A., Laghrouche, O., & Medero, G. (2012b). Breaking the ground speed barriers for ultra-speed trains: Rayleigh ground wave modelling and mitigation. International Journal of Railway Technology, 1(1), 105-119.

Woodward, P., Laghrouche, O., & El Kacimi, A. (2013). Ground dynamics of high-speed trains crossing soft soils. Institute for Infrastructure & Environment Scotland, Heriot-Watt University.

Wu, T. X., & Thompson, D. J. (2001). Vibration analysis of railway track with multiple wheels on the rail. Journal of Sound and Vibration, 239(1), 69-97.

Xia, H., Cao, Y., & De Roeck, G. (2010). Theoretical modeling and characteristic analysis of moving-train induced ground vibrations. Journal of Sound and Vibration, 329(7), 819-832.

Yang, L., Powrie, W., & Priest, J. (2009). Dynamic stress analysis of a ballasted railway track bed during train passage. Journal of Geotechnical and Geoenvironmental Engineering, 135(5), 680-689.

Yang, Y., Hung, H., & Chang, D. (2003). Train-induced wave propagation in layered soils using finite/infinite element simulation. Soil Dynamics and Earthquake Engineering, 23(4), 263-278.

Zhai, W., Wang, Q., Lu, Z., & Wu, X. (2001). Dynamic effects of vehicles on tracks in the case of raising train speeds. Proceedings of the Institution of Mechanical Engineers, Part F: Journal of Rail and Rapid Transit, 215(2), 125-135.

Zou, C., Wang, Y., Wang, P., & Guo, J. (2015). Measurement of ground and nearby building vibration and noise induced by trains in a metro depot. Science of the Total Environment, 536, 761-773.